Effect of Shear Energy Input on the Rheology of Flocculant-Dosed Kaolinite Suspensions

By

Ravi Neelakantan

A thesis submitted in partial fulfillment of the requirements for the degree of

Master of Science

in

Chemical Engineering

Department of Chemical and Materials Engineering

University of Alberta

Abstract

Thickened tailings technology is implemented in some oil sands operations in order to recycle warm process water, thereby reducing net water draw, and to reduce the size of tailings impoundment areas. The rheology of thickened tailings is complex and time-dependent, and the underlying mechanism of rheological degradation (J.M. Treinen and R. Cooke, HYDROTRANSPORT 18, BHR Group, Cranfield, UK, 487-499, 2010) is not well understood. In the present study, the time evolution of the particle size distribution (PSD) and vane yield stress of a kaolinite dispersion mixed with polymer flocculants is examined as a function of shear energy input. Size distributions are obtained using the Focused Beam Reflectance Measurement technique. The shear energy input was quantified with the use of a large-volume, customized concentric cylinder shearing apparatus which allowed for the testing of about 300cm^3 of flocculated tailings per experiment.

It was found that decreases in vane yield stress and aggregate size were correlated with energy input when acrylamide polymers were used as flocculants. In particular, very large aggregates appeared to break down to produce a significant population in the 10-100µm size range as shear energy input was increased, which was seen in other studies, e.g. Vaezi et al. (*J. Colloid Int. Sci,* **355**, 96-105, 2011), who observed both size and structure (porosity) changes. A decrease in apparent volume is the main mechanism for rheological degradation of acrylamide flocculated thickened tailings. Lowering the slurry pH before flocculation from 8.5 to 7.0 resulted in a much greater equilibrium yield stress; however initial rates of yield stress decay and floc degradation were unaffected. Dual polymer flocculation with Magnafloc® LT27AG and HyChem HyperFloc CD650 resulted in increased rates of decay in both rheology and size distribution. Data obtained for non-conventional polymers (e.g. PEO) demonstrate the potential for elastic polymer structures to flocculate in high shear environments and the importance of other factors (aggregate shape, zeta potential) which require further investigation.

Acknowledgements

I would like to thank my supervisor Dr. Sean Sanders, not only for guiding me through sticking points in the project, but mostly for taking a chance by bringing a chemist into the field of hydrotransport. I also have to give credit to my friend Cody Kupferschmidt for his help commissioning the concentric cylinder shear apparatus and Kyle Minor for his hard work writing Matlab code for statistical analysis. I also need to thank Brad Komishke from Teck for supplying the tailings for an experiment. In addition I would like to extend the highest gratitude to Herb Green from the machine-shop for his fantastic work when constructing my shearing apparatus. I also need to thank Terry Runyon and the rest of the Pipeline Transport Processes Research Group for their help throughout the project.

I would like to thank the Institute for Oil Sands Innovation (IOSI) and the NSERC Industrial Research Chair in Pipeline Transport Processes for their funding of the project.

Last, but not least, I would like to thank my parents for their moral support throughout my studies. I could not have done this without them.

Table of Contents:

Chapter 5: Conclusions and Recommendations

List of Figures:

List of Tables:

List of symbols

ω	angular velocity	$(rad \cdot s^{-1})$
T	torque	$(N \cdot m)$
t	time	(s)
E	shear energy per unit volume	$(kJ \cdot m^{-3})$
τ_w	wall shear stress	(Pa)
τ_V	Vane yield stress	(Pa)
τ_B	Bingham yield stress	(Pa)
$\dot{\gamma}$	shear rate	(s^{-1})
ζ	zeta potential	(mV)
C_f	volume concentration of fines	(C_{solids}/C_{total})
λ_D	Debye length	(m)
ρ	density	$(kg \cdot m^{-3})$
C_i	concentration of the i^{th} species	$(atoms \cdot m^{-3})$
V(x)	potential energy at distance x	(J)
F(x)	Force at distance x	(N)
C_f	Volume concentration of fines	(Volume of fines/Total volume)
D_p	Particle diameter	(m)
α_i	volume fraction of the i^{th} species	$(\frac{\alpha_i}{\sum_i \alpha_i})$
dCL/dt	time derivative of chord length d_{50}	$(\mu m/s)$
C_D	Drag coefficient	(dimensionless)
Re	Reynolds number	(dimensionless)
d[3,2]	Sauter mean diameter	(μm)
d[3,0]	Number volume mean	(μm)
P	power	(W)

A_H	Hamaker constant	(J)
η	refractive index of a material	(dimensionless)
ε	dielectric constant	(dimensionless)
ε_o	permittivity of free space	(F/m)
ν_e	frequency of electron	(s^{-1})
k_B	Boltzmann constant	($J \cdot K^{-1}$)
$\varphi(x)$	potential at distance 'x'	(mV)
Ω	advective flow correction factor	(dimensionless)
g	force of gravity	($m \cdot s^{-2}$)

Chapter 1: Introduction

1.1 Oil sands overview

In 2009, the Alberta Energy Regulator (AER) issued Directive 074 to create strict regulations in an effort to make oil sands operations more environmentally sustainable. The overall goals of Directive 074 were to reduce the production of fluid fine tailings, reduce the size of current tailings ponds, and decrease net draw from the Athabasca River, while producing highly dewatered tailings suitable for relatively rapid land reclamation[1]. Fluid fine tailings are a byproduct of mining operations and consist of fine particles, defined as particles with diameters less than 44μm. Due to their small diameters, fine particles experience competition between body forces and surface forces. At a certain pH, aqueous environment and hydrodynamic conditions these particles will form stable colloidal suspensions and require a large volume of storage space. Despite efforts to reduce fluid tailings, oil sands operators have not met the targets set out in their applications and inventories of fluid tailings have continued to grow. As a result, oil sands operators were required to submit strategies outlining their plans to meet the required levels of fines capture set out by the Alberta Energy Regulator.

In March 2015, the Government of Alberta released the Tailings Management Framework (TMF) for Mineable Athabasca Oil Sands while at the same time suspending Directive 074.[2] The TMF was created to provide direction to the AER on regulating fluid fine tailings volumes and oil sands operators are now no longer obliged to meet the requirements outlined in Directive 074, but are expected to continue working towards progressive tailings management strategies while the specific goals of the TMF are developed[2]. The TMF is working towards setting achievable goals of fines capture and aims to set limits of total volume of accumulated fine tailings during mine operation and have these tailings in a reclaimable form within 10 years of the end of the mine life. The amount of fluid tailings which can be accumulated is referred to as the Total Volume Limit, and operators which surpass this amount of

accumulated tailings will receive severe penalties as it poses both environmental risk and potential long term liability. In essence, the overall goals of TMF and Directive 074 are the same and will require oil sands operators to reduce fluid fine tailings which will require implementation of new technologies in order to convert fluid fine tailings to trafficable deposits used for land reclamation.

The strategies used in dewatering of fluid tailings involve a wide variety of process equipment which will depend on the specific requirements of each mining site or tailings area[3-9]. Table 1.1 lists each operator's strategy to capture fines in accordance with Directive 074 from 2013. In 2012 the Consortium of Tailings Management Consultants (CTMC) released a report called, Oil Sands Tailings Technology Deployment Roadmap, which outlines the process equipment currently being implemented in the oil sands[10]. Nearly all of these strategies involve injection and mixing of polymer flocculants which bind fine particles together through molecular bridges[11] forming large fractal aggregates called flocs[12]. The formation of flocs causes de-stabilization of clay suspensions which allows recovery of water. In addition to recovering water, the flocs will increase the solids concentration of the tailings deposits which produces a high yield stress mixture. Injection of polymer flocculants can be in-line or can be done in large mixing vessels after which the concentrated mixture must be pumped to a designated disposal area where additional drainage occurs through shear from beaching, under drainage, and environmental effects (drying)[10,13]. Maintaining a high yield stress is crucial to avoiding deposition of coarse particles in laminar pipeline transport of the slurry[14,15] while also having adequate strength to be used in land reclamation efforts, which requires yield stresses > 10 kPa[1].

Though one of the benefits of using flocculants for thickening tailings is an increase in yield stress, in practice this is not a permanent change. In fact, once the tailings are transported in a pipeline, the rheology changes, reducing the slurry's yield stress and at least partially off-setting this benefit. Predicting the rheology change of such complex mixtures has proven to be difficult and currently only

Table 1.1: List of oil sands operators and their tailings management technology being implemented as of the June 2013 Directive 074 reports.

Operator – Mine Site	Technology (date of implementation)	Cumulative fines capture goal
CNRL – Horizon Mine[3]	-Non-segregating tailings (NST) (2015) -Thin-lift dewatering (TLD) (2015)	December 2025
Imperial Oil Resources Ventures Limited Kearl Oil Sands Project[4]	- Flotation tailings thickener (2016) - Thickened tailings solvent recovery unit will deposit tailings in pit (2018)	December 31, 2023
Shell Canada Jackpine Mine[5]	-Thickened tailings (2010 – end of mine life) -Fluid tailings centrifugation (2014-2027) -Non-segregating tailings (2027 – end of mine life)	December 31, 2019
Shell Canada Muskeg River Mine[6]	-Atmospheric fines drying (AFD) (2013) -Composite tailings (CT) technology (2012) -Non-segregating tailings (NST) (2019)	2023
Suncor[7]	mature fine tailings drying (MFTD) technology and tailings reduction operations (TRO)	December 31, 2021
Syncrude Canada Aurora North Mine[9]	- Composite tailings (CT) technology - Will develop additional fines capture technology and implement (2017)	2030
Syncrude Canada Mildred Lake Mine[8]	- Using composite tailings (CT) technology - Centrifuges and thin lift deposition to be used commercially by 2015	2023

empirical studies, which demonstrate a general power-law type decay in rheology of these mixtures can be found in literature[16-18]. Initial yield stresses and extent of rheological degradation vary significantly from one batch of tailings to another and a more quantitative model that takes into account physical, chemical and hydrodynamic conditions of the mixture has yet to be developed. The present study is focused on providing new research results in this area.

1.2 Context and Research Objective

Studies have demonstrated that rheological degradation of tailings is directly related to the amount of shear energy input into the tailings during transport and show a power-law type degradation under all conditions examined[17,18]. In addition, Treinen and Cooke (2010)[16] demonstrated that the degradation is not affected by the shearing device used and is only dependent on the amount of shear energy input. However these studies were empirical in nature and many fundamental aspects are still to be explored. In order to predict yield stress, knowledge of solids volume concentration[19,20], mineralogy[21], pH[22], water chemistry[23] and chemical additives[11,24,25] are essential. Coarse particles are generally not porous and hence have a constant volume and can be assumed to have a constant size when being pumped in a thickened tailings mixture through a pipeline. Fine clay particles exhibit more complex behaviour and can have up to three faces of varying surface chemistry. Each surface can be negative, neutral or positive in charge depending on water chemistry[26]. Consequently clay particles can form structural networks called flocs and can associate in different configurations depending on pH and ion concentration[27,28]. The water chemistry and pH affects floc structure and also mixture rheology. For example the maximum yield stress of a fine clay particle suspension occurs at the pH of the iso-electric point of the edge[29]. In addition, polymer additives can form alter structure and rheology through bridging, charge neutralization and other forces[11,24,30-33]. Vaezi et al. (2011)[34] showed that a dilute kaolinite suspension flocculated with a high molecular weight anionic polymer forms flocs that are increasingly porous with size. In that study, the largest flocs (>400μm) were found to have porosities of approximately 95%. Flocs between 200-400μm in diameter had porosity values between 60-90%. Recently, Klein (2014)[35] found that excessive mixing of tailings during flocculation with high molecular mass anionic polymers leads to dramatic size reduction of flocs. Flocs formed by charge neutralization with the use of cationic polymers results in smaller, dense and more rigid flocs when compared to those

formed by high molecular weight anionic polymers[24,32,33]. Non-conventional poly(ethylene oxide) produces large robust flocs which densify when subject to shear thereby increasing yield stress[11].

Given the dramatic differences in floc properties produced by various polymer flocculants and the importance on yield stress thereof, it is logical that the effects on time-dependent rheology of these various additives should be explored. Current empirical studies on rheological reduction have only investigated the phenomena for tailings flocculated with anionic acrylamides, and no quantitative study exists for tailings flocculated with cationic polymers or poly(ethylene oxide). In addition there is no study in literature which examines changes in particle size distribution (PSD) of flocculated aggregates and their effect on rheology.

Hence the goals of the present study are to determine:

- The relationship of floc size and rheology of a polymer-flocculated kaolinite paste as a function of energy input
- The effects of polymer type and structure on the relationship between floc size and rheology changes with energy input on polymer-flocculated kaolinite paste
- The effect of pH on both floc size reduction and rheology of a polymer-flocculated kaolinite paste as a function of energy input

The most important activities required to fulfill the research objectives include the following:

- Construction of a concentric cylinder shearing apparatus capable of accommodating large volumes of paste. This apparatus is used to control the energy input into the mixture;
- Create shearing protocols which give a broad range of energy inputs;
- Develop a method to consistently reproduce a concentrated homogenous paste of polymer-flocculated kaolinite from a dilute kaolinite suspension (8% wt.);

- Experimentally measure a broad range of yield stresses of 41% wt. paste using a vane viscometer
- Develop a method for Focused Beam Reflectance Measurement (FBRM) chord length measurements. In particular, the following guidelines must be met:
    - Minimal amount of shear energy input into the system during chord length measurements such that the size measurement is not affected;
    - Ensure that the measurement protocol does not alter the floc size;
    - Reproducible chord length measurement at a known solids concentration must be obtained.

1.3 Thesis Contents

The thesis contains five chapters, including the current chapter. The second chapter is a literature review, which contains an overview of relevant literature and the importance of the contributions of the present study. Chapter 3 contains a list of materials, while Chapter 4 and 5 contain results and discussion, and conclusions respectively.

Chapter 3 also contains all procedures, materials, and equipment used throughout the thesis. The materials section contains all information regarding materials used and the supplier from which they were obtained. The equipment section lists information regarding all equipment/instrumentation used in the experiments, their dimensions and any other relevant information. A large portion is directed to the description of a customized concentric cylinder shearing apparatus which was constructed specifically for this experiment. The sub-chapter on procedures includes protocols for vane rheometry measurements, paste shearing, focused beam reflectance measurements and flocculation experiments. Due to the unique application of FBRM, a section of the appendix is dedicated to the

validation of the experimental technique and contains supplementary experiments and statistical analysis using Matlab.

Chapter 4 discusses the results of the experiments for all conditions tested and their relevance in the current literature. This chapter is focused on the importance of floc size reduction as a function of shear energy input and the relation to reduction in yield stress of the mixtures studied. It also covers the importance of polymer selection and mixture chemistry on floc size and yield stress reduction. In addition, it discusses the importance of non-conventional poly(ethylene oxide) and the need for added research into its distinct rheological properties. Lastly, the concepts are tested against real tailings to demonstrate their validity.

The fifth chapter contains an extended discussion and concluding remarks. The discussion covers the significance of the present study in the current literature and how the study can be used to fuel a new stream of research. In addition methods of improving the procedures and recommendations for future work are included.

1.4 Contributions

The underlying mechanisms of time-dependent rheology are not well understood and predicting rheology of tailings can be difficult. Presented here are some mechanisms of time-dependent behaviour and methods of predicting the behaviour using fundamental properties of a mixture, such as particle size, size distribution, initial yield stress, polymer type and mixture chemistry. It also provides the design of an instrument which can be used to accurately characterize the time-dependent behaviour of tailings without the use of a thickener and, in addition, does not rely on concentric cylinder viscometer measurements. Although the time dependent behaviour can be examined using a concentric cylinder viscometer, the effects of slip do not provide the true material property of the mixture. In addition,

subsequent yield stress measurements cannot be taken on a mixture sheared in a benchtop concentric cylinder rheometer due to lack of volume.

Finally, the present study outlines the importance of studying flocculation as a function of mixing energy to be scalable to industrial applications. Simple studies which including mixing time and spindle angular velocity do not suffice and are qualitative at best.

The study provides a new stream of research to be examined and offers a wide range of future work to be done. With enough added research, the concepts obtained from this study can provide methods to accurately predict tailings rheology in an industrial setting using in-line measurements of particle size, size distribution and solution chemistry.

2. Literature Review

2.1 Introduction

This chapter consists of a practical review of the most relevant literature related to the characterization of a fluid-particle system – in particular a flocculated kaolinite clay suspension. First, methods of characterizing fine-particle suspensions are discussed, with a focus on particle size and rheology measurements, as they pertain to the experimental results of the present study. The system characterization literature was pivotal for the present study, in particular for developing reproducible procedures. A basic understanding of rheology – from a primarily practical point of view – is necessary for interpretation of the results presented in Chapter 4. Specifically, a thorough breakdown of factors that affect suspension rheology – particle diameter, surface chemistry and volume concentration, chemical additives such as polymers and water chemistry – are discussed in relation to this project. The relationship between floc structure and rheology will be established. In addition, the effects that polymer type and structure have on clay floc formation and suspension rheology are reviewed.

Finally, the additional complexity that shear adds on the previous list of factors affecting suspension rheology will be discussed. The effect of shear on flocculated suspensions is typically time-dependent and is affected by polymer additives, and other suspension properties such as particle size distribution and mixture chemistry. Previous work in this area is limited and mostly qualitative (described in terms of mixing times, not shear energy) and the importance of this work to the development of the present study is provided in Section 2.4.

2.2 Fine-particle suspension characterization

2.2.1 Floc size

Floc size can be measured using a variety of methods, and the appropriate method depends entirely on the application and the type of information required. Some experiments may require particle shape factors which will require visual imaging, whereas others may only be interested in particle diameters, which can be obtained through a variety of methods. Considerations must be made based on the fundamental limitations of the measurement technique as well as the implications of the experimental procedures – for example, sampling technique and shear forces imparted on the flocs. Typical methods are laser diffraction experiments and visual imaging[36] and more recently focused beam reflectance measurement (FBRM)[37].

Laser diffraction experiments are an excellent tool for in-line measurements of dilute suspensions, as a stirred sample can be directly fed to the detector through a feed tube. An illustration of this system is shown as Figure 2.1. In this technique, small particles scatter light at high angles whereas larger particles will scatter light at much smaller angles[38]. The diffracted light can be measured and converted to a size distribution; however; is not a direct measurement of particle size. This experimental technique has been used to monitor flocculation as well as monitoring fractal dimensions of flocs[38-40]. There are several drawbacks of this experimental technique in the context of the present study. The sample must be homogenous and hence in the presence of settling particles, the slurry must be subject to pre-mixing of the sample in order to achieve homogeneity. As a consequence, mixing energy is added to the system which alters floc size[35]. In addition, as the sample is drawn through the narrow tube, the flocs are subjected to very high shear rates, and the effect of shear on reducing floc size is well documented[35], thus altering the sample and influencing the size measurement. Samples must be very dilute, which for

Figure 2.1: (LEFT) Dynamic light scattering instrumentation showing premixing chamber with feed tubes to the detector (RIGHT) Focused beam reflectance measurement showing direct immersion of probe into the mixture

the present study, contributes to the uncertainty of the measurement given that the samples will be very dense (approximately 41% by mass).Vaezi et al. (2011)[34] used image analysis to monitor the floc size of very dilute kaolinite suspensions flocculated with an anionic acrylamide (Magnafloc® 1011). The advantage of using image analysis is that it provides a particle image from which a diameter can be obtained and does not require the conversion of a signal to a cross-sectional diameter. In addition, the amount of shear can be minimized by modification of the experimental apparatus and sampling technique. However, in order to obtain clear images, a very dilute suspension must be used, and analysis can be very time consuming when large populations of particles are required (e.g. when producing a size distribution), or when a large number of samples are being analyzed.

Focused beam reflectance measurement (FBRM) has been used since the 1990s in the paper industry to optimize flocculation and has been used to study floc strength by monitoring flocculation, de-flocculation and re-flocculation[37,41-43]. The apparatus consists of a probe which is directly immersed into a stirred mixture as shown in Figure 2.1, thus eliminating the high shear experienced in the feed

tube in laser diffraction experiments. The probe tip contains a 780nm laser which oscillates in a circular path at very high speeds. The backscattered light is used to generate a chord length distribution based on the cross-sections of particles in the circular path of the laser. Due to the high rotational speeds, FBRM can count thousands of particles per second when producing size distributions. One of the disadvantages of FBRM is that it does not provide a true particle diameter, but rather a chord length taken along the path of the laser and for this reason should only be used when measuring a trend (e.g. optimizing flocculation). Yu and Erickson (2008)[44] outlined some of the limitations when using FBRM for size analysis and found that the reported size is affected by solids volume concentration and may suffer from counting overlapping particles as one particle, hence reporting a greater apparent chord length. However, FBRM is very practical for measuring changes in size or size distribution and can be applied to dense mixtures up to 40 % by mass. In addition, FBRM has recently been used by Klein (2014)[35] for optimizing flocculation of oil sands tailings.

In the present study, FBRM was selected to obtain size distributions of the mixture because it is the change in particle size and size distribution that is of greatest importance. In order to minimize shear energy input into the sample, a 'paste-drop' method is employed which involves dropping a desired amount of paste into stirring water rather than pre-stirring a mixture. This procedure is explained in detail in Chapter 3. Laser diffraction experiments were not used due to the fact that this method introduces an unquantified amount of shear which can break down (destroy) flocs[35], making it impossible to measure the un-altered sample. Image analysis was not used due to the complexity of sampling, sample dilution and data processing and would not be practical given the large number of counts required to produce each size distribution.

The population of particles can be viewed as a particle size distribution, either as a differential frequency or a cumulative distribution which can provide qualitative information with regards to the

population such as number of modes and the shape of the distribution which are not provided by a mean particle diameter[45]. Using a differential frequency distribution is essential when making measurements of individual particles which are classified by bin size or when converting distributions[46], which is the case for FBRM raw data. The y-axis of this distribution is denoted dF/dx, where 'F' is frequency, and 'x' is bin size. In order to produce cumulative distributions, the integral of differential frequency is taken ($F = \int \frac{dF}{dx} dx$) , and the y-axis is denoted F.

In order to describe a population of particles, several different particle mean diameters can be used, and the appropriate one will depend on the type of size information produced and on the specific application for which a mean diameter is needed. The number volume mean, d[3,0] is defined as[47]:

$$d[3,0] = \left(\frac{\Sigma(n_i {d_i}^3)}{\Sigma n_i}\right)^{1/3} \tag{2.1}$$

In the present study, number volume mean tracks the fragmentation of the larger flocs effectively. Sauter mean diameter, d[3,2], is defined as[34]:

$$d[3,2] = \left(\frac{\sum(n_i {d_i}^3)}{\sum(n_i {d_i}^2)}\right) \tag{2.2}$$

Sauter mean diameter tracked floc size but was mostly unaffected by the presence of fragmentations and kaolinite particles. This mean diameter was used to optimize flocculation due to the volume term in the numerator, and in some statistical analysis of 'paste-drop' experiments as it tracked the homogenization of the mixture with greater sensitivity. A more detailed description of the use of those mean diameters is presented in Sections 4.2 and Appendix B and C.

2.2.2 Rheology

Within the field of rheology, there are two main classifications of fluids – Newtonian and non-Newtonian fluids. Newtonian fluids are defined by a linear relationship between shear rate ($\dot{\gamma}$) and shear stress (τ), where the proportionality constant is the viscosity, μ[48]. Non-Newtonian fluids can be time-dependent or time-independent. Time-independent non-Newtonian fluids can fall into one of many classifications – dilatant (shear thickening), pseudoplastic (shear thinning) and Bingham just to name a few, shown qualitatively in Figure 2.2. Couette flow is used in the present study in the concentric cylinder shearing apparatus and an understanding of the behaviour of fluids with yield stresses in this geometry is required.

The Bingham fluid model is applied in present study, as the Bingham yield stress is a fitted parameter commonly used in Couette (concentric cylinder) flow. Bingham fluids require a minimum amount of stress to initiate flow, known as the Bingham yield stress[49]. For a Bingham fluid, or any fluid with a yield stress, this is the point of transition between solid-like and fluid-like behaviour[22]. The constitutive relationship for Bingham fluids in Couette flow is[49]:

$$\tau - \tau_B = -\mu_p \frac{du}{dr} \tag{2.3}$$

The Bingham yield stress is denoted τ_B, while 'u' is the fluid velocity in the tangential direction and 'r' is the radial position. The proportionality constant between shear stress and shear rate after flow is initiated is called the Bingham plastic viscosity, denoted μ_p. The integrated equation for Couette flow of a Bingham fluid is defined as[49]:

$$\omega = \frac{T}{4\pi L \mu_P}\left[\frac{1}{{R_1}^2} - \frac{1}{{R_2}^2}\right] - \frac{\tau_B}{\mu_P} ln\left(\frac{R_2}{R_1}\right) \tag{2.4}$$

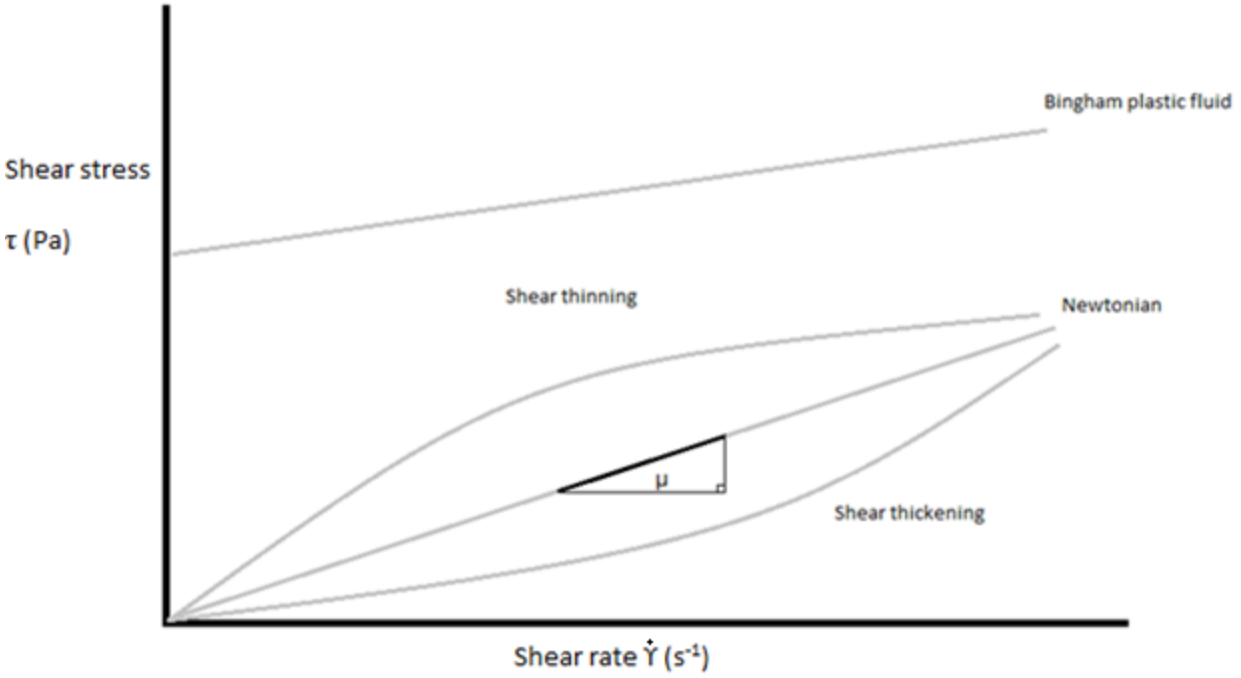

Figure 2.2: Qualitative rheogram showing basic time independent rheological classifications

In this equation, ω is angular velocity (rad/s), T is torque (N·m), τ_B is Bingham yield stress (Pa), μ_P is the plastic viscosity of the fluid (Pa·s), R_1 and R_2 are the inner and outer radii of the fluid filled annulus (m) and L is the length of the rotating spindle (m). The physical dimensions relevant to Equation 2.4 are represented in the illustration shown in Figure 2.3. Direct measurement of yield stress is generally not possible due to lack of data at low shear rates, and in the case where low shear rate data is available, instrument limitation such as wall slip may lead to an inaccurate result[50]. In dilute colloidal systems, wall slip arises from a thin annulus of fluid existing between the particles and the wall of the test geometry and thus the particles interact weakly with the wall[51]. For concentrated suspensions, the local concentration of solids is lower near the wall than in the bulk mixture. When the mixture is sheared,

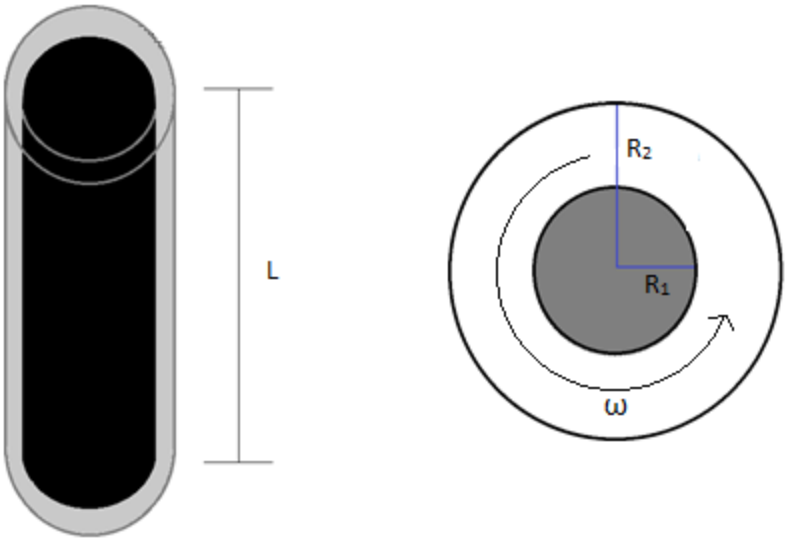

Figure 2.3: Illustration of physical dimensions relevant in Couette flow

a large velocity gradient is produced in this region as a result of lowered viscosity near the wall resulting in apparent wall slip[52,53]. Since low shear (low velocity) measurements cannot be made for Bingham fluids in Couette flow, Bingham yield stresses are obtained by fitting Equation 2.4 to a set of torque-angular velocity data[52]. It is important to remember that shear stress across the gap is not constant and that a minimum torque is required for complete shearing[54]:

$$T_{min} = 2\pi {R_2}^2 L\tau_B \tag{2.5}$$

Here R_2 is the outer radius, L is the length of the cylinder wall and τ_B is the Bingham yield stress. It is very important that the Bingham yield stress be used in Equation 2.5, and should not be confused with vane yield stress. Unfortunately, this method provides a yield stress value which can be as much as 5 times the true yield stress[50]. The key difference is that vane yield stress is a true property of the fluid and is independent of any fluid model, whereas Bingham yield stress is a fitted property[55]. In addition,

measurement of Bingham yield stress of shear-sensitive mixtures may not be possible due to the high rotational velocities required and the resulting shear energy imparted to the mixture. Hence, in the present study, concentric cylinder geometries will not be used to obtain rheological data and will only be used to quantify shear energy input.

As previously stated, non-Newtonian mixtures can be time-dependent in which case they could be classified as thixotropic (decrease in rheology with time) or rheopectic (increase in rheology with time) and can be reversible or irreversible[49]. Normally, if one could experimentally determine the Bingham yield stress and plastic viscosity, the minimum angular velocity for complete shearing across the gap can be obtained. However, due to the time-dependent behaviour of polymer-flocculated suspensions, the Bingham yield stress is reduced during an experiment as shear energy is imparted to the mixture. An alternative approach to determine complete shearing across a gap can be identified when there is a power-law decay in rheology, observed by Treinen et al. (2010)[16] and Salinas et al. (2009)[18]. Both authors used concentric cylinder geometries to study the effect of energy input of flocculated tailings from several mining sites. They determined that complete shearing was obtained when a strict power-law decay was observed after the maximum spindle speed was obtained. This technique is employed in the present study to select an appropriate angular velocity for shearing experiments to ensure the mixture is sheared uniformly.

As a result of the drawbacks associated with Bingham yield stress measurements for time dependent fluids, vane yield stress will be used as the main parameter for characterizing the mixture rheology in the present study. Vane yield stress measurements are discussed in the following section.

2.2.3 Vane Yield Stress

For fluids with yield stresses greater than 20 Pa, the most reliable method of analyzing yield stress is with vane rheometry[55]. To obtain yield stress information, a vane should be set to very low angular velocity (less than 0.5 RPM)[56], and the maximum measured torque can then be related to the vane yield stress through the equation developed by Nguyen and Boger (1983)[55]:

$$T_m = \frac{\pi D^3}{2}\left(\frac{H}{D} + \frac{1}{3}\right)\tau_V \tag{2.6}$$

where D is the diameter of the vane, H is the height of the vane and τ_v is the vane yield stress. The maximum torque in Equation 2.6 is taken as the peak torque value from a torque versus time graph produced during a vane yield stress experiment, shown as point 'A' in Figure 2.4. Nguyen and Boger (1983)[55] also recommend that, to minimize effects caused by the walls of the container, the mixture depth must be twice the vane height (H), and the diameter of the container must be at least twice that of the vane diameter (D).

Vane yield stress measurements have been recently used in several fundamental studies in the characterization of polymer-flocculated clay suspensions[11,24,31] as well as in the characterization of fine particle suspensions in the absence of polymer flocculant[21,57,58]. This technique has also been used in the study of rheology reduction conducted by Gillies et al. (2012)[17] when thickened oil sands tailings were flocculated with anionic acrylamide polymers.

The vane technique is used in the present study to characterize the rheology of the mixtures for three reasons. As discussed above, it has been commonly used in the study of polymer-flocculated clay suspensions, kaolinite suspensions, and real tailings. Also, because the angular velocity of the vane is very low, it does not add an appreciable amount of shear energy to the system. Finally, the vane yield stress is a material property; it is not affected by slip or particle size and is a far more reliable

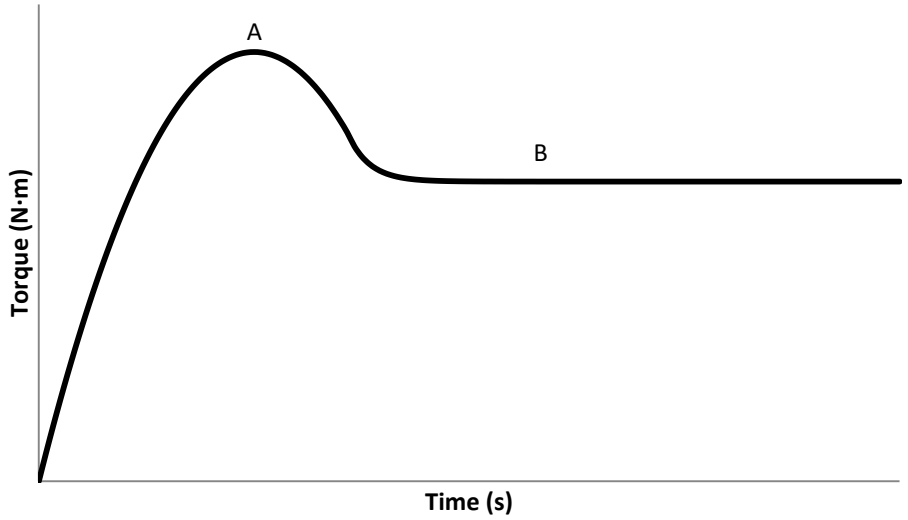

Figure 2.4: Qualitative diagram of yield stress measurement showing: A -Maximum Torque - B Equilibrium Torque

method of characterizing yield stress than concentric cylinder viscometry, particularly for mixtures with high yield stresses (τ>20 Pa)[55] which will be encountered in the present study.

2.3 Factors affecting suspension rheology

2.3.1 Overview

There is no stringent definition of 'fine particles,' but the implication is that the particles are small enough (and have a sufficient surface area to volume ratio) to exhibit colloidal behaviour[59]. Masliyah (2004)[60] defines fine particles in the oil sands as those which have a particle diameter less than 44µm. The key distinction between fines and coarse particles is that as particle size decreases, the surface area to volume (or mass) increases, and as a result the surface forces begin to dominate over body forces. The two main components of the surface forces are described by the well-known DLVO theory, where the summation of van der Waals forces and electrostatic double layer forces provides the

total particle interaction force[61-64]. Whether the attractive or electric double layer forces dominate will depend on the pH, water chemistry, and the size and surface chemistry of the particles involved. When van der Waals forces are greater than the repulsive double layer forces, the particles coagulate and are able to form three dimensional structural networks which contribute to the yield stress of a mixture[22,65]. In the event that the repulsive forces dominate, inter-particle associations which lead to three dimensional structures are limited and a stable suspension is formed[66]. Other non-DLVO forces can contribute a system's rheology, particularly when dealing with polymers. These non-DLVO forces include bridging, depletion, charge neutralisation and hydrophobic forces and are discussed in Section 2.4.1 and 2.4.2. The impact of surface forces on suspension rheology is discussed in this Chapter.

The rheology of a fine particle suspension is also dependent upon solids on volume concentration. Some literature describing the importance of volume concentration on suspension rheology is discussed first, followed by a review of the effects of particle size and surface forces on rheology.

2.3.1 Volume concentration

One of the main contributors to the rheology of a system is the volume fraction of solid particles present in the system. Thomas (1961)[21] developed a correlation between Bingham yield stress and particle properties from 20 different fine particle suspensions including thorium oxide, kaolinite, titanium oxide, aluminum oxide, graphite, magnesium and uranium oxide and observed relationships between Bingham yield stress and particle size and volume fraction. Thomas (1963)[67] found that the yield stress was dependent on particle diameter, D_p, volume fraction, C_f, and a dimensionless shape factor, φ[21]:

$$\tau_B = \frac{A\varphi {C_f}^3}{{D_p}^2} \tag{2.7}$$

The coefficient A is an empirical constant and must be determined when fitting the data. The shape factor accounts for increases in surface area due to particle asymmetry. Coussot and Piau (1995)[19] suggested an exponential correlation with two coefficients, where 'A' and 'B' are determined experimentally for a given set of conditions:

$$\tau_B = Ae^{BC_f} \tag{2.8}$$

Shook et al. (2002)[20] fitted data from several mature fine tailings samples to develop an exponential correlation:

$$\tau_B = e^{13C_f} \tag{2.9}$$

As the aforementioned examples illustrate, the yield stress of a fine particle suspension cannot be predicted until the coefficients are determined experimentally.

Despite differences between the relationships provided above, the volume fraction of fines, C_f, is the dominant term and hence yield stress will be most sensitive to this parameter. In the present study, volume fraction of fines is kept constant in order to compare the impacts of other parameters, such as shearing and surface forces, on rheology.

2.3.2 Particle diameter

The rheology of fine particle suspensions will also depend upon on the diameter of the particles present. Thomas (1961)[21] found that for a wide variety of fine particle suspensions, the yield stress was related to $\frac{1}{{D_p}^2}$ as, shown in Equation 2.7. This is the case for two reasons – firstly, as the particle diameter decreases the surface forces become more dominant and the particles can become flocculating under the appropriate conditions (e.g. pH, water chemistry, etc.), forming structural

networks which trap water. This effectively creates a larger apparent volume thus contributing to the yield stress of the mixture[68]. Secondly, as the surface area to volume ratio of the particles increases, the overall net forces between the particles per unit mass increase, which further augments the yield stress of the mixture[58,69].

Zhou et al. (1999)[58] studied fine particle alumina suspensions and also found that the yield stress was inversely proportional to the square of the particle diameter. In addition they found that the surface average diameter, d_s, could be used to characterize the effects of particle size on yield stress of the mixture, thus confirming the importance of surface forces of fine particles on the yield stress of a fine particle suspension.

A study conducted by Leong et al. (1995)[70] examined the effects of particle size on yield stresses of fine zirconia particle dispersions. Similar to previous work, the authors concluded that the rheology was dictated by particle size and was proportional to $\frac{1}{D_p{}^2}$. In the event of more complicated size distributions, the authors recommend using the fine particle concentration to predict the rheology. Kapur et al. (1997)[22] observed that yield stress increased with decreasing particle diameter for fine particle suspensions. In addition, for skewed or bimodal distributions, the rheology was largely dictated by the particles in the lower size range.

The contribution of small particles to the yield stress of a polymer-flocculated kaolinite suspension is crucial in the present study. As flocs are sheared they decrease in size[35] producing fragmentations and free kaolinite particles. An understanding of the effect of fine particles on rheology is essential in interpreting time-dependent behaviour. A more thorough description of surface forces is described in the next section, with particular attention paid to kaolinite particles.

2.3.3. Surface forces

Kapur et al. (1997)[22] state that the presence of a yield stress implies a mechanically rigid 3D structure formed by the particles. In an earlier study, Michaels and Bolger (1962)[68] experimented with kaolinite suspensions in water, and found that the yield stress was directly related to the volume fraction of flocs rather than the fine kaolinite particles. They proposed the Bingham yield stress was directly related to the square of the floc volume. Similarly, Pignon et al. (1997)[71] studied the influence of volume fraction of floc structure in fine particle suspensions and their relation to yield stress. The volume fraction was found to influence the 3D structure of the flocs, which governs changes in yield stress of the suspension. The formation of these 3D structures arises from associations of kaolinite particles – mainly edge-edge and edge-face[27] depending on the inter-particle forces.

As mentioned previously, the type and magnitude of surface forces acting between particles will have a significant effect on suspension rheology, and thus an understanding of surface forces is highly relevant in the context of understanding the time-dependent behaviour observed in the present study. Specifically, Leong et al. (1993)[69] concluded that vane yield stress of flocculated fine particle suspensions was directly related to inter-particle force. The magnitude of attractive van der Waals forces between spherical particles is dependent on the materials in question, their radii and separation distance, x[61]. The magnitude of van der Waals forces will be important in predicting rheology as increased inter-particle bonding will result in higher yield stresses. For any two spherical particles, the interaction energy in a vacuum can be quantified as follows[61]:

$$V_{vdW}(x) = -\frac{A_H R_1 R_2}{6x(R_1+R_2)} \tag{2.10}$$

$$F_{vdW}(x) = -\frac{A_H R_1 R_2}{6x^2(R_1+R_2)} = -\frac{dV_{vdW}}{dx} \tag{2.11}$$

$$A_H = \pi^2 \rho_1 \rho_2 C_{12} \tag{2.12}$$

Here, A_H is the well-known Hamaker constant, which quantifies the strength of the interaction between two particles, ignoring any effects of the medium. It is dependent on the relative concentration of atoms per unit volume, ρ_1 and ρ_2, and the coefficient of particle-particle interaction, C_{12}[61].

Lifschitz[72,73] advanced this theory to predict Hamaker constants between two particles in a medium. In this instance, the particle-particle interaction energy is far more complicated and becomes dependent on refractive index of the material, η, its dielectric constant, ε, and the frequency at which the electron travels around the nucleus of an atom, ν_e. For particles of different materials '1' and '2' interacting in medium '3', the Equation is an infinite series, of which the first two (and most dominant) terms are[74]:

$$A_{132} = \left(\frac{\varepsilon_1-\varepsilon_3}{\varepsilon_1+\varepsilon_3}\right)\left(\frac{\varepsilon_2-\varepsilon_3}{\varepsilon_2+\varepsilon_3}\right)\frac{3}{4}k_BT + \frac{3h\nu_e}{8\sqrt{2}}\frac{(n_1{}^2-n_3{}^2)(n_2{}^2-n_3{}^2)}{\sqrt{n_1{}^2+n_3{}^2}\sqrt{n_2{}^2+n_3{}^2}(\sqrt{n_1{}^2+n_3{}^2}+\sqrt{n_2{}^2+n_3{}^2})} \quad (2.13)$$

When there are two identical materials interacting in any medium, Equation (2.13) becomes[74]:

$$A_{131} = \left(\frac{\varepsilon_1-\varepsilon_3}{\varepsilon_1+\varepsilon_3}\right)^2\frac{3}{4}k_BT + \frac{3h\nu_e}{16\sqrt{2}}\frac{(n_1{}^2-n_3{}^2)^2}{(n_1{}^2+n_3{}^2)^{3/2}} \quad (2.14)$$

An important consequence of Equation (2.14) is that two particles of the same material interacting in any medium will have a positive value for the Hamaker constant. In the context of the present work, kaolinite particles interacting in any medium will have a positive Hamaker constant and hence will always experience attractive van der Waals forces.

In an aqueous, fine-particle suspension there will also be repulsive forces present in the form of an electric double layer surrounding the particle. Depending on the pH and water chemistry, the surface charge of colloidal particles can be positive, neutral or negative. This surface charge generates an electric double layer – the Gouy-Chapman model represent the double layer as a region in which there is

a statistically much higher concentration of counter-ions to screen the surface charge[62]. For low surface potentials (<25mV), the Poisson-Boltzmann model[62] can be applied to characterize the double-layer:

$$\lambda_D = \sqrt{\frac{\varepsilon\varepsilon_o k_B T}{e^2 \sum_i C_i^o {Z_i}^2}} = \kappa^{-1} \tag{2.15}$$

$$\varphi(x) = \varphi_o e^{-x/\lambda_D} \tag{2.16}$$

The decay length, known as the Debye length ($\lambda_D = \kappa^{-1}$), is strongly dependent on the concentration (C_i) and valency (Z_i) of salts as well as temperature. The term φ(x) is the potential at a distance 'x' from the surface and for solutions with high concentration and/or valence salts, the surface charge will be screened resulting in a compressed electric double layer. The potential energy and force resulting from the electric double-layer are[62]:

$$z = 64\pi\varepsilon_o\varepsilon\left(\frac{k_B T}{ze}\right)^2 tanh^2\left(\frac{ze\varphi}{4k_B T}\right) \tag{2.17}$$

$$V_{edl}(x) = \left(\frac{R_1 R_2}{R_1 + R_2}\right) ze^{-x/\lambda_D} \tag{2.18}$$

$$F_{edl}(x) = -\frac{dV_{edl}}{dx} = \left(\frac{R_1 R_2}{R_1 + R_2}\right)\frac{ze^{-x/\lambda_D}}{\lambda_D} \tag{2.19}$$

Classic DLVO theory considers only attractive van der Waals forces and repulsive electric double-layer forces between two surfaces in a liquid medium[61-64]. The total energy of the system defined by DLVO theory, V_{Tot}, can be expressed as the sum of van der Waals and electric double layer forces shown in Equation 2.20:

$$V_{Tot}(x) = V_{vdW}(x) + V_{edl}(x) \tag{2.20}$$

where 'x' represents the separation distance between two particles. For a given chemical environment, the total energy is a function of separation distance, x and is shown qualitatively in Figure 2.5.

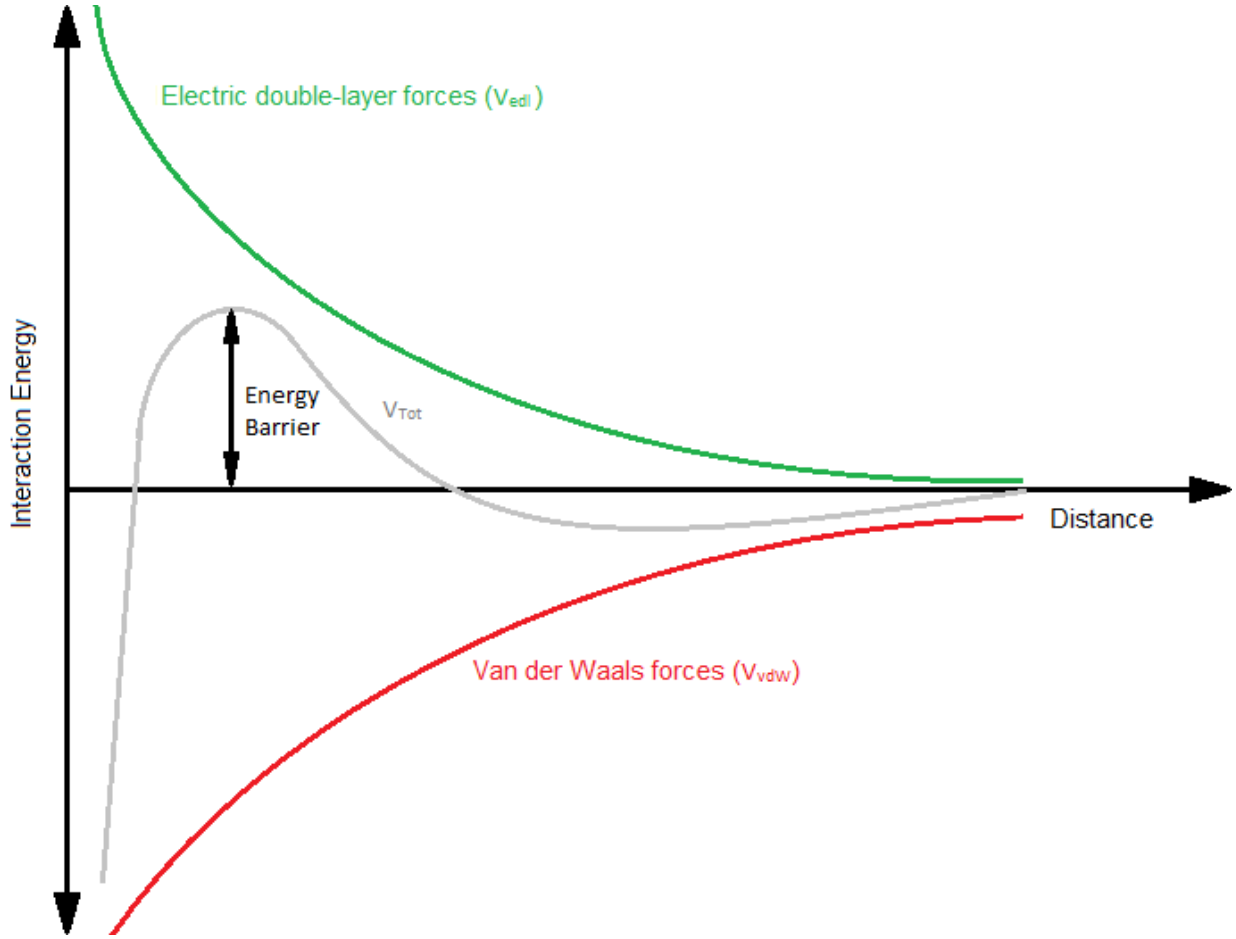

Figure 2.5: Qualitative diagram illustrating classic DLVO theory

The rheology of fine particle suspensions is affected by DLVO forces. At constant solids volume concentration, the maximum yield stress of a fine particle suspension occurs at a pH referred to as the isoelectric point[66,75,76]. At the isoelectric point, the fine particles acquire a zeta potential of zero[66]. The zeta potential is the solid surface potential at the shear plane, the first layer of unbound molecules, of the surrounding liquid[77]. At a pH above or below the isoelectric point the particle surface is charged, and acquires a positive or negative zeta potential. At the isoelectric point the attractive van der Waals forces dominate, and the net attractive inter-particle forces are at a maximum as the electric double layer is

depleted. At appreciable zeta potentials (>20mV) colloidal particles may become stabilized due to overlapping double layers resulting in low yield stresses and very commonly, Newtonian fluid behaviour[66].

In the present study, a model clay is selected rather than real tailings in order to remove the effects of varying concentration, of particle size and size distribution, as well as differing mineralogy and chemistry, which vary from one site to another. Kaolinite is used in the present study due to its widespread abundance in ore bodies and its well characterized chemistry and morphology[11,26,30,31,78,79]. Kaolinite is a two-layer mineral and hence has two different basal faces[26]. One is composed of a tetrahedral siloxane layer and the other is an octahedral aluminium oxide layer[26]. The basal face carries a negative charge due to isomorphous substitution of lower valence cations for Si^{4+} in the tetrahedral sheet or Al^{3+} in the octahedral sheet, shown in Figure 2.6[26]. The basal plane has been shown to occupy 90% of the surface area of kaolinite clays with the remaining 10% accounted for by the edge sites[30]. The overall isoelectric point of kaolinite particles occurs at a pH of ~2[78], and that of the edge, as determined by Braggs et al. (1994)[80] occurs at a pH of 5.25. Thus in the present study, where tests are conducted at pH values of 7 and 8.5, the particles will be inherently negative.

In summation, the pH of the medium will directly affect the surface properties of kaolinite particles. The surface charge of the faces of kaolinite will vary with pH and thus the strength of the repulsive electric double layer force will also vary with pH. The optimum yield stress of a kaolinite suspension occurs at the isoelectric point and decreases as pH deviates from it. In the present study, kaolinite suspensions are flocculated at pH 8.5 and 7. Given the data on isoelectric points of kaolinite, it is expected that the yield stress of well-sheared suspensions will be higher at pH 7 than at pH 8.5.

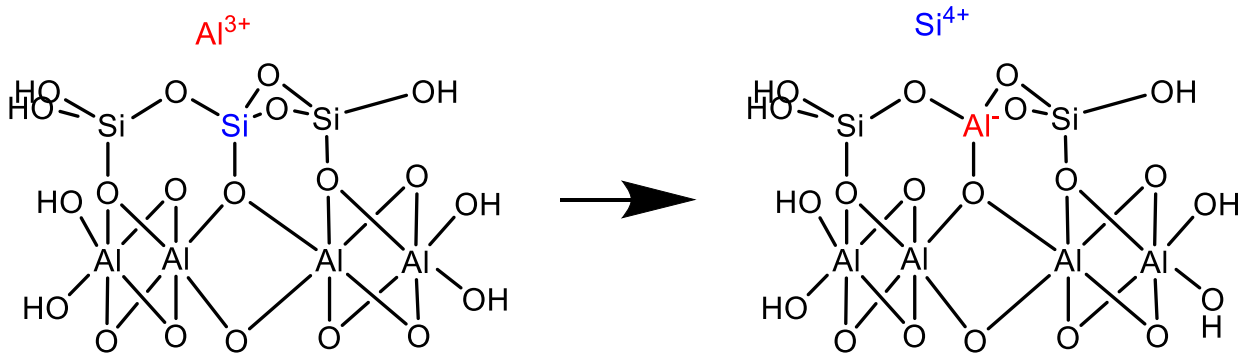

Figure 2.6: Tetrahedral siloxane lattice on top of octahedral aluminum oxide layer. Substitution of Si^{4+} for Al^{3+} is shown from left to right, bringing a permanent negative charge.

2.3.4 Floc size & structure – "apparent" volume concentrations

This section presents studies pertaining to the formation of flocs using polymer flocculants, typical sizes of these flocs, and their structural properties. The structure of flocs will be examined in terms of their strength and porosity-size relationships. As will be demonstrated in this section, the formation of porous flocs results in suspensions where the apparent volume fraction is significantly greater than the true solids volume fraction. The consequence is that as floc porosity increases, the suspension yield stress also increases

The adsorption of high molecular weight polymers to a particle or floc is strong and essentially irreversible[81]. The polymer will preferentially adsorb to the outer surface of large flocs, leaving the interior of the flocs as well as small particles devoid of adsorbed polymer[81]. In order to obtain equal distribution of polymer throughout the flocs one must take advantage of floc breakage and reformation while slowly adding a dilute solution of polymer[82]. Numerous studies have demonstrated that slow addition of polymer will result in a more even distribution throughout the flocs and has been shown to result in larger and faster settling flocs[83-85].

Studies[86-88] have examined the structures of flocculated fine particles and have demonstrated their fractal nature which results in increasingly porous structures with increasing size. These studies have shown that as aggregate size increase, the effective density decreases via a power-law correlation of the form:

$$\rho_{eff} \propto L^{D_F-3} \tag{2.21}$$

In this equation ρ_{eff} is the effective density of the aggregate, L is the diameter, and D_F is the fractal dimension which is a fitted parameter. As D_F increases, the particles are less porous and become more dense. Vaezi et al. (2011)[34] studied the fractal dimensions of flocs generated in very dilute kaolinite suspensions at pH 8.5 flocculated with high molecular weight acrylamides (Magnafloc® 1011). In this study, floc sizes and densities were related using:.

$$\frac{\rho_a-\rho_L}{\rho_p-\rho_L} = 1-\varepsilon = \frac{3\rho_L C_D {V_a}^2 \Omega}{4g(\rho_p-\rho_L)d_a} \tag{2.22}$$

Equation 2.22 assumes a spherical porous aggregate settling steadily in an infinite medium and has also been used in numerous other studies[86,89-91]. In this equation ρ_a is the aggregate density, ρ_L is the density of the liquid medium, Ω is the advective flow correction factor, ε is the void fraction, C_D is the drag coefficient, V_a is the settling velocity in an infinite medium, g is the force due to gravity and d_a is the aggregate diameter. The study showed that during the early stages of the flocculation process, floc growth is the dominant mechanism. However, as the flocs are further subjected to shear, floc breakage becomes more significant. As larger flocs are broken and pseudo-equilibrium between floc growth and fragmentation is established, the average floc size stays relatively constant. The study also found that large aggregates (with diameters > 400μm) had porosities between 90-95%. Additionally, a sharp decrease in porosity was observed for aggregates below 400μm in diameter. This porous nature of flocs results in a dramatic increase in the apparent volume of the solids in the mixture, and may be

responsible for the dramatic increase in yield stress of polymer flocculated mixtures observed in many studies[11,24,31,33]. Klein (2014)[35] flocculated dilute mature fine tailings (MFT) with Hychem AF246 (a high weight anionic acrylamide) with an overhead stirrer while monitoring size using FBRM and observed an initial increase in size during polymer addition, followed by a decrease in mean diameter to equilibrium after one hour.

The initial increase in floc size upon polymer injection, followed by a decrease to an equilibrium condition, can be explained as follows. As flocculation progresses, growth rates will eventually be slowed for two reasons - the existing flocs will be broken due to disruptive shear forces[92], and the collision efficiency decreases as particles become larger[93]. Floc breakage will be strongly dependent on the intensity of the shear and on the floc strength[94]. Flocs formed from high molecular mass bridging polymers tend to be stronger than those produced by charge neutralization or destabilization through inorganic salts[95]. Flocs formed by high molecular mass polymeric flocculants tend not to re-form when they are broken down, which may be the result of polymer chain scission or re-conformation of polymer at the particle surface[95]. On the other hand, flocs formed through charge neutralization seem to readily reform after breakage[95]. Hence it is expected in the present study that aggregates flocculated through charge neutralization may experience re-structuring of flocs in low shear environments resulting in higher equilibrium yield stresses.

One of the main goals of the present study is to determine the effect of floc breakage, and hence reduction in apparent volume, in the presence of anionic acrylamides (bridging polymers) on rheology. In addition, the ability of flocs produced through charge neutralization mechanisms to re-flocculate and their effect on rheology is also of importance in the present work.

2.4 Polymer flocculation of fine-particle suspensions

2.4.1 Polymer-particle interactions

Given that Leong et al. (1993)[69] and Kapur et al. (1997)[22] conclude that yield stress is correlated to the strength of inter-particle forces, the contribution from polymer flocculants must be considered when predicting rheology .Often in the presence of polymers, compliance with DLVO theory is not observed and additional forces must be considered. In addition Mpofu et al. (2003)[11] demonstrate that dramatic increases in rheology resulted from non-DLVO forces when kaolinite dispersions were mixed with poly(ethylene oxide) or high molecular mass anionic acrylamide[11]. Depending on the chemistry – pH and (polymer) additives – as well as the mineralogy of the dispersion a number of non-DLVO forces must be considered such as bridging, steric, hydrophobic, hydration, hydrodynamic and depletion forces[66]. Hence the total interaction including non-DLVO forces can be defined as:

$$V_{Tot} = V_{vdW} + V_{edl} + [V_{ster} + V_{dep} + V_{hydroph} + V_{bridge} + V_{hydro} + V_{hydra}] \quad (2.22)$$

For polymer-flocculated thickened tailings, bridging, steric, hydrophobic and hydrodynamic forces will be of particular importance.

Bridging forces result from a polymer chain adsorbing to the surface of particles, simultaneously binding them together through molecular bridges[11]. These forces arise from high molecular mass of polymers (large chain length) and a low coiling index in a particular liquid medium, resulting in an extended conformation capable of bonding to multiple particles[82,96,97]. In order for bridging to occur the polymer must be able to adsorb to the surface and may be inhibited my steric forces

Steric force defined by Biggs (1995)[98] is a repulsive force which arises from surface saturation of a particle. In the study, atomic force microscopy was used to quantify forces between zirconia particles and poly(acrylic acid). When the surface of a zirconia particle was saturated with poly(acrylic acid), the

force on an approaching poly(acrylic acid) polymer was repulsive. Steric forces will be important in the binding and attachment of polymers to the surface of kaolinite, as bulky or electrostatically repulsive groups can limit adsorption and lead to the formation of more open, loose and fragile flocs as noted by Mpofu et al. (2003)[11] when describing the structure of flocs produced by anionic acrylamides. Alagha et al. (2011)[99] witnessed a limited and reversible adsorption of Magnafloc® 1011 to alumina and silica sheets as a result of steric repulsions between acrylate pendant groups.

Hydrophobic forces arise in molecules or surfaces which lack hydrogen bonding acceptors, donors and polar groups and thus interact poorly with water[78]. As a result the water molecules near the surface become highly ordered which generate forces that are entropic in nature[78]. The range of these forces can be quite large and have been experimentally measured to be stronger and have longer range than typical van der Waals interactions but are still not well understood[78]. Rubio (1976)[100] described that attachment of poly(ethylene oxide) to silica arises from entropic effects from the displacement of water at the surface (hydrophobic force).

Hydrodynamic conditions will affect the structural properties and size of flocs[95,101] which will impact both settling and dewatering behaviour[102-104], as has been shown with anionic acrylamides mixed with kaolinite[104], as well as poly(ethylene oxide) flocculated smectite dispersions[105]. When kaolinite was flocculated with high molecular mass anionic acrylamides, the structures showed significant rupturing when subjected to moderate shear[11,31]. On the other hand when kaolinite dispersions were flocculated with poly(ethylene oxide), the flocs densified when subjected to moderate shear without rupturing[11,31].

Once adsorbed, it is not likely that polymer chains will reach an equilibrium conformation due to the constant collisions between polymer chains and particles during the flocculation process[95] and has been visually observed through scanning electron microscope (SEM) imaging through altered floc structures with increasing mixing time[11,31]. If the polymer adopts a flat conformation (e.g. cationic

acrylamides) it is likely it will not be able to bridge to other particles and may saturate the surface preventing further adsorption of polymer molecules[95]. Hence the mechanism of adsorption will be important in the re-structuring of flocs and will influence how flocs break and whether they can reform.

2.4.2 Effects of polymer type and chemical structure on rheology

The main types of flocculants that are applied in thickening operations are cationic and anionic acrylamides due to their high settling performance and relatively low cost[24]. High settling rates and good supernatant clarity are generally achieved through a combination of salt (e.g. Al^{3+}) and flocculant, the most common of which are high molecular mass polyacrylamides[106]. An appropriate flocculant for a particular application must be of the right molecular mass, charge density and must have a functional group present which will adsorb to the particle surface[33,82]. Anionic acrylamides are the most commonly used due to their superior settling rates, clearer supernatant and distinct sediment structures when compared to cationic acrylamides while also avoiding re-suspension of particles due to overdosing [24,33]. Anionic acrylamides contain roughly 65-90% (mol ratio) of non-ionic acrylamide sub-units with the remaining 10-35% commonly comprised of acrylates or 2-acrylamido 2-methylpropane sulphonate derivatives, as shown in Figure 2.7[11,24]. Molecular masses and charge densities of anionic acrylamides can vary depending on the character of the particles being flocculated. Also shown in Figure 2.7 is a basic cationic polymer structure (pDADMAC), composed of a quaternary amine derivative. The charge density can be reduced by polymerizing the subunit with non-ionic species. Lastly, a non-conventional polymer, poly(ethylene oxide) is shown. It is a homo-polymer composed of only ethylene oxide monomers. Poly(ethylene oxide) has gained attention due to its ability to rapidly flocculate clay suspensions and produce large robust flocs; however, due to its high cost, it has not gained widespread

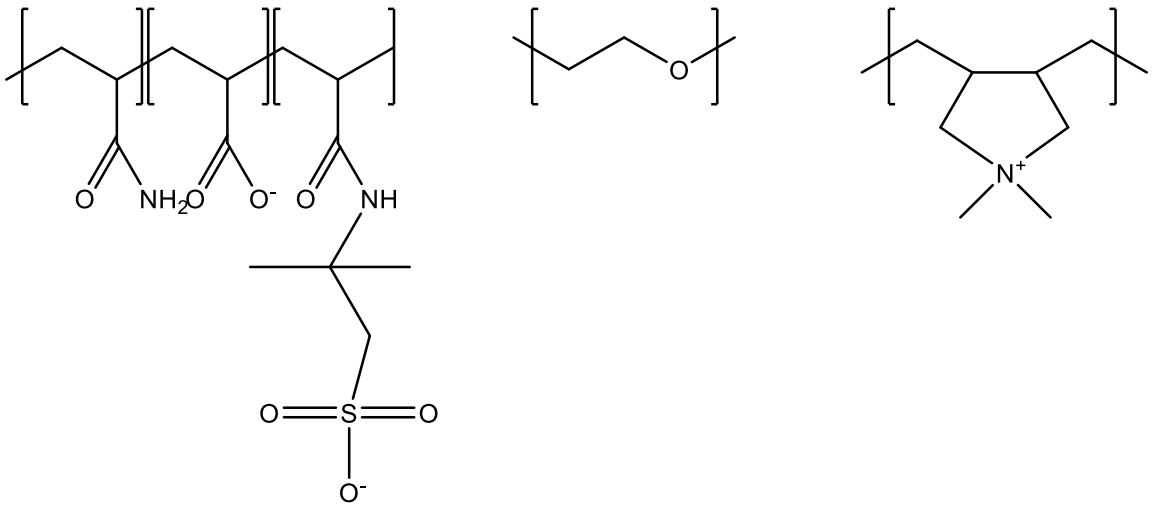

Figure 2.7: **(LEFT)** Common anionic acrylamide components – acrylamide, acrylate and 2-acrylamido 2-methylpropane sulphonate **(CENTRE)** Poly(ethylene oxide). **(RIGHT)** poly(DADMAC). Here subscripts 'n' and 'm' infer molar fractions

application[106]. Along with having different structures, these three polymer types produce distinctly different floc structures and suspension rheology.

Numerous studies[11,107,108] have demonstrated that the primary mechanism of flocculation with anionic acrylamides is through polymer bridging. The bridging mechanism requires that the polymer be of high enough molecular weight and of the right charge density to project itself past the electric double-layer, allowing it to come in contact with another particle. Adsorption to the surface of kaolinite occurs primarily through hydrogen bonding with aluminol and silanol groups and 94% of bonding occurs at the edge surface of the clay[109,110]; however, repulsions between negatively charged pendant groups and the surface results in limited polymer adsorption[11]. In addition, the interaction between negatively charged kaolinite surfaces and anionic pendant groups also influences the conformation at the surface, as electrostatic repulsions will repel charged components allowing the polymer to adopt a more extended conformation which will be beneficial to bridging[33].

For anionic acrylamides, the resulting sediment will have an augmented yield stress arising from bridging forces between particles. In a study from Mpofu et al. (2003)[11] kaolinite dispersions of 40% wt. at a pH 7.5, a strong correlation between flocculant dosage and yield stress is found. In a dose range of 150g/tonne to 1000g/tonne, yield stresses increased from 150 Pa to 300 Pa as the number of polymer bridges increased[11]. Adsorbed layer thickness was limited to 4nm as a result of electrostatic repulsions between adjacent polymer chains and negatively charged clay surfaces[11]. In a separate study, Nasser and James (2007)[24] demonstrated the effect of polymer size and charge on the compressive yield stress of flocculated kaolinite at neutral pH. They found that higher charge densities resulted in higher compressive yield stresses resulting from the increased number of polymer bridges, thus requiring more consolidating pressure than the more deformable, low charge density polymers. In the present study, two anionic acrylamides of different mass and charge density will be examined to determine if there will be any differences in time-dependency of the resulting suspension.

Cationic polymers produce flocculation through charge neutralization and charge-patch (dual-polymer) mechanisms. The basic principle behind the use of cationic polymers is to form small oppositely charged patches on the surface of the particle, which will form attractive forces with neighbouring anionic particles. Collision of the positively charged patch with the negative surface of another particle produces aggregation[111]. Flocs produced by cationic acrylamides are generally smaller and denser than those produced by anionic acrylamides due to the stronger inter-particle bonding[24,33]. Adsorption of cationic polymers occurs through hydrogen bonding with the amide functional group and electrostatic bonds on the negatively charged surfaces of the clays and positively charged quaternary amines– the electrostatic bonds are much stronger than hydrogen bonding seen in anionic acrylamides-particle interactions, and as a result will adopt a flat conformation on the surface which restricts the bridging mechanism[24,33]. Due to the overall negative charge of kaolinite particles at pH 8.5[27,78,80], the flat

conformation of adsorbed cationic polymers result in charge neutralization as the primary flocculation mechanism, whereas bridging will play little to no importance[24,33].

At pH 7, kaolinite dispersions flocculated with cationic acrylamide were able to achieve higher shear and compressive yield stresses when compared to anionic acrylamides of similar mass and charge density, because of the greater inter-particle bond strength produced from electrostatic attractive forces[24,25]. Zhou et al. (2009)[112] observed that polymer dose has an effect on yield stress, but is dependent on charge density. Charge densities of 10% displayed the highest dose dependence on yield stress, and this dependence decreased as charge density increased. Given that the maximum yield stress of flocculated fine particle suspensions is attained at an isoelectric point of zero[66,75,76], an augmented equilibrium yield stress is expected for well sheared suspensions flocculated with cationic polymer flocculants when compared to suspensions flocculated strictly by anionic acrylamides.

The study of Mpofu et al. (2003)[11] demonstrated the superior adsorption of poly(ethylene oxide) over anionic acrylamides to kaolinite at a pH of 7.5. Although poly(ethylene oxide) and anionic acrylamides adsorb to kaolinite particles through hydrogen bonding, anionic acrylamides have lower adsorption due to electrostatic repulsions between anionic pendant groups. Poly(ethylene oxide) had a much higher affinity for kaolinite surfaces and could form much thicker adsorbed layers, which drastically reduced surface potential with doses above 500g/tonne. The study demonstrated that the method of adsorption was primarily through hydrogen bonding between the ether oxygen of poly(ethylene oxide) and aluminol and silanol hydroxyl groups. Koskal et al. (1990)[113] suggested that entropic effects arising from the release of water from the surface of particles play a significant role in the attachment of poly(ethylene oxide). The mechanism of flocculation was determined by Mpofu et al. (2003)[11] to be through bridging at doses over 400g/tonne.

Poly(ethylene oxide) has a much stronger dose dependence on yield stress than acrylamides. For example, Mpofu et al. (2003)[11] studied 40% solids by mass kaolinite suspensions and found that yield stresses increased from 150 Pa to 750 Pa by increasing the poly(ethylene oxide) dose from 100g/tonne to 1000g/tonne. They also found that very dramatic changes occurred at dosages of approximately 500g/tonne, where yield stresses increased exponentially with dose. The dramatic increase in yield stress was found to have a strong correlation with decrease in magnitude of the zeta-potential (surface potential) to a near-zero value, resulting from the formation of a thick adsorbed layer reaching 14nm in thickness. At doses of 500g/tonne of poly(ethylene oxide) or more, it was found that non-DLVO forces had become dominant and were responsible for the dramatic increases in yield stress.

As described above, different polymer structures and types adsorb to particles through different mechanisms, producing specific floc structures and thereby influencing suspension rheology. The following Section discusses the shear dependence of polymer-flocculated dispersions. In particular, the change in yield stress of flocculated dispersions with shear energy input will be addressed, as well as the corresponding changes in floc structure.

2.4.3 Factors affecting rheology "reduction"

An early fundamental study on fine-particle suspensions by Pinder (1964)[114] demonstrated the relationship between thixotropy (time dependent decrease in rheology) and size reduction of a monodisperse system of particles. It was shown that size reduction was well correlated with a decrease in rheology. However, a decrease in particle size also results in an increase in surface area to volume ratio which should increase the importance of inter-particle surface forces and thus does not directly explain the reduction in rheology. The authors suggested that a change in structure was the reason for the decrease in rheology. The study did not examine other factors, such as the surface chemistry of the particles, differing size distributions, effects of bimodal distributions or the addition of flocculants to the

system. In addition, the data are not presented in a practical and reproducible form and are shown as a function of mixing time. Reporting changes as mixing time introduces issues, one of which being container/impeller size and shape. Additionally, the amount of shear imparted will vary with the rheology of the suspension, even when mixing times are identical. Due to the factors mentioned, it is more practical to report the results as a function of mixing energy for scaling purposes. Finally, the suspension rheology is determined with a concentric cylinder viscometer which can provide unreliable data if care is not taken to avoid, for example, wall slip. The present study expands on this previous work by correlating rheology changes with particle surface chemistry, water chemistry and the use of flocculants.

Fundamental studies on the response of anionic acrylamide flocculated dispersions to shear are limited and are restricted to yield stress measurements as a function of mixing time[11,31]. When a sediment produced by anionic acrylamides was subjected to moderate shear from an overhead stirrer, its yield stress decreased dramatically[31]. Images (obtained using SEM) showed that flocs were ruptured due to shear forces; however, no quantitative information with regards to changes in floc size and size distribution were obtained. The present study seeks to connect changes in rheology with changes in the size distributions of the flocculated suspensions.

The rheology of PEO-flocculated sediments is very dependent on shear forces both during flocculation and on flocculated sediment. Structurally, PEO is completely linear and there is freedom of rotation about any axis as all the carbon and oxygen atoms are sp^3-hybridized, resulting in a highly elastic structure when compared to acrylamides. This structure allows the polymer to re-conform more easily. Carboxylate and amide (COO^- and $CONH_2$ respectively) functional groups on acrylamides are sp^2-hybridized so there is no freedom to rotate about carbon-oxygen and/or carbon-nitrogen bonds due to electron delocalization[115], fixing them in a plane and making them somewhat 'bulky'. This structure gives

rise to steric effects[11] which may restrict bonding and/or re-conformation at the particle surface. Consequently, the elastic structure of PEO facilitates the formation of more robust flocs when compared to those formed by anionic acrylamides. One should expect that flocs produced using PEO will which re-structure and densify when subjected to moderate shear[11] rather than fragmenting. This capability may provide PEO-flocculated mixtures to continue to release water in high shear environments, thus allowing flocculation of high solids content suspensions. For examples, when PEO-flocculated kaolinite pulps were mixed for 10 minutes at 50RPM with an overhead stirrer, the pulps increased dramatically in density and yield stress[11,31]. For kaolinite pulp flocculated by a poly(ethylene oxide)/anionic acrylamide mixture, a similar result was also observed[31]. However, quantification of the effect of shear of poly(ethylene oxide) flocculated dispersions on rheology remains in question as the data are limited to qualitative mixing time rather than energy input. In addition, there is no study which examines the change in floc size and size distribution of poly(ethylene oxide) flocculated dispersions when subjected to shear.

Flocs produced by charge neutralization mechanisms became smaller and denser in response to shearing[116]. In addition higher polymer concentrations resulted in flocs which were more robust and stayed intact in higher shear rate ranges than flocs produced at lower doses[116]. Li et al. (2006)[117] showed that flocs produced by charge neutralization mechanisms fragmented more quickly in response to shear and produced smaller and denser flocs at steady state when compared to those produced by bridging mechanisms. The more rapid decrease in size and increase in density of flocs produced through charge neutralization mechanisms would suggest more rapid decrease in yield stress due to rapid reduction of apparent solids volume fraction. However, no study that compares the effects of shear on floc structure and rheology can be found in the literature.

Salinas et al. (2009)[18] tested the shear induced rheological degradation of anionic polymer flocculated tailings using a customized shearing apparatus with three different geometries. The results were independent of the geometry of the shearing apparatus and showed that rheological degradation was directly related to energy input. Complete shearing across the gap of the rheometers was identified by a well correlated power-law reduction in rheology as a function of shear energy. In addition, the characteristic power-law degradation curve was shown to be independent of flocculant type. However, it was assumed that chemical environment such as pH, flocculant type and dosage would affect the amount of energy to achieve equilibrium rheology, but was not tested. The independence of test results on geometry is the basis for the use of the concentric cylinder shearing apparatus in the present study.

Treinen et al. (2010)[16] investigated the effect of energy input on yield stress of anionic polymer flocculated tailings. A benchtop scale Haake Viscotester 550 with MV-II concentric cylinder geometry was used (2.6mm gap, 55mL volume) and their results were compared to the previous experiments of Salinas et al. (2009)[18], who used a more complex shearing apparatus. They concluded that rheology reduction could be studied using a benchtop scale concentric cylinder shearing apparatus, although the settling of coarse particles made equilibrium measurements unreliable. In the present study, a fine particle suspension is used to eliminate effects of coarse particle settling.

Gillies et al. (2012)[17] contined the study of energy induced rheological degradation, but did so with a pilot-scale 265mm pipeline. Flotation tailings from CNRL's Horizon oil sands operation were used as the feedstock and were diluted to 10% solids by mass. Tailings were flocculated using 200g/tonne of HyChem AF 309 (anionic acrylamide type polymer) and concentrated in a 1.5m FLSmidth deep cone thickener. Two batches were produced with varying fine-to-coarse solids ratios and in both cases it was observed that after approximately 1500kJ/m^3 of shear energy input, the mixture's vane yield stress could be reduced by half. Both batches experienced a power-law type yield stress degradation but had

completely different initial and final yield stresses. There was, however, no information regarding the chemical environment of the slurry such as pH, salt concentrations, size distribution of tailings and mineralogy.

The current literature on this topic is lacking in several aspects. There is no study which aims to find mechanisms of rheology reduction, and all of the studies are focused on either the effect of shear energy input on rheology flocculated tailings, or the qualitative effect of mixing and polymer selection on yield stress. In addition, it is well known that floc structures are highly dependent on hydrodynamic conditions and yet there is no study which pairs floc size (distribution) and vane yield stress data. It is therefore the focus of the present work to quantitatively determine the relationships among of polymer selection, mixture chemistry and particle size distribution on rheology as a function of mixing energy.

Chapter 3: Experimental Method

3.1 Introduction

In this chapter, technical information concerning the materials and equipment used in the experiments are described. The customized concentric cylinder shearing apparatus is described in detail as it is unique to this project. Section 3.4 lists all experimental procedures used in the Project. In order to achieve reproducible procedures, many preliminary tests were required in order to determine the proper rotational speed for vane rheometry, impeller speed during flocculation, flocculant dose, impeller speed and mixing time for kaolinite suspension, polymer solution preparation, rotational speed for the concentric cylinder shearing apparatus, and FBRM size measurement. Supplemental information regarding the experiments conducted to develop these reproducible procedures is included in Appendix D.

Due to the complicated and lengthy nature of the overall test procedure, a flow chart is shown in Figure 3.1 which outlines the steps involved to obtain a single data point. Each data point first required the preparation of a dilute model tailings at 8% by mass, which was concentrated to 41% by mass using a combination of polymer flocculant and customized drying apparatus. A sufficient volume of paste to fill the concentric cylinder shearing apparatus was produced and was divided into two portions – one which was used as a pre-shear or 'initial' measurement and the other portion was sheared in the concentric cylinder mixing apparatus. Vane yield stress and size measurements were performed on both the initial and sheared samples. The data obtained for the sheared samples were normalized so that size reduction and rheology reduction graphs could be compared.

Tailings samples obtained from Teck were tested for congruency with the model tailings samples. Due to differences in solids concentration and physical properties of the resulting paste, the

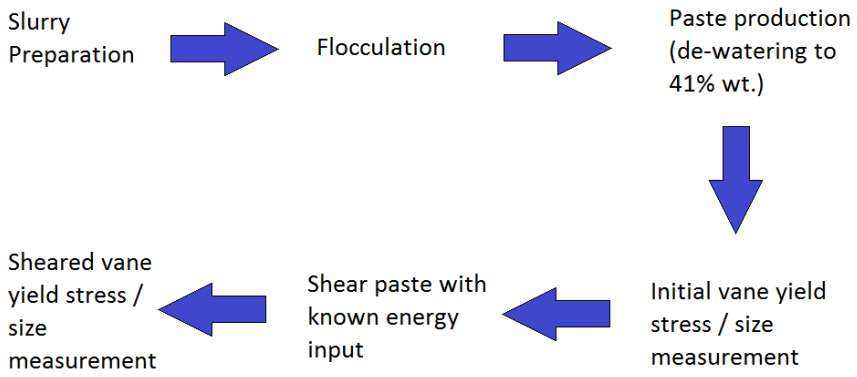

Figure 3.1: Flow chart of experimental procedure

test procedures were modified to ensure that the right amount of paste was produced, and that the paste was uniformly sheared in the concentric cylinder shearing apparatus.

In Table 3.1, a concise list of test conditions is summarized. The first three conditions listed were most heavily tested, as 30 samples were analyzed for each. In the table 'A-C-A' stands for 'anionic-cationic-anionic' and refers to a method of addition of a dual polymer system to a clay suspension. The method recommended by the Saskatchewan Research Council[118]. The last two conditions (Magnafloc® LT27AG at 100g/tonne and pH 7, Magnafloc® LT27AG + poly(ethylene oxide) 100g/tonne + 150g/tonne pH 8.5) were used to demonstrate the importance of particle surface chemistry and non-DLVO forces arising from poly(ethylene oxide) on time-dependent rheology of flocculated clay dispersion.

3.2 Materials

Kaolinite

Kaolinite was obtained from Kentucky Tennessee Clay Company, and supplied by Plainsman Pottery in Edmonton. The supplier reports an average particle diameter between 1 – 1.2µm. According to the SRC database[57], the average density of kaolinite is estimated to be 2696 kg/m^3.

Table 3.1: Conditions tested for size and rheology reduction using 41% by mass solids paste

Polymer flocculant	Dose (g/tonne)	pH	Energy input (kJ/m^3)
Magnafloc® LT27AG	100g/tonne	8.5	0 - 1200 kJ/m^3
Magnafloc® LT27AG + Hyperfloc CD650 (A-C-A)	65g/tonne – 85g/tonne – 35g/tonne	8.5	0 – 1200 kJ/m^3
Magnafloc® 1011	100g/tonne	8.5	0 - 1200 kJ/m^3
Magnafloc® LT27AG	100g/tonne	7	0 - 3000 kJ/m^3
Magnafloc® LT27AG + poly(ethylene oxide)	100g/tonne / 150g/tonne	8.5	0 – 7000 kJ/m^3

Polymers

Both anionic acrylamides were obtained through BASF/CIBA chemicals. The anionic acrylamides used in the study were Magnafloc® LT27AG, an 'ultra-high' molecular mass poly(acrylamide-co-acrylate) of medium charge density and Magnafloc® 1011, a very high molecular mass anionic acrylamide of 30% charge and unknown chemical composition. The cationic polymer used was Hyperfloc CD650 which is a pDADMAC derivative of unknown chemical composition and charge density. Poly(ethylene oxide), or 'PEO', was purchased through SigmaAldrich chemicals in the form of a fine white powder. The molecular mass average, M_V, of the PEO was 8,000,000.

Milli-Q water, KOH, KCl, HCl

De-ionized water was obtained from an in-lab Milli-Q water system. To ensure consistent water chemistry, all beakers used throughout the study were washed with detergent and tap water and rinsed

several times with de-ionized water to remove any remaining salts before being used. KOH pellets and KCl salt were purchased from EMD Millipore and J.T. Baker respectively.

Calibration standards

Calibration standards for the pH probe as well storage and cleaning solutions were purchased from Rice Engineering & Operating Ltd. Viscosity standards used for the concentric cylinder shearing apparatus and Haake Viscotester 550 were purchased through Cannon Instrument Company viscosity standard. The 'S60' viscosity standard was used to calibrate the concentric cylinder shearing apparatus.

3.3 Equipment

3.3.1 Concentric cylinder shear apparatus

The concentric cylinder shear apparatus constructed for this project is shown in Figure 3.2a, and a dimensional schematic of the mixing chamber is shown in Figure 3.2b. The apparatus consists of a Teflon spindle R_1=25mm with a glass cup R_2=29.5mm with a total height of L=385mm for a total volume of approximately 308$cm^{3.}$ The spindle torque, angular velocity and power were monitored using a 3-channel torque sensor that has a 5 N·m capacity and USB interface for live torque and angular velocity measurements (Burster GmbH model 8661-5005-V0110 purchased through A-Tech instruments Ltd). The mixer was powered by a belt-driven system consisting of an IKA Eurostar 60 digital mixer, with a custom built gear with 0.200" pitch and 17.26mm diameter, in-line with a 78mm diameter gear attached through a 27" fiber-glass timing belt (PowerGrip 236XL037).

3.3.2 Focused Beam Reflectance Measurement (FBRM)

A Mettler Toledo S400A FBRM probe was used to measure particle size within the paste. A solid state laser provides a continuous beam of monochromatic light (780nm wavelength) which rotates about a circular path at the interface of the probe lens and the particle dispersion. As particles pass by

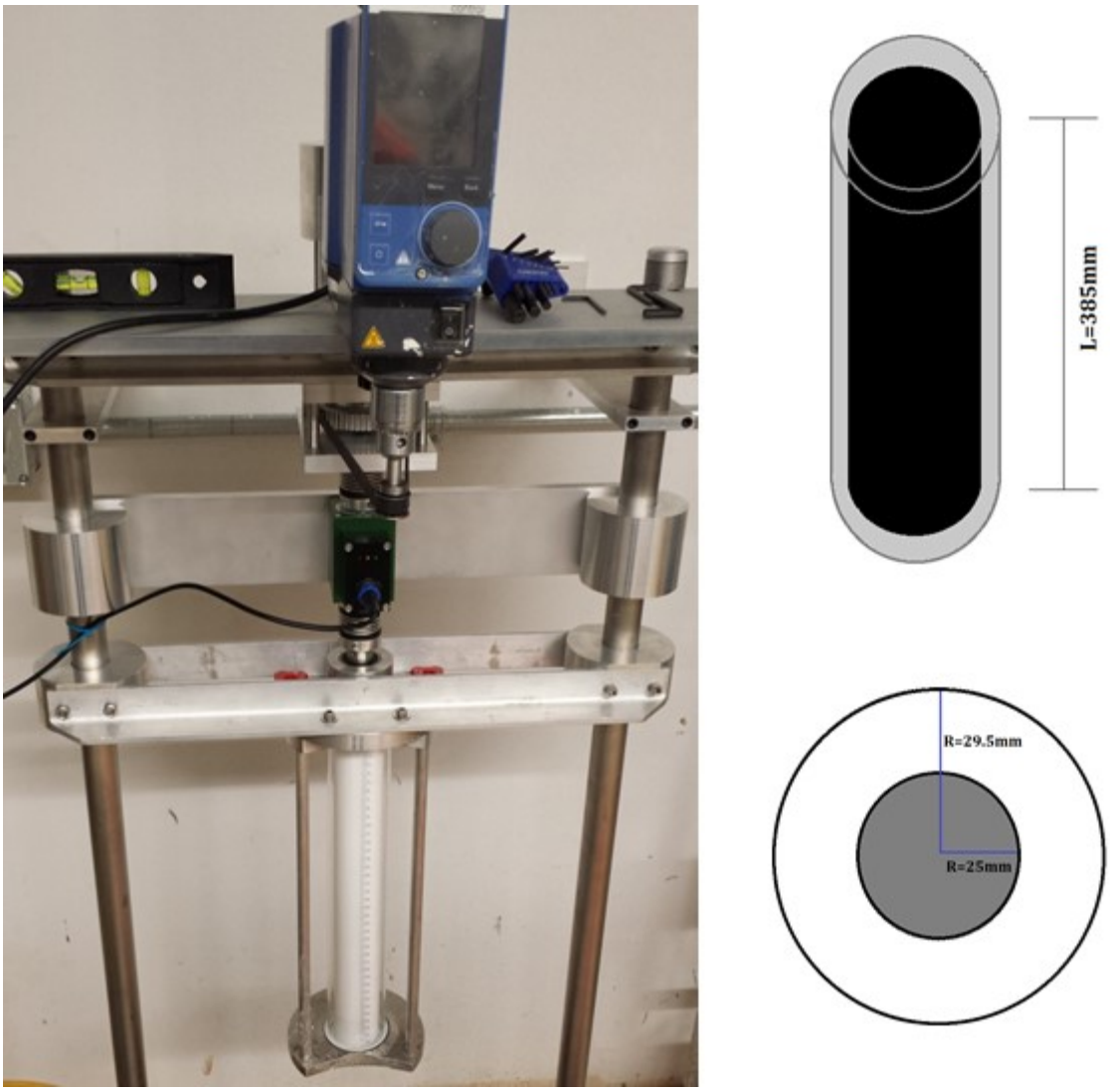

Figure 3.2: Concentric cylinder shearing apparatus

the probe tip, light is scattered back into the probe. The backscattered light is converted into a chord length using a simple calculation based on the scan speed multiplied by the pulse width (time). The chord length represents the length of the cross-section of the particle in question and does not provide a 'true' diameter for irregular shaped particles. The probe generally scans thousands of chord lengths in

a second to produce a chord distribution – analogous to a particle size distribution. The advantage of FBRM is that it allows the measurement of a large sample without visual observation of individual flocs.

In addition the amount of shear energy input into the system can be minimized through appropriate selection of solids concentration of the mixture and impeller speed of the mixing apparatus.

3.3.3 Haake Viscotester 550

All vane measurements were made with FL100 geometry on the Haake 550, as shown in Figure 3.3 (which includes a dimensional schematic). The vane has six blades with a diameter D=22mm and a blade height of H=16mm. Based on recommendations from Nguyen and Boger (1983)[55] requiring a mixture of twice the vane height and twice the vane diameter, the minimum volume required for a cylindrical container would be roughly 100cm^3:

$$V = \pi r^2 h = \pi(\tfrac{2D}{2})^2 2H = \pi\left(\tfrac{2*1.1cm}{2}\right)^2 (2 * 3.2cm) = 97cm^3 \quad (3.1)$$

Given the dimensions and volume, this criterion is satisfied with 300mL of sample.

An estimate of the Bingham yield stress of each paste produced was obtained with MV-III concentric cylinder geometry (R_1=15.2mm, R_2=21mm, L=60mm) attached to the Haake Viscotester 550. The experiments were conducted using a temperature control set to 20^{o}C. The purpose of these experiments was to be able to estimate what range of angular velocities was required to achieve the minimum torque required for complete shearing across the gap of the concentric cylinder shearing apparatus. The small sample size required for the MV-III concentric cylinder allowed many tests to be conducted on each batch of paste produced.

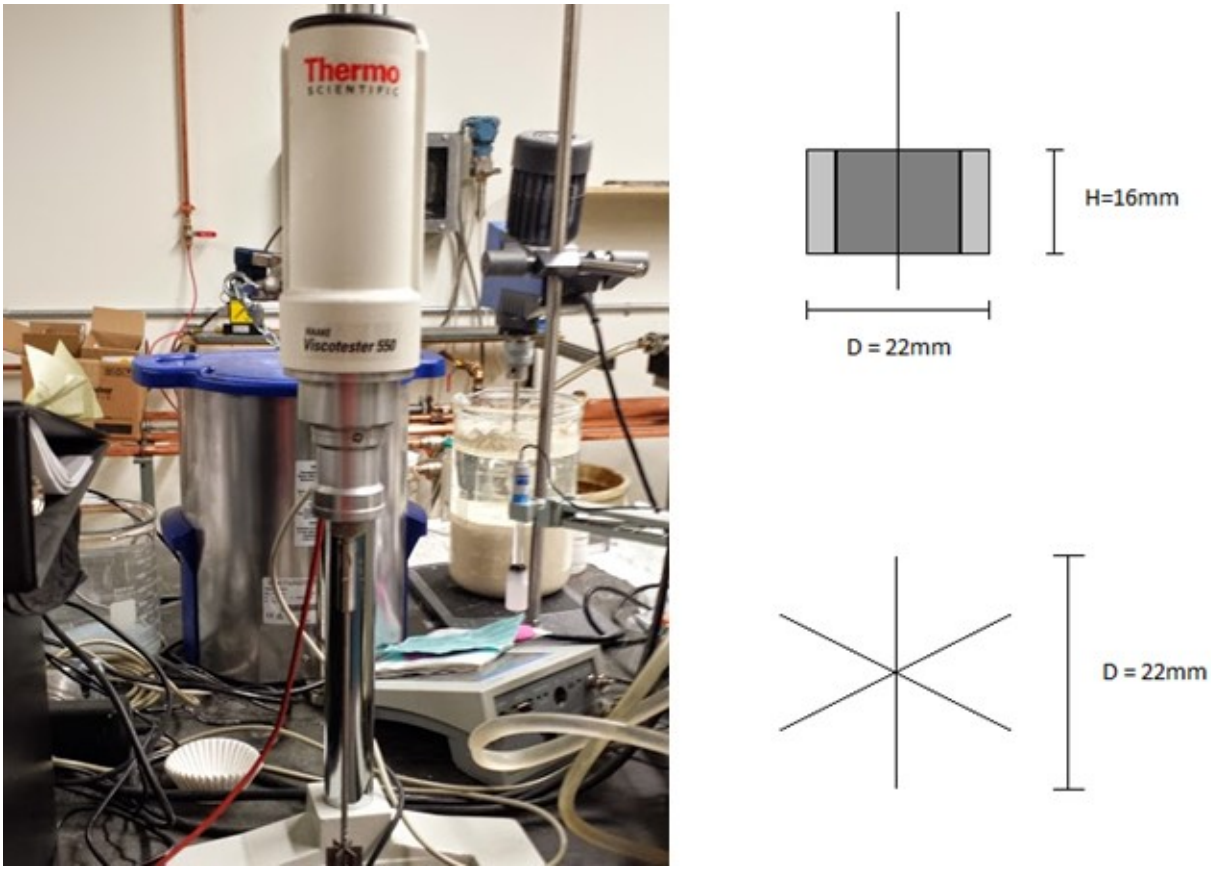

Figure 3.3: FL100 vane geometry attached to Haake 550 viscometer

3.3.4 pH measurements

pH measurements were conducted with a Mettler Toledo SevenMulti system using an InLab Expert Pro pH probe (shown in Figure 3.4). The pH probe was calibrated several times per week to ensure water chemistry was kept as consistent as possible. The probe was thoroughly cleaned weekly during use. Once the experimental procedures had been fully developed, a new probe was used to collect all data reported in this thesis.

Figure 3.4: pH probe used throughout all experiments

3.4 Procedures

3.4.1 Polymer solution preparation

Stock and feed solutions were prepared and kept in 100mL re-sealable glass beakers. The beakers were 7.5cm in diameter. The mixer used was an IKA Eurostar 60 overhead stirrer with a four-bladed impeller that was 5cm in diameter. Unlike a vane, the impellers are 45^{o} to the direction of rotation. Stock solutions of acrylamides (Magnafloc® LT27AG, Magnafloc® 1011 and HyChem CD 650) of 1% by mass were discarded after two days of used to ensure consistency. Mixtures containing poly(ethylene oxide) were produced daily and discarded at the end of the day.

Preparation of Magnafloc® LT27AG and Magnafloc® 1011 solutions

100mL of 1% by mass **stock** solutions were prepared via the following method:

1) 1.0g of solid polymer was placed in 100mL of de-ionized water

2) The impeller was placed in the centre of the beaker 3mm from the base

3) The solution was stirred at 60RPM for 12 hours

100mL of 0.1% by mass **feed** solutions were prepared daily via the following method:

1) 10mL of 1% by mass stock solution was combined with 90mL of deionized water

2) Impeller placed 1cm above the base of the glass beaker

3) Stirred at 200RPM for 30 minutes

Preparation of poly(ethylene oxide) solutions

320mL of 0.25% by mass solution

1) 80mL de-ionized water was combined with 0.80g of poly(ethylene oxide) powder

2) Impeller placed 3mm from the base of the beaker

3) Stirred at 150RPM for 30 minutes

4) 20mL of de-ionized water was added

5) Stirred at 150RPM for 5 hours

6) 220mL water added

7) Stirred at 300RPM for 1 minute

8) Impeller placed 3.5cm from base of beaker

9) Stirred at 150RPM for 4 hours

Mixtures were prepared daily and discarded after being used. Several other methods were attempted and are described in Appendix D. The most important conditions were beakers with rounded edges and proper impeller placement. Using an ice bath also aided in solubilisation as reported by many authors[119-121], but was not used out of simplicity in order to eliminate any temperature dependent effects during flocculation.

Preparation of poly(ethylene oxide) and Magnafloc® LT27AG solution

A solution of approximately 0.1% by mass Magnafloc® LT27AG and 0.15% by mass poly(ethylene oxide) was prepared in order to achieve doses of 100g/tonne and 150g/tonne respectively. The solution was prepared from 1% by mass Magnafloc® LT27AG solution and 0.25% by mass poly(ethylene oxide solution as follows:

1) 10mL of 1% by mass Magnafloc® LT27AG solution was added to 40mL of de-ionized water in the 7.5cm diameter beaker
2) The impeller was placed in the centre of the beaker 3mm from the base
3) The solution was stirred at 150RPM for one hour
4) 60mL of 0.25% by mass poly(ethylene oxide) solution was added
5) The impeller was placed 1 cm from the base
6) The solution was stirred at 150RPM for 1.5 hours

The poly(ethylene oxide) / Magnafloc® LT27AG solutions were prepared daily and discarded immediately after being used.

Preparation of HyChem CD 650 solutions

100mL of 1% by mass **stock** solutions were prepared via the following method:

1) 1.0g of solid polymer was placed in 100mL of de-ionized water
2) The impeller was placed in the centre of the beaker 3mm from the base
3) The solution was stirred at 100RPM for 1 hours

100mL of 0.1% by mass **feed** solutions were prepared daily via the following method:

1) 10mL of 1% by mass stock solution was combined with 90mL of deionized water

2) Impeller placed 1cm above the base of the glass beaker

3) Stirred at 100RPM for 1 hour

3.4.2 Kaolinite suspension preparation and Flocculation

The kaolinite suspensions of 8% by mass were prepared in 4L beakers (D=15cm, H=24cm). An overhead stirred with a four-bladed impeller of 5cm diameter was used to homogenize the suspension.

1) 3.5L of de-ionized water and 0.25g of KCl were combined in the 4L beaker
2) The impeller was placed 12cm from the base of the beaker
3) Approximately 310g of kaolinite powder was added to the beaker
4) The mixture was stirred at 1000RPM for 30 minutes to suspend the particles
5) pH was modified using KOH pellets and concentrated KOH solution

The kaolinite suspension was immediately dispensed into 500mL beakers to be flocculated.

<u>Flocculation of 8% by mass kaolinite suspension using Magnafloc® LT27AG and Magnafloc® 1011</u>

The flocculation was performed in 500mL beakers (500mL mark at 9cm) with a 5cm diameter four-bladed impeller. The suspension was stirred at 350RPM throughout the flocculation process, and mixing times were optimized using FBRM and the data are shown in Appendix D.

1) The impeller was placed 6cm from the base of the beaker
2) The suspension was stirred at 350RPM
3) 100g/tonne of polymer was dispensed as 0.1% by mass solution was dispensed over 40 seconds
4) Stirring continued for 20 seconds after polymer addition
5) The impeller was stopped
6) Flocculated suspension was gently poured into 500mL stoppered graduated cylinder

7) The 500mL stoppered graduated cylinder was inverted twice and left to settle
8) Initial settling rate (ISR) was determined based on the time required for the mudline to travel from the 450mL mark to the 350mL mark (5.5cm)

The dose used in all experiments for anionic acrylamides was selected based on a peak in dose efficiency on initial settling rates (ISR) at 100g/tonne, shown in Figure 3.5. Doses beyond 100g/tonne of polymer resulted in minimal increases in yield stress and supernatant clarity. The dose was also not increased beyond 100g/tonne to avoid local overdosing of polymer to the kaolinite particle surfaces which can result in poor floc formation. The procedure produced large (confirmed by FBRM in Appendix D), fast-settling flocs.

Flocculation of 8% by mass kaolinite suspension using A-C-A (Magnafloc® LT27AG and HyChem CD 650)

The flocculation was performed in 500mL beakers (500mL mark at 9cm) with a 5cm diameter four-bladed impeller. The suspension was stirred at 350RPM throughout the flocculation process, and mixing times were optimized using FBRM and the data are shown in Appendix D. In order to compare effects between a strictly anionic flocculated mixture and a dual-polymer system 'A-C-A' (anionic-cationic-anionic), 100g/tonne of Magnafloc® LT27AG was used in addition to 85g/tonne of Hyperfloc CD 650.

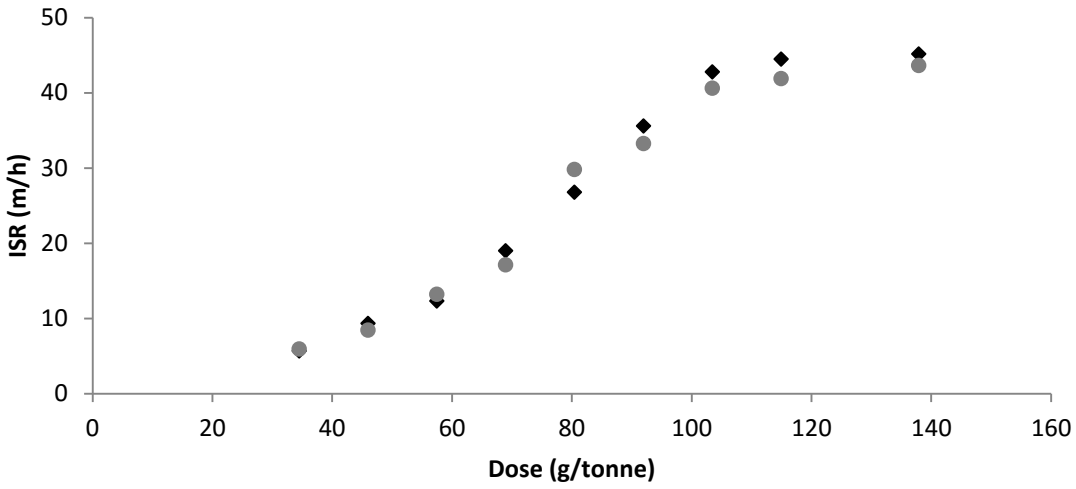

Figure 3.5: Initial settling rate (ISR) versus dose dependence of pH 8.5 kaolinite suspension flocculated with Magnafloc® LT27AG (●) and Magnafloc® 1011 (◆)

For the A-C-A system, the mixing protocol is as follows:

1) The impeller was placed 6cm from the base of the beaker
2) The suspension was stirred at 350RPM
3) 65g/tonne of Magnafloc® LT27AG was dispensed as 0.1% by mass solution was dispensed over 30 seconds
4) Stirring continued for 10 seconds after polymer addition
5) 85g/tonne of 0.1% by mass solution of HyChem CD650 was dispensed over 40 seconds
6) Stirring continued for 10 seconds after polymer addition
7) 35g/tonne of Magnafloc® LT27AG was dispensed as 0.1% by mass solution was dispensed over 20 seconds
8) Stirring continued for 10 seconds after polymer addition
9) The impeller was stopped
10) Flocculated suspension was gently poured into 500mL stoppered graduated cylinder

11) The 500mL stoppered graduated cylinder was inverted twice and left to settle

A list of other combinations (sequence of addition, doses, stirring times) is shown in Appendix D. The optimal dose for the A-C-A system was selected based on sediment height, supernatant quality, and ease of collection. When too much cationic polymer was used, the flocs would adhere to the walls of the glass due to the negative surface charge of glass (silica)[122] at the pH of the mixture (pH 8.5). Also included in Appendix D are other cationic polymers considered for the present study.

Flocculation of 8% by mass kaolinite suspension using poly(ethylene oxide) and Magnafloc® LT27AG/Poly(ethylene oxide)

Consistent settling behaviour with poly(ethylene oxide) could not be achieved and will be discussed in section 4.6. To obtain consistency and compare effects of poly(ethylene oxide) to conventional acrylamides, a solution containing approximately 0.1% by mass Magnafloc® LT27AG and 0.15% by mass poly(ethylene oxide) was prepared.

1) The impeller was placed 6cm from the base of the beaker
2) The suspension was stirred at 450RPM
3) 100g/tonne Magnafloc® LT27AG and 150g/tonne poly(ethylene oxide) was dispensed as 0.1% by mass solution was dispensed over 40 seconds
4) Stirring continued for 30 seconds after polymer addition
5) The impeller was stopped
6) Flocculated suspension was gently poured into 500mL stoppered graduated cylinder
7) The 500mL stoppered graduated cylinder was inverted twice and left to settle

Higher RPM was required to dispense the significantly more viscous polymer solution. Lower doses of poly(ethylene oxide) showed little to no effect on settling, whereas higher doses gave increasingly unpredictable behaviour (see Appendix Figure A.1).

3.4.3 Sediment preparation

After the kaolinite suspension had been flocculated and left to settle in the 500mL graduated cylinders for 30 minutes, the supernatant was decanted and the sediment was gently poured onto filter paper covering a 1mm stainless steel strainer (D=20.5cm, H=8.5cm) that was placed within large ceramic Buchner funnel (D=20cm, H = 6.5cm), as shown in Figure 3.6. The paste was left to dry to remove excess water and obtain a paste-like consistency. Drying times of approximately 90 minutes were required for the paste to achieve a consistent density in all conditions. After the designated drying time, the paste was gently scooped using a large spoon into two separate beakers. Each beaker contained roughly 310mL of paste and were used to produce an 'un-sheared/initial' and 'sheared' sample such that yield stress and size reduction graphs could be normalized. Normalization of yield stress and size reduction graphs was essential for two reasons. The variability in initial yield stress and mean chord length, and hence that of a sheared sample at a particular energy input, would result in graphs which are not well correlated. Thus normalization provides much more distinct correlations. Secondly, in order to compare size reduction and yield stress, the graphs were required to be normalized.

Figure 3.6: Filter paper in 1mm stainless steel within a large Buchner funnel used for paste densification

3.4.4 Density estimation

To achieve a reasonably accurate estimate of paste solids content, 500mL of paste was sheared at 2000 RPM using an overhead stirrer with a four-bladed 5cm diameter impeller for five minutes for acrylamides, and 10 minutes for PEO-flocculated mixtures to destroy the floc structure and reduce yield stress. A 100mL sample of the paste was then poured into a 500mL Erlenmeyer flask and placed under vacuum using an aspirator type vacuum pump for ten minutes to remove air bubbles that were entrapped during mixing. Using a 5mL syringe, 5mL increments of the sheared paste were transferred to a beaker on scale accurate to 0.001g. The mass of ten samples was recorded, and three batches were produced to ensure reproducibility (30 measurements total). The same 5mL syringe was used for all measurements. A consistent solids content of approximately 40-43% solids by mass and volume

concentration of 20-22% was achieved for all conditions. The data are shown in Table 3.2 and the full data set from all samples can be found in Appendix A. Density of Magnafloc® LT27AG + poly(ethylene oxide) flocculated pastes were not calculated due to relatively (relative to acrylamide flocculated suspensions) inconsistent behaviour.

3.4.5 Paste shearing protocols

The spindle angular velocity required for complete shearing across the gap of the concentric cylinder shearing apparatus was determined experimentally since there was no way to accurately measure Bingham yield stress or plastic viscosity due to the time- and shear-dependency of each sample. Estimation of the minimum required torque for complete shearing across the gap was first estimated using a benchtop rheometer. A concentric cylinder MV-III geometry was used (R_2=21mm and L=60mm) and an example is shown:

1) First 600mL of flocculated dispersion of 41% by mass was produced

2) Approximately 70mL of the flocculated dispersion was placed in the benchtop rheometer and sheared at a given angular velocity

3) The resulting apparent torque versus time curve was fitted as a power-law function on Excel

4) If the R^2 = 0.99 complete shearing had occurred, as noted in Treinen et al. (2010)[16] and Salinas et al. (2009)[18]

5) If R^2<0.99, incomplete shearing across the gap occurred

6) The next 70mL sample was sheared at a higher spindle angular velocity until an R^2=>0.99 was achieved

7) When a sample with R^2=0.99 was achieved, the peak torque value was taken from this graph, and an example is shown in Figure 3.7

8) In the case of the curve in Figure 3.7, the maximum torque was T=0.021580 N·m

9) The torque value from **Step 8** is used at the minimum torque to obtain complete shearing across the gap in Equation 2.2

10) Substituting L=60mm, R_2=21mm and T_{min}=0.021580 N·m into Equation 2.2, we have:

$$\tau_B = \frac{T_{min}}{2\pi L {R_2}^2} = 130\ Pa$$

11) We use the estimated Bingham yield stress from **Step 10** (τ_B = 130 Pa), along with the dimensions of the concentric cylinder shearing apparatus (L=385mm, R_2=29.5mm), to estimate the minimum torque for complete shear in the concentric cylinder shearing apparatus using Equation 2.2

$$T_{min} = 2\pi L {R_2}^2 \tau_B = 0.27\ N\ m$$

The estimation of the torque required to achieve complete shear across the gap is necessary because achieving an R^2 = 0.99 was quite difficult using the concentric cylinder shearing apparatus. Using this method, numerous samples were attempted at increasing spindle angular velocities (on the concentric cylinder shearing apparatus) until peak torque values greater than 0.27 N·m were attained. This procedure resulted in concentric cylinder spindle angular velocities of 117 RPM. An example of a trial is shown in Figure 3.8, and a peak torque greater than 0.30 N·m is observed. The initial peak 3 seconds into the experiment at 0.45 N·m is a result of the torque required to accelerate the spindle to the desired angular velocity.

Table 3.2: Summary of paste densities and volume fractions

Condition	Weight percentage (%)	Volume fraction (C_s/C_{total})
Magnafloc® LT27AG	42	0.21
Magnafloc® 1011	41	0.21
A-C-A	40	0.20
Magnafloc® LT27AG pH 7	43	0.22

For each condition, 30 samples were produced and characterized. Energy input was calculated using:

$$E = \frac{1}{\pi\left({R_2}^2-{R_1}^2\right)L}\int_{t=0}^{t=t1}(\omega T - k)dt = \frac{1}{\pi\left({R_2}^2-{R_1}^2\right)L}\int_{t=0}^{t=t1}(P - k)dt \quad (3.2)$$

$$= 3371m^{-3}\int_{t=0}^{t=t1}(P - k)dt$$

where R_2 and R_1 are the outer and inner radii of the concentric cylinder, L is the length of the spindle, ω is angular velocity (rad·s^{-1}), T is torque (N·m), P is power (J·s^{-1}) and k is the mechanical energy loss (J·s^{-1}). A range of 10 seconds to 10 minutes of shearing time was used to test a broad range of energy input values, and a matrix is provided in Table 3.3 and provides the exact time of shearing for the 30 samples. Of note is that most of the shearing times for the 30 samples are below 2 minutes in length and this is due to the fact that initially the energy input is very high until yield stress has decayed.

The time integral of power was calculated using a Riemann sum given the very small step sizes resulting from the fast data accumulation rate of 20 data points/second. Riemann sums involve taking the sum of a large number of trapezoids:

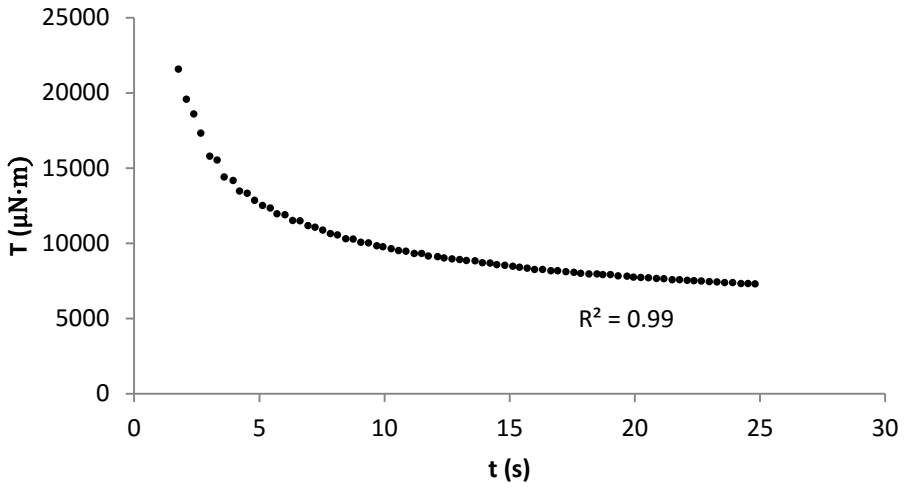

Figure 3.7: Torque reduction trace 41% by mass paste flocculated with Magnafloc® LT27AG sheared in concentric cylinder MV-III geometry at 20 rad/s

$$E = \sum_{m=1}^{n} \frac{(P(t_m) + P(t_m + dt))}{2} dt$$

where 'P' is the power at time 't_m', there are an 'n' number of data points, and 'dt' is the time between each data point (0.05s, since there are 20 data points/second).

3.4.6 Vane rheometry

For all polymer flocculated dispersions, the vane was rotated at very low angular velocity (0.0075 rad/s) for 450 seconds. The maximum torque was generally attained at the 100 second mark, and equilibrium was generally attained after 150-200 seconds.

Normalization of yield stress graphs were essential for two reasons. The variability in initial yield stress, and hence that of a sheared sample at a particular energy input, would result in graphs which are not well correlated. Thus normalization provides much a more distinct correlation. Secondly, in order to

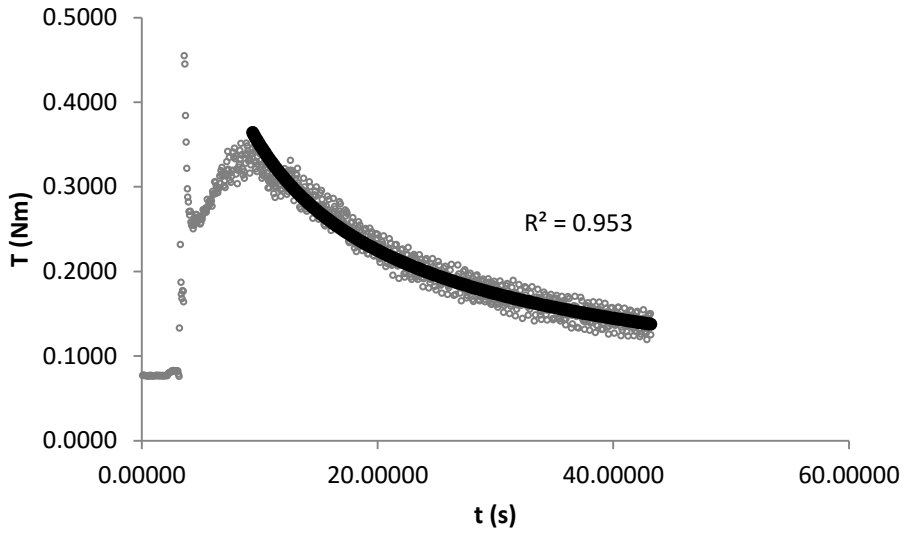

Figure 3.8: 41% by mass paste flocculated with Magnafloc® LT27AG sheared at 500RPM (motor speed) in the concentric cylinder shearing apparatus

compare size reduction and yield stress, the graphs were required to be normalized. In order to normalize the yield stress, vane rheometry tests conducted on sheared samples were normalized using with a pre-shear sample, made from the same 620mL batch of paste.

For pre-shear (or 'initial') vane yield stress measurements, approximately 310mL of paste was gently placed in the cup of the concentric cylinder shearing apparatus (Figure 3.2). The cup was slowly moved into place over a period of 18 seconds and then slowly removed over a period of 18 seconds. The sample was gently poured into a 300mL beaker and three initial vane yield stress measurements were taken. The vane placement was staggered such that each measurement was taken on an undisturbed portion of the sample, shown in Figure 3.9. Placement of the vane often introduced lateral movements which disturbed the sample in the area in which the vane was placed. In addition, the paste was not completely homogenous and hence staggering of the vane provided an average yield stress which was representative of the entire sample.

Table 3.3: Matrix of shearing times for the three most heavily studied conditions (pH 8.5: Magnafloc® LT27AG, Magnafloc® 1011, A-C-A)

Sample number	Time (mm:ss)*
1	10:00
2	7:00
3	5:00
4	3:00
5	2:00
6	1:35
7	1:20
8	1:10
9	1:03
10	0:59
11	0:55
12	0:51
13	0:47
14	0:45
15	0:41
16	0:37
17	0:33
18	0:31
19	0:30
20	0:27
21	0:24
22	0:21
23	0:18
24	0:15
25	0:13
26	0:12
27	0:11
28	0:10
29	0:09
30	0:08

*Time measured from 00:10 to 10:00 (mm:ss)

The post-shear measurement was acquired after shearing of the remaining paste (the other half of the original sample). The sample loading and removal steps were conducted following the same procedure described previously for the initial 'pre-shear' measurement. No temperature control is required during vane yield stress measurements as the amount of heat being generated can be neglected. The peak torque value defined in Figure 2.3 (Section 2.2.3) was used to calculate the suspension yield stress.

3.4.7 FBRM

Dilution of the paste was required in order to make reproducible size measurements. Probe tip fouling was very common in high solids content pastes and did not provide reproducible size measurements. In addition, mixing of concentrated pastes added shear energy due to the high yield stresses of the material. A complete review of the methods attempted in developing a FBRM procedure is shown in Appendix C. Dilution of the concentrated paste to 8% by mass solids was necessary for two reasons. First, as noted above, dilution was required to obtain consistent size measurements without probe tip fouling and minimal energy input into the sample. Additionally dilution of the paste to 8% by mass allowed direct comparison with the dilute suspension produced prior to addition of polymer flocculant.

In a 500mL beaker, 420mL of de-ionized water at a pH 8.5 was stirred at 350 RPM. Once data acquisition began, one large spoonful of paste (~80mL) from a sample was gently poured into the beaker with continuous stirring. The protocol was set for the maximum data-rate acquisition of $0.5s^{-1}$ and the shortest period of time (30 minutes). The overhead stirrer was set to 350RPM for acrylamide-flocculated kaolinite and 450RPM in the case of PEO-flocculated kaolinite for the duration of the experiment. Particle chord length, CL (μm), was selected from the first equilibrium value which was attained when dCL/dt of the Sauter mean chord length reaches an equilibrium value, as shown in Figure 3.10.

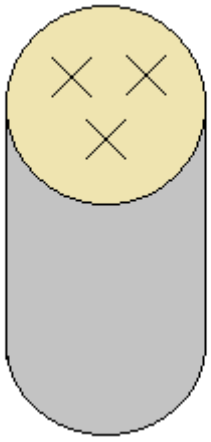

Figure 3.9: Staggered vane placement in 300mL paste sample

The derivative is calculated with respect to subsequent measurements in time (e.g. $\frac{dCL}{dt} = \frac{CL(2)-CL(1)}{t_2-t_1}$). The initial spike occurs when paste is initially mixed into the stirring beaker of water. The subsequent negative spike arises from the mixture being homogenized, as initially larger particles settled more quickly. The equilibrium was defined as the first point after which dCL/dt > -3 which provided reproducible results. Statistical analysis, shown in Appendix B, showed that dCL/dt reached a steady state for all samples once dCL/dt > -3. The average particle diameter used in the statistical analysis was the Sauter mean diameter (Equation 2.2). A full statistical analysis with regards to the effect of dilution is in Appendix C and the validity of the 'paste-drop' method is included in Appendix B.

3.5 Tailings samples

3.5.1 Stock mixture preparation

Tailings were supplied by APEX Engineering and were obtained from a batch extraction of oil sands ore taken from a Teck Mine site. The tailings were roughly 15% by mass with a pH of 7.9. The remaining tailings data (e.g. salt concentrations, initial particle size distribution, bitumen content, etc.) is shown in the Appendix A. In order to remove effects from coarse particles, the tailings sample (16L, 15%

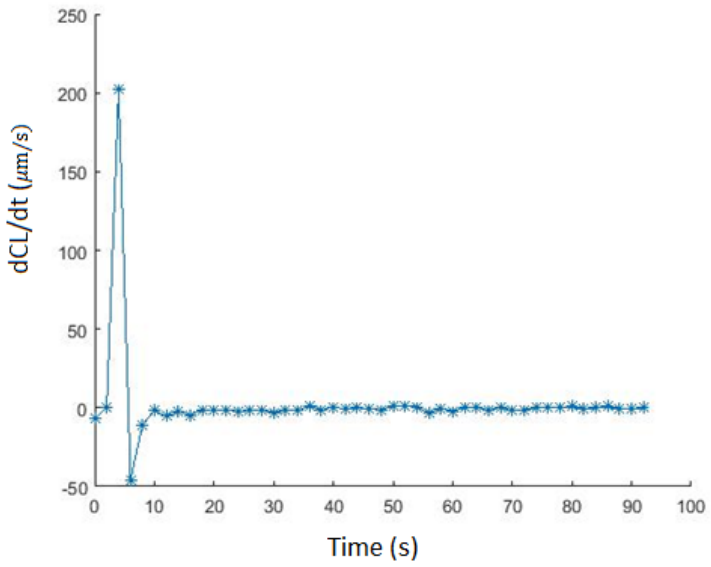

Figure 3.10: dCL/dt 'paste-drop' experimental method using FBRM. Measurement is conducted at 8% by mass diluted from 41% by mass

by mass) was first stirred at 250RPM for one hour with a large three bladed impeller approximately 13cm in diameter in a large vessel of 36cm diameter. The well dispersed tailings sample was then passed through a 300µm sieve on recommendation[123] that using a smaller sieve size would result in a large number of clay particles not passing through and filtration time could take many hours. The 16L sample was used as a stock mixture for flocculation.

3.5.2 Flocculation Procedure

The stock 15% by mass tailings suspension was kept in a 36cm diameter vessel, and was stirred in this vessel to disperse/homogenize the suspension prior to sampling. The stock mixture was stirred for 30 minutes at 250RPM using a 13cm diameter three-bladed impeller in a the 36cm diameter vessel. The blades of the impeller are at a 45^{o} angle to the base of the vessel and each blade is of a triangular

shape. While stirring, four 500mL samples were drawn from the stirring 15% by mass tailings suspension using four 500mL beakers. The 500mL samples were flocculated using A-C-A (Magnafloc® LT27AG + Hychem Hyperfloc CD650) at 400RPM through the following procedure. Doses are based on the estimated weight percentage of solids and are not exact.

1) The impeller was placed 6cm from the base of the beaker
2) The suspension was stirred at 400RPM
3) 170g/tonne* of Magnafloc® LT27AG was dispensed as 0.1% by mass solution was dispensed over 50 seconds
4) Stirring continued for 10 seconds after polymer addition
5) 130g/tonne* of HyChem Hyperfloc CD650 was dispensed as 0.1% by mass solution was dispensed over 40 seconds
6) Stirring continued for 10 seconds after polymer addition
7) 130g/tonne* of Magnafloc® LT27AG was dispensed as 0.1% by mass solution was dispensed over 40 seconds
8) Stirring continued for 10 seconds after polymer addition
9) The impeller was stopped
10) Flocculated suspension was gently poured into 500mL stoppered graduated cylinder
11) The 500mL stoppered graduated cylinder was inverted twice and left to settle

3.5.2 Sediment preparation and shearing protocol

The sediment was dried using the procedure described in **Section 3.3** using the same drying apparatus, drying times, etc. Density data was not obtained due to lack of available sample. Hence experiments on tailings samples are used to validate the experimental concepts and results described in the Section 4.7.

Determining the shearing protocol was more complicated due to lack of available sample. It was determined experimentally by gradually increasing the spindle angular velocity on samples until a steady power-law decay was observed and visual observation of the concentrated paste being sheared in the concentric cylinder shearing apparatus. The method demonstrated in the detailed example of **Section 3.4.5** (which will not be re-stated due to the length) could not be used due to the lack of available sample and significant wall slip effects.

Optimizing flocculation required the use of four samples (8L out of 16L) leaving very little remaining stock tailings to study Finally, a spindle speed of 350RPM was used for the tailings experiment. Complete shear was estimated though visual observation and power-law decay of the torque response of the concentric cylinder shearing apparatus. However, a strict power-law decay could not be confirmed (R^2=0.99) as a result of instrument noise due to vibrations at such high spindle angular velocity. To ensure uniform shearing of the flocculated tailings, the concentric cylinder shearing apparatus was set to 10 minutes of shearing. After significant shear-induced rheology reduction of the flocculated tailings, complete shear could be visually observed. The contributing factors to the significant wall-slip are discussed in Section 4.7.

Chapter 4: Results and Discussion

4.1 Introduction

In this chapter, tests to investigate the effect of shear energy input on polymer-flocculated kaolinite suspensions are reported. A limited data set for real, industrial tailings is also presented. Before the effects of shear energy are discussed, however, the initial properties – namely yield stress and particle size – of kaolinite dispersions prior to shearing will be discussed. A comparison of the initial properties for the five conditions tested here (see Table 4.1) will be made. The comparison will show that differences in both particle size and yield stress were related to both flocculant type and suspension pH.

After the initial paste properties have been displayed, the five main conditions will be discussed in order of increasing complexity. First, anionic acrylamides at pH 8.5 are discussed together as the results for the two polymers tested are very similar in both rheology and size reduction. The main mechanism is a reduced apparent volume through floc breakage and densification. Next, the addition of cationic flocculant in dual-flocculation at pH 8.5 is compared to the case of single polymer (anionic acrylamide) flocculation. The comparison shows that yield stress and particle size reduction occur more rapidly. Furthermore, the flocs in dual-polymer flocculation show a slight recovery after long mixing times in low shear environments. These results can be explained by differences in floc structure arising from the cationic polymer. Next, dispersions flocculated with anionic acrylamides at pH 7 and pH 8.5 are compared. The initial rate of yield stress reduction was nearly identical at both pH values and was caused by a reduction of apparent solids fraction in both cases. However, as the pH was lowered from 8.5 to 7, the equilibrium yield stress was raised quite substantially, by a factor of approximately 3. Finally, the effects non-conventional PEO are introduced and compared to the previous conditions. In the presence of 150g/tonne of PEO, flocs continued to flocculate in a thickened mixture even up to 1000

kJ/m^3 of shear energy input and was the only condition where average particle size increased with shearing. In addition, high yield stresses were measured even at high energy inputs.

Real tailings were also studied and the results are interpreted using knowledge from the kaolinite suspension experiments listed above. The tailings were flocculated using A-C-A and the equilibrium (well-sheared) yield stress was slightly higher than that measured for the model tailings A-C-A experiment. The higher equilibrium (well-sheared) yield stress was expected considering the pH was lower for the real tailings. Interesting differences in the evolution of size distribution indicate there may be effects related to gap width which will need further investigation.

The real industrial tailings had a much broader size distribution when dosed with polymer flocculants, and a substantial amount of flocs in the size range of 1-10μm were produced. The flocs in the 1-10μm size range grew when a large amount of shear energy was added to the system; after approximately 7000kJ/m^3 there were almost no particles of this size range remaining. This phenomena was not observed with model tailings. In addition, the chord length distribution was nearly identical for all tailings samples (model and industrial tailings).

4.2 Paste properties before shearing

A sample torque versus time graph is provided in Figure 4.1 taken from a Magnafloc® LT27AG flocculated paste at 41% wt. The peak torque can clearly be seen at approximately 100 seconds after which an equilibrium torque is established. The form of the torque versus time curve shown in Figure 4.1 was observed for all conditions tested here. It was found that the time at which peak torque appeared was dependent on the angular velocity, but did not seem to impact the magnitude of the torque. Samples containing PEO could not be studied at lower angular velocity as the torque would reach a plateau rather than a peak, and did not decrease thereafter. The remaining peak torque values, yield stresses, and several characteristic torque versus time curves can be found in Appendix A.

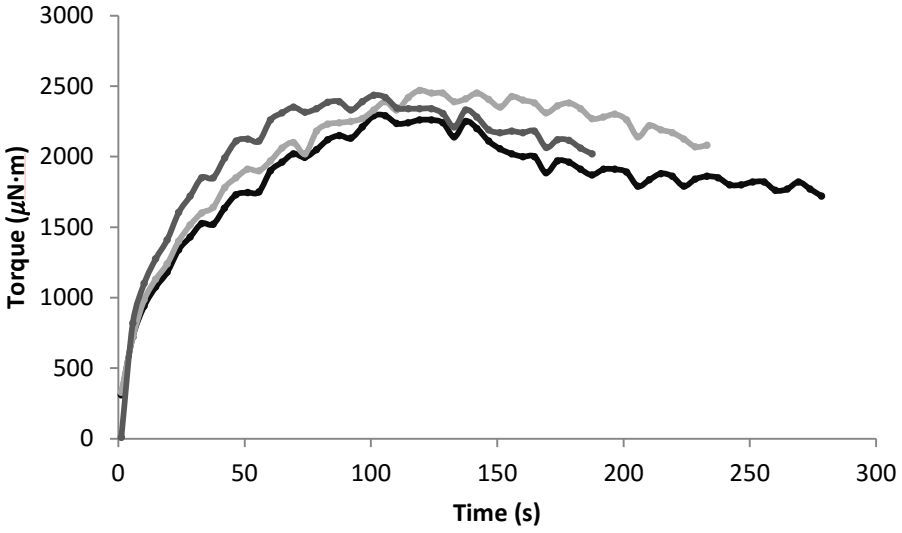

Figure 4.1: Torque versus time traces of vane yield stress experiment of a kaolinite suspension flocculated with Magnafloc® LT27AG

Particle mean diameters (d[3,2] and d[3,0]) were calculated using Equation 2.1 and 2.2 with the raw data provided from the FBRM software, which provides number counts over a chord length range of 1-1000μm. The Sauter mean diameter, d[3,2], was selected to optimize flocculation as it tracks the change in floc size with time and/or shear energy input. Additionally, d[3,2] was used in statistical analysis of the 'paste-drop' method because it was more sensitive to floc size. In the 'paste-drop' method, the true particle size distribution was obtained after homogenization of the mixture which required suspension of larger particles. The d[3,2] was more sensitive to larger particles and thus was used to track homogenization. The number volume mean, d[3,0], more efficiently tracks the fragmentation of flocs. The number based distributions provided by the software were converted to a volume based distribution by multiplying each number count by the cube of the corresponding chord length to produce a volume distribution. The volumes were then divided by the bin sizes to produce a

differential frequency distribution. An initial chord length distribution for a kaolinite suspension flocculated with Magnafloc® LT27AG is shown in Figure 4.2. The chord length distributions are initially mono-modal and the majority of particles are greater than 100μm in size. Chord length distributions will be discussed in detail in following sections, and all size distributions are provided in Appendix A.

It is important to understand that chord length distributions do not represent a true particle size distribution and should only be used to identify trends. In addition, as mentioned in Chapter 2, there is also a solids concentration of effect on the measured chord length. At higher solids concentrations, overlapping particles can be counted as one particle; and a full discussion of this issue is presented by Yu and Erickson (2008)[44]. In the present study, samples were diluted in order to achieve reproducible chord length distributions, as reproducible results were not obtained at high solids contents. The effect of solids concentration on measured chord length was evaluated by measuring size distributions at 3 different solids concentrations. For the diluted suspensions test in the FBRM in the present study there was almost no effect of changing the solids concentration from 6-12% by mass on the measured chord length distribution. A full analysis of the effect of solids concentration on measured chord length is provided in Appendix C.

In an attempt to at least qualitatively validate the size results obtained, the chord length distribution obtained for flocculation of kaolinite dispersions using Magnafloc® 1011 (from the present study) is compared to the particle sizes obtained from the image analysis technique of Vaezi et al. (2011)[34]. In their study, the same flocculant, similar kaolinite samples and slurry pH were tested. Floc diameters were in the range of 200μm to roughly 1200μm. In the present study, floc chord lengths during flocculation (shown in Figure 4.2) range from 200-1000μm. The chord length range obtained from FBRM is quite comparable to the size range obtained through the though image analysis technique of Vaezi et al. (2011)[34]. One

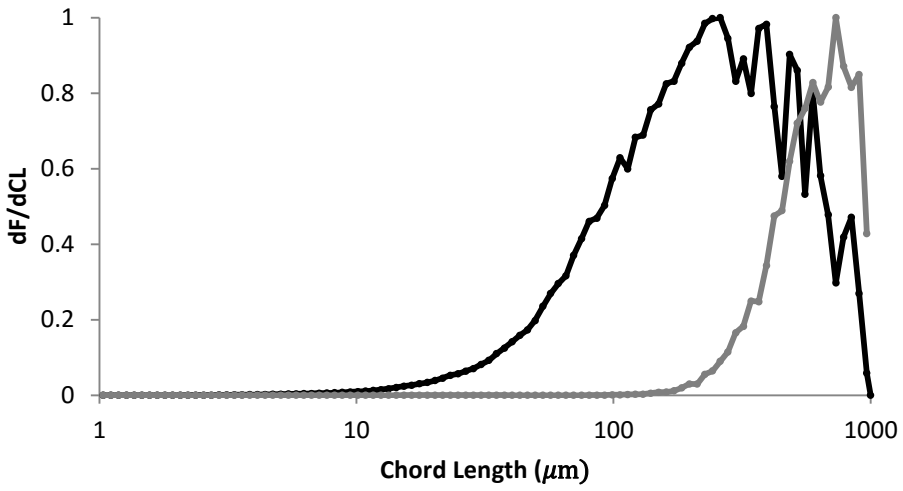

Figure 4.2: Volume based size distribution of kaolinite suspension flocculated with Magnafloc® LT27AG before insertion into shearing apparatus ( ) and after insertion into shearing apparatus ( )

limitation of FBRM is the upper size limit of 1000μm and hence the largest flocs cannot be measured during flocculation. However this does not affect the results of the present study; the shear imparted during sample loading (into the concentric cylinder shearing apparatus) causes a significant reduction in floc size, shown in Figure 4.2. The significant reduction in floc size brought about during sample loading shifts the chord length distribution into an ideal range (<1000μm).

Initial floc chord length distributions and vane yield stress measurements were dependent on flocculant type and pH, and can be seen in Table 4.1. Suspensions produced with anionic flocculants (Magnafloc® LT27AG or Magnafloc® 1011) yielded very similar results, with the two suspensions having similar initial yield stress values. The substantially larger floc sizes, measured as d[3,2], of Magnafloc® LT27AG arises from differences in polymer structure.

Table 4.1: Initial paste properties prior to energy input tests.

Polymer	Magnafloc® LT27AG pH 8.5 (100g/tonne)	Magnafloc® 1011 pH 8.5 (100g/tonne)	A-C-A pH 8.5 (65g/tonne – 85 g/tonne – 35g/tonne)	Magnafloc® LT27AG + PEO pH 8.5 (100g/tonne – 150g/tonne)	Magnafloc® LT27AG pH 7 (100g/tonne)
Initial Yield Stress (Pa)	130±10	130±20	140±20	360*	160±10
Sauter Mean Diameter d[3,2] (μm)	250±20	220±10	270±20	360**	240±20
Volume Number Mean d[3,0] (μm)	100±10	90±10	110±10	143**	110±10

*Limited number of measurements taken – standard deviation not applicable. **True size is much greater than reported - see Section 4.6

The addition of cationic flocculant for the A-C-A system produced a larger d[3,2] and d[3,0] (shown in Table 4.1) than the anionic flocculant alone and a slightly higher yield stress as a result of the added electrostatic bonds. Magnafloc® LT27AG produced a suspension with a greater yield stress, along with smaller and denser flocs at pH 7 than at pH 8.5. This difference is due to the weaker electrostatic repulsions between the surface of kaolinite and the polymer chains at pH 7, thus resulting in stronger adsorption at the cost of lowered bridging efficiency. The net effect is the production of smaller, denser flocs (smaller d[3,2] at pH 7) but left fewer kaolinite particles un-flocculated (larger d[3,0] at pH 7), as shown in Table 4.1. When Magnafloc® LT27AG was combined with PEO, the floc size and mixture yield stress produced were much higher than those measured under any other condition (see Table 4.1). In fact, the reported d[3,2] and d[3,0] values are lower than the true values as a significant portion of particles were beyond the range of the instrument (>1000μm).This will be discussed in greater detail in Section 4.6.

4.3 Magnafloc® LT27AG and Magnafloc® 1011 flocculated suspensions at pH 8.5

Changes in yield stress were well correlated with overall size reduction of flocs (Figure 4.3) as well as accumulation of fragmented particles in the size range of 10-100μm (Figure 4.4). Yield stress, size reduction and particle size evolution profiles were nearly identical between the two pastes; therefore data for Magnafloc® LT27AG flocculated pastes are shown here, while the corresponding data for Magnafloc® 1011 flocculated pastes are shown in Appendix A. The form of the rheology reduction is qualitatively similar to reports in the literature for real tailings sheared in a concentric cylinder viscometer[16,18] and pipe flow[17]. Quantitatively, though, the reduction is more dramatic when compared to the results of Salinas et al. (2009)[18] and Treinen et al. (2010)[16], who observed reductions to 30-50% of the pre-shear value in concentric cylinder viscometers. Gillies et al. (2012)[17] saw a reduction to 50% of the initial vane yield stress in their pipe flow experiments. There are two main differences between the test conditions of those earlier studies and the present work. The presence of coarse particles in the previous work accounted for a substantial amount of the total solids volume fraction and has been shown to augment yield stress by up to 80% in kaolinite dispersions[57] . The present study does not contain coarse particles and hence the reduction is more enhanced. Also the previous studies involve more complex mixture chemistries (i.e. the presence divalent cations), which can adsorb to particle surfaces and enhance floc structure[124].

The dramatic 90% reduction in yield stress (Figure 4.3) for flocculated kaolinite clay suspensions at pH 8.5, with low salt concentration, can be explained as follows. The large porous flocs are fragmented and decrease in size, as shown in Figure 4.3. A decrease in floc size, as noted by Vaezi et al. (2011)[34], was well correlated with a dramatic increase in floc density. Flocs greater than 400μm were very porous and contained roughly 90-95% water whereas flocs near 200μm were roughly 65% water. Thus as flocs are fragmented and decrease in size, the overall apparent solids volume fraction of the

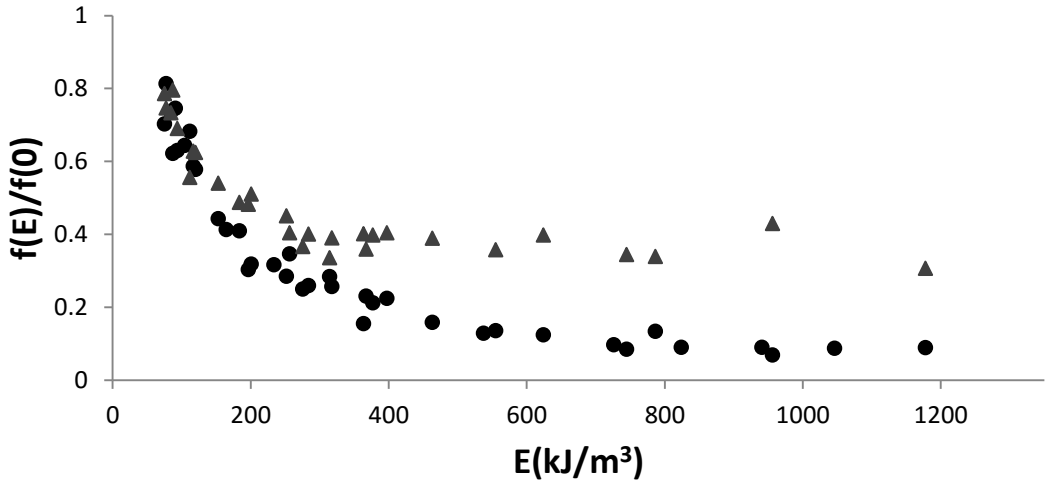

Figure 4.3: Normalized functions of yield stress (●) and number volume mean diameter (▲) plotted as a function of shear energy input for 41% wt. paste flocculated with Magnafloc® LT27AG at 100g/tonne. The function 'f(E)' is substituted for $\tau_v(E)$ and $d_{[3,0]}(E)$

mixture decreases substantially. Particles below 200μm account for 85% of the solids volume fraction of a well sheared mixture (E=1000 kJ/m^3), whereas they only account for 47% of the volume fraction before shear. Fine particle suspension yield stress has an exponential[19,20] or cubic[67] relationship to solids volume fraction. Thus a dramatic rheology reduction to 10% of initial rheology would occur at approximately a 50% reduction in apparent volume through the relation from Thomas (1963)[67], shown in Equation 2.7.

Flocs formed by high molecular weight anionic acrylamides do not reform once broken. Thus the accumulation of fragmentations (see Figure 4.3 Figure 4.4) is irreversible. As previously mentioned, the fragmentations (and kaolinite particles) account for 85% of the solids volume fraction of the mixture of a well sheared mixture. At this stage of mixing, the large porous flocs (>400μm) account for only 2% of the solids volume fraction and do not contribute to yield stress (see Figure 4.4). Hence the rheology of a well

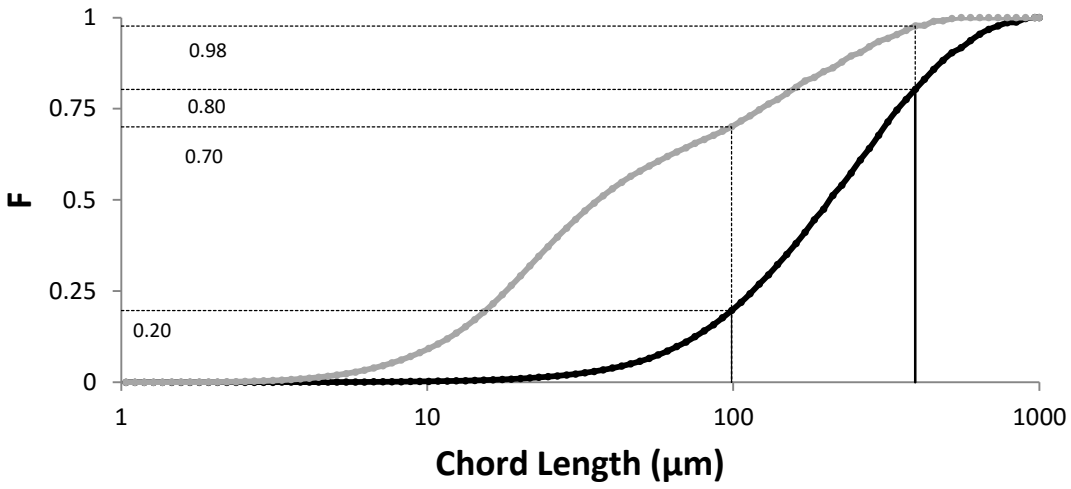

Figure 4.4: Cumulative volume distribution as a function of particle chord length for un-sheared paste (—) and paste sheared with 1000 kJ/m^3 of shear energy input (—)

sheared mixture (E=1000 kJ/m^3) is dictated by the fragmentations, and their contribution is explained as follows. Due to the dramatic difference in size, fragmentations have a much higher surface area to volume ratio which is much closer to that of the initial kaolinite slurry shown (Figure 4.5); thus inter-particle surface forces become increasingly important. The maximum yield stress of a fine-particle suspension occurs at the isoelectric point[66,75,76], which for kaolinite is at approximately pH 2[78]. The pH of the test suspension is 8.5, and much greater than that of the isoelectric point of kaolinite. The large difference in pH of the suspension and isoelectric point creates substantial surface charge, which results in considerable repulsive forces. The repulsive forces result in weakly interacting fragmented particles, thus producing very low yield stresses.

Interestingly, despite the normalized yield stress decreasing from 0.2 to 0.1 from (E=400 kJ/m^3 to E=1000 kJ/m^3 e.g. $\frac{\tau_V(400)}{\tau_V(0)} = 0.2$ and $\frac{\tau_V(1000)}{\tau_V(0)} = 0.1$), the chord length distributions and d[3,0] do not seem to significantly change. Changes in yield stress have been attributed to shape factors in previous

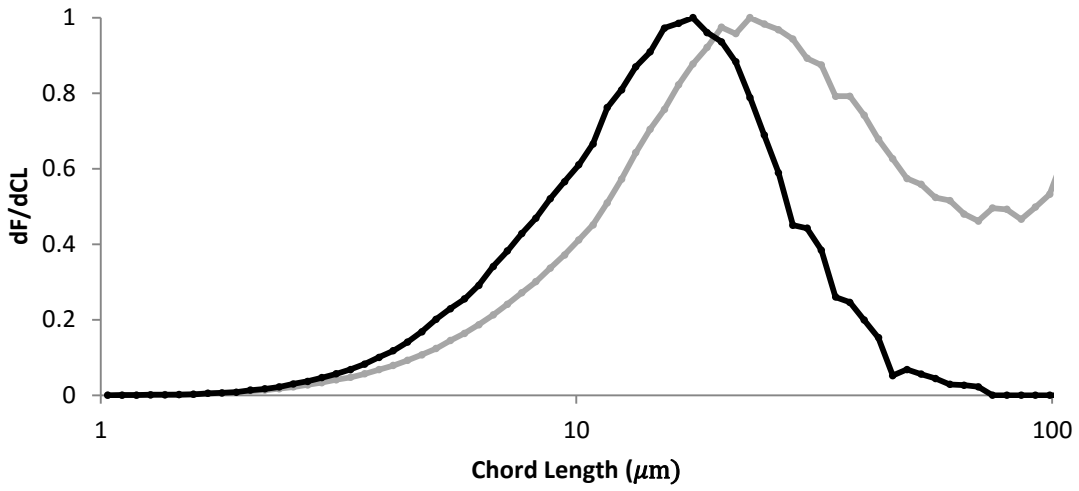

Figure 4.5: Chord length distribution of kaolinite slurry at pH 8.5 after 30 minutes of stirring prior to polymer addition (—) and Magnafloc® LT27AG paste after 1000 kJ/m^3 of shear energy (—)

studies, and may be responsible for the reduction in rheology from E=400 kJ/m^3 to E=1000 kJ/m^3. In future work particle shapes should be studied as a function of shear energy.

Finally, the results suggest that the structure of anionic acrylamides is unimportant in predicting time-dependent rheology. The evolution of vane yield stress and d[3,0] were identical for both anionic acrylamide dosed kaolinite suspensions. The precise structure of the acrylamides, however, is provided qualitatively and strict conclusions cannot be drawn. Kaolinite dispersions dosed with low charge density anionic acrylamides are more deformable than high charge density acrylamides, and, this may result in flocs which first densify rather than fragmenting. A further investigation into charge density should be conducted in order to gain a more complete understanding on polymer structure and type on time-dependent rheology.

4.4 Effect of cationic polymers in a dual-polymer system (A-C-A)

A reduced apparent solids volume fraction was the main factor in yield stress reduction for a dual-polymer system. Initial rates of decrease in both yield stress and fragmentation were more pronounced in the presence of cationic polymer (Figure 4.6 and 4.7). The increased rates of yield stress and floc size reduction are the result of altered floc structure. The addition of cationic polymers to negatively charged particles results in flocs formed through charge neutralization. It is well documented[92-95] that flocs formed through charge neutralization fragment more quickly than flocs formed through bridging associations. In Figure 4.7, we can see a clear bi-modal distribution has been established for A-C-A dosed kaolinite dispersions (charge neutralization) at E=200 kJ/m^3, and this bi-modal distribution is not present for kaolinite dispersions dosed with only anionic acrylamides (bridging).

The effect of cationic flocculant is observed when comparing the fragmentation patterns of dispersions flocculated with A-C-A and those of Magnafloc® LT27AG only, shown in Figure 4.8. The fragmentations have enhanced structure for well sheared dispersions (E=1000 kJ/m^3) due to the presence of cationic polymers. The cationic polymers produce positively charged patches on the fragmentations, allowing them to associate through electrostatic attraction with negatively charged patches of neighbouring fragmentations. Additionally, it is known that flocs produced through charge neutralization mechanisms have the ability to re-aggregate under the right hydrodynamic conditions [95]. The slight recovery of d[3,0] and chord length distribution from E= 900 to 1100 kJ/m^3 is shown in Figure 4.9.This effect of floc recovery may be more dramatic in the presence of higher doses of cationic flocculant, as noted in theliterature[112].

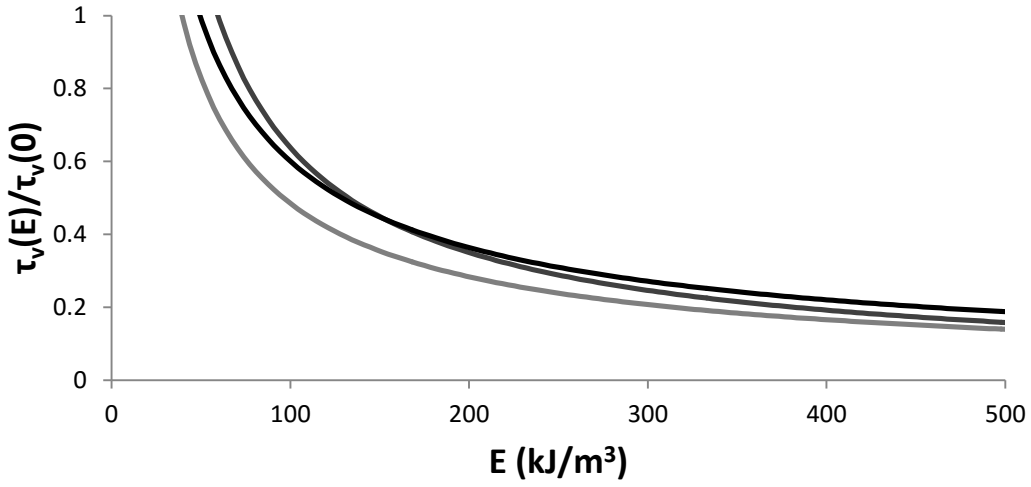

Figure 4.6: Power-law least squares regression models of yield stress decay for acrylamide flocculated suspensions at pH 8.5. Magnafloc® LT27AG R^2=0.9689 (———). Magnafloc® 1011 R^2=0.9579 (———).A-C-A R^2=0.8579 (———)

Finally, when compared to kaolinite dispersions dosed only with anionic acrylamides, the vane yield stress at high energy inputs (E > 400 kJ/m^3) exhibits different behaviour. The yield stress does not decrease after E=400 kJ/m^3 for A-C-A dosed kaolinite dispersions and is the result of enhanced inter-particle forces.

4.5 Effect of pH

Kaolinite dispersions flocculated at pH 7 and pH 8 had similar initial rates of rheology reduction (Figure 4.10a) up to E=200 kJ/m^3, but deviated significantly thereafter (Figure 4.10a). The initial rates of rheology reduction were a result of floc size and apparent solids volume reduction (Figure 4.10b). However, the chord length distributions do not change accordingly for Magnafloc® LT27AG flocculated kaolinite dispersions at pH 7 and 8.5, despite similar normalized d[3,0] evolutions, shown in Figure 4.11a. A clear bi-modal chord length distribution is not established until 500 kJ/m^3 of shear energy input

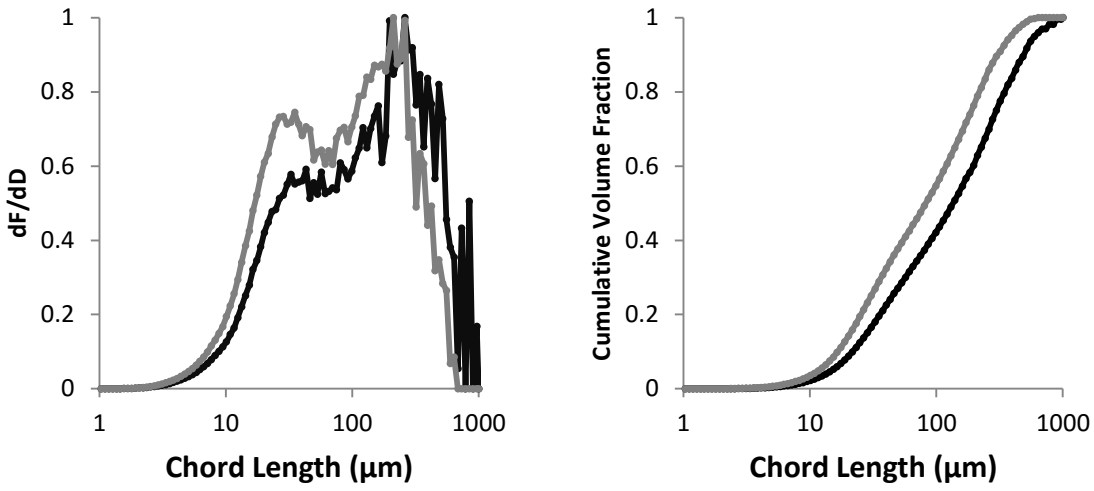

Figure 4.7: Qualitative difference in particle size distributions of paste sheared by Magnafloc® LT27AG (—●—) and A-C-A (—●—) at 200kJ/m^3 of shear energy input.

at pH 7 (as compared to 200-250 kJ/m^3 at pH 8.5), as the flocs undergo densification first rather than fragmentation shown in Figure 4.11b. Additionally, the fragmentations produced do not reach their equilibrium size until E > 500 kJ/m^3 inputs (compared to 350-400 kJ/m^3 of shear energy input for previous other conditions). The initial densification event is due to the flocs being more deformable as a result of lower surface potential. The lowered surface potential of kaolinite results in lowered electrostatic repulsions between acrylate pendant groups on anionic acrylamides and the kaolinite particle surface. Hence the mechanism of rheology reduction changes with reductions in pH, and hence surface chemistry, of the fine particles. Increase in yield stress of a well-sheared mixture is a result of enhanced bonding between fragmented particles, and can be explained as follows. The increase in inter-particle bond strength is a result of the inherent changes in kaolinite particles as pH is decreased. The kaolinite particles at pH 7 are much closer to the edge isoelectric point, pH 5.25, thus reducing surface charge and producing enhanced inter-particle bond strength when compared to pH 8.5. As previously

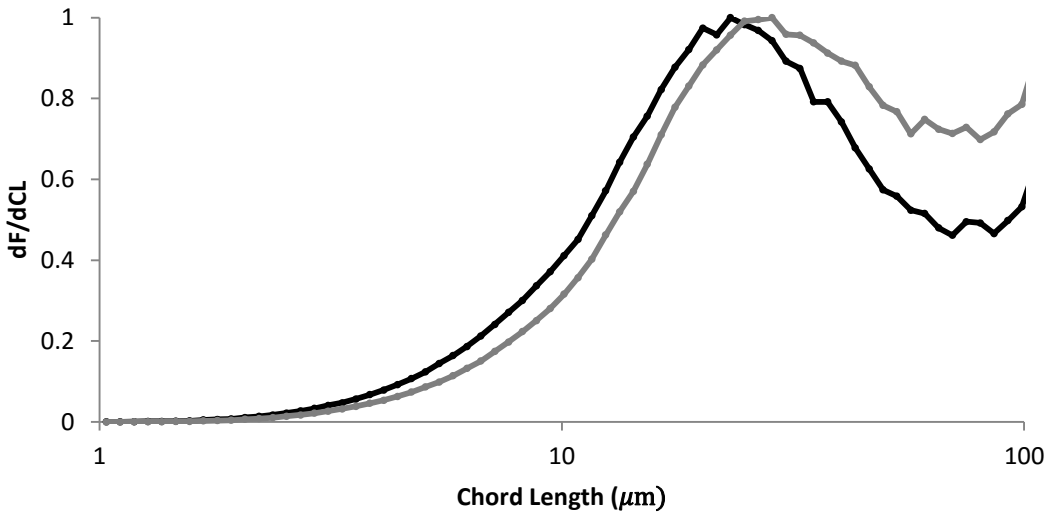

Figure 4.8: Fragmentations at equilibrium (>1000 kJ/m^3) for dispersions flocculated with Magnafloc® LT27AG (—•—) and A-C-A (—•—)

noted, the maximum yield stress of fine-particle suspensions occurs at the isoelectric point; hence yield stress increases at pH decreases. The effect of decreased pH can be seen in Figure 4.12a, where fragmentation sizes are substantially larger due to increased inter-particle bond strength.

The importance of surface chemistry over zeta-potential is outlined. Zeta-potential of kaolinite particles at pH 8.5 is reduced when either cationic polymers are added, or pH is reduced to 7. Depending on the method used to reduce zeta-potential (cationic polymer or reducing pH) structure is affected (4.12b), and clearly rheology is also dramatically affected, as shown in Figure 4.13.

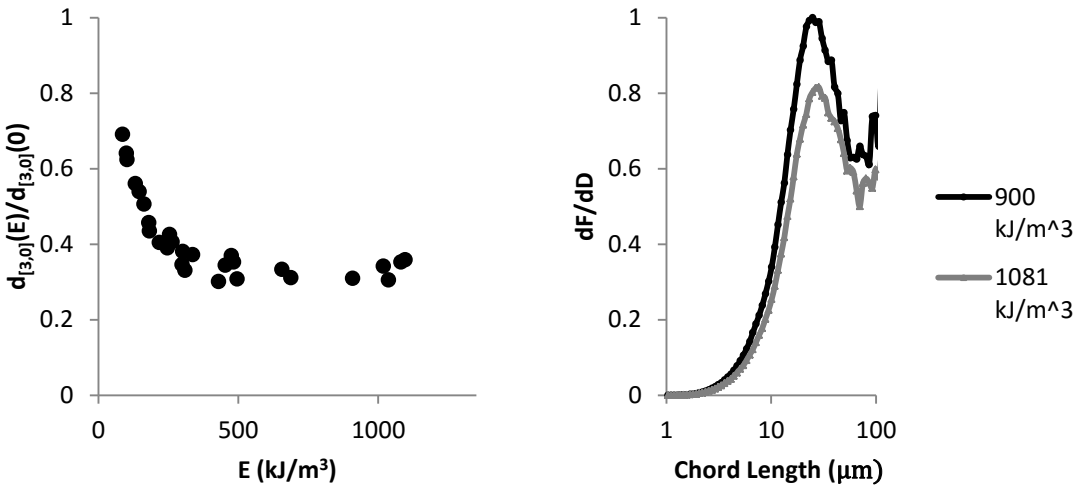

Figure 4.9: (a,**LEFT**) Normalized function number volume mean chord length plotted as a function of shear energy input for 41% wt. paste flocculated with an A-C-A system (Magnafloc® LT27AG at 100g/tonne + Hychem Hyperfloc CD 650 85g/tonne) (b,**RIGHT**) Differential frequency size distribution at 900 kJ/m^3 (—) and 1081 kJ/m^3 (—) showing slight recovery in chord length

4.6 Effect of PEO

4.6.1 A brief note on the issues of using PEO

Studying the properties of flocculated kaolinite at pH 8.5 using PEO was troublesome. Consistent settling rates could not be obtained at reasonably low doses comparable to those used in other experiments. Each 3.5L batch of kaolinite suspension produced a different settling rate for doses below 500g/tonne. This dose was much higher than doses in previous conditions and thus difficult to draw comparisons without, of course, bringing into question the effect of drastically differing doses. The system could be 'titrated' such that PEO solution was slowly dispensed until a 'flocculating point' was observed, in an attempt to achieve consistency. This 'flocculating point' was the dose at which the system would change from a stable dispersion to one with large robust flocs and clear supernatant. The change was very abrupt and intermediate conditions were rarely observed. This method produced

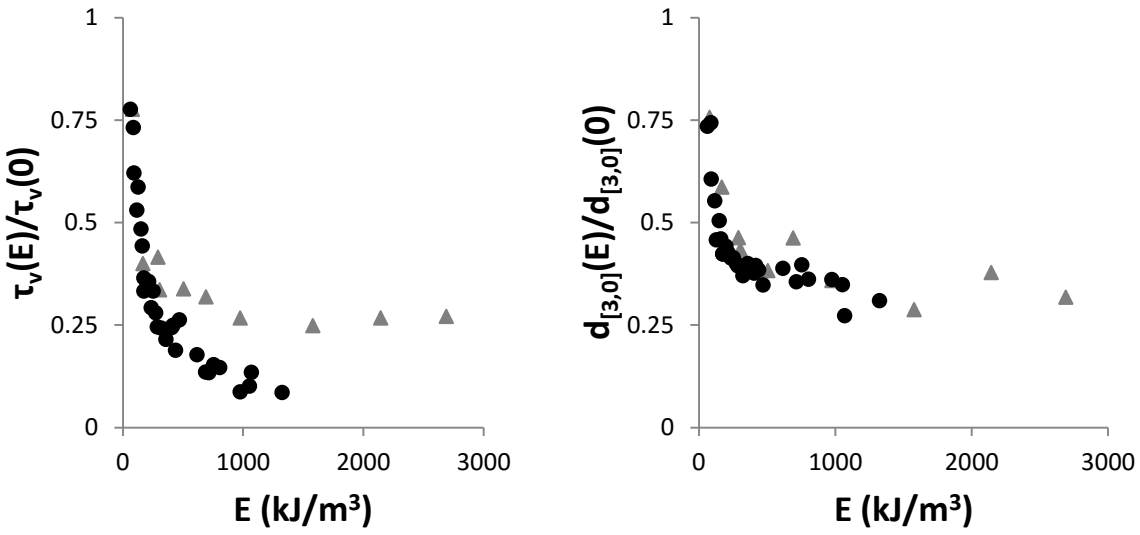

Figure 4.10: (**a**) Normalized rheology reduction as a function of shear energy input (**b**) Normalized size reduction as a function of shear energy input. Magnafloc® LT27AG at pH 7 (▲) and pH 8.5 (●)

consistent, reproducible yield stresses for subsequent experiments. However, the paste produced could not be sheared in the concentric cylinder apparatus.

Various apparatus were attempted to overcome wall slip effects arising in PEO-flocculated suspensions. Using a Haake Viscotester 550, MV-II and MV-III (2.6mm and 5.8mm gap widths) geometries were attempted, as well as large batch samples in the customized concentric cylinder (4.5mm gap) shearing apparatus. Complete shear was unattainable even at very high spindle speeds -80 rad/s for Haake 550 Viscotester, 42 rad/s spindle speed for concentric cylinder shearing apparatus. The incomplete shear was observed visually - the paste would remain stationary as an annulus of water formed between the paste and cylinder wall. PEO was mixed with Magnafloc® LT27AG which provided both more consistent settling properties and the ability to shear it in a concentric cylinder mixer. When combined with Magnafloc® LT27AG, doses of PEO greater than 150g/tonne resulted in increasingly unpredictable behaviour (see Appendix A). Doses of 100g/tonne of PEO or less resulted in little to no

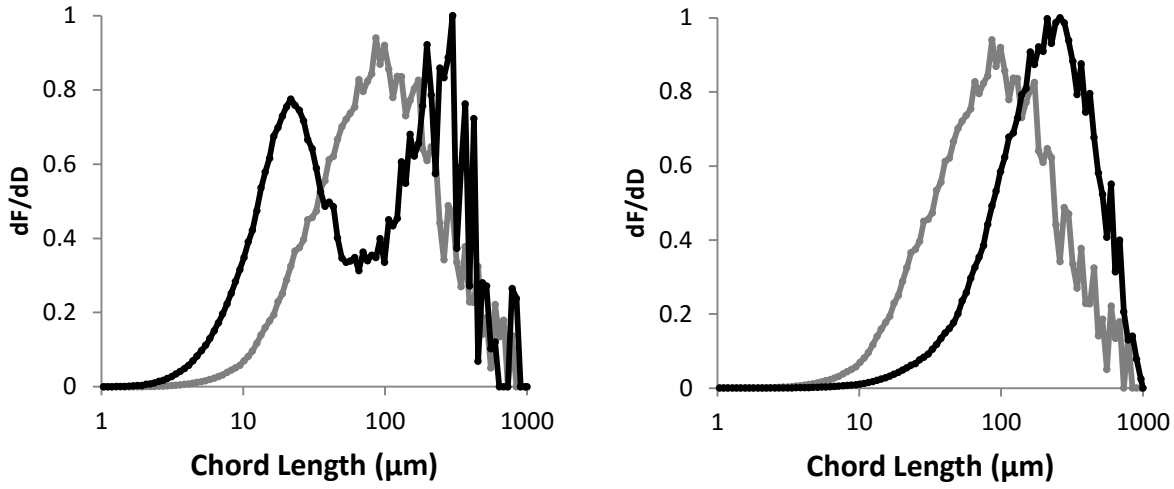

Figure 4.11: (**a**) 300kJ/m^3 of shear energy input for paste at pH 7 (—) and pH 8.5(—). (**b**) pH 7 paste at 0 kJ/m^3 (—) and 300 kJ/m^3 (—) of shear energy input.

noticeable effect on settling and rheology. Confirming a steady power-law decay for PEO-flocculated dispersions was also difficult. The complete shearing of the mixture could not be confirmed by a steady power-law decay in viscosity used in previous studies[16,18], as the apparent viscosity was increasing during the first 60 seconds followed by a steady power-law decay, which is discussed in the following section. The spindle speed was selected based on visual observation of complete shearing of the mixture and will require further investigation. Measurements of sheared samples were not made until 60 seconds of shearing was imparted to the mixture. This minimum amount of shear was to ensure complete shearing had occurred.

4.6.2 Effect shear energy on kaolinite dispersions flocculated with PEO

The elastic structure of PEO allows re-conformation of polymer chains and thus floc structure. PEO produced flocs with a dramatically reduced rate of yield stress decay, requiring nearly an order of magnitude more energy to achieve similar reductions in yield stress compared with other flocculants at

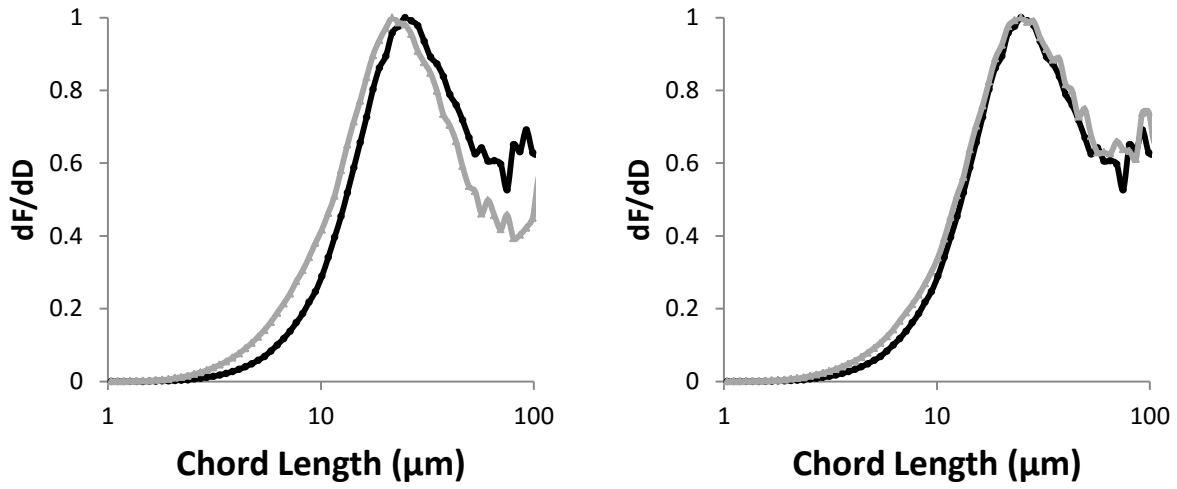

Figure 4.12: (**a**) Size distribution of well sheared paste (1000 kJ/m^3) using Magnafloc® LT27AG pH 7 (—) and pH 8.5 (—). (**b**) Size distribution of well sheared paste (1000 kJ/m^3) using Magnafloc® LT27AG at pH 7 (—) and A-C-A at pH 8.5 (—).

pH 8.5 (Figure 4.14). The resistance to yield stress decay is due to the robustness of the flocs and their ability to withstand moderate shear forces without rupturing, as reported by Mpofu et al. (2003)[11] and McFarlane (2005)[31]. In contrast to the present study, they observed an increase in yield stress when the flocs were subject to moderate shear. However, in their studies, the yield stress before and after shear were measured at different solids concentrations. The densification of flocs when subjected to shear resulted in higher solids content for the post-shear yield stress measurements. In the present study, solids concentration is kept constant, and hence a decrease in yield stress is observed as a result of a reduction in apparent solids volume concentration. The reduction in apparent volume up to 1000 kJ/m^3 can be confirmed by the following observations. PEO-flocculated suspensions were left to stand quiescently for 10 minutes after 1000 kJ/m^3 of shear. The suspension settled and a large amount of clear water rose to the top of the mixture, which account for roughly 10% of its volume (of the entire mixture). This result is concurrent with McFarlane (2005)[31] which observed kaolinite suspensions

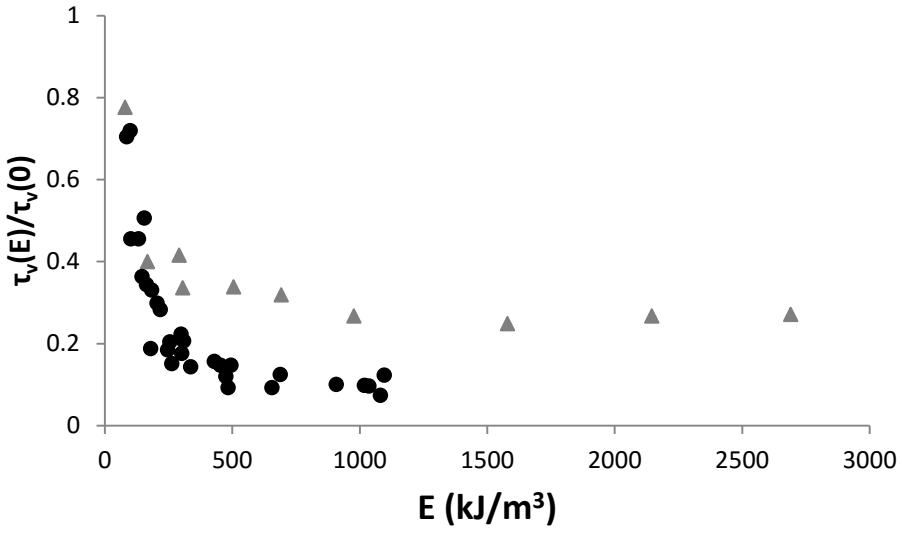

Figure 4.13: Rheology reduction of kaolinite dispersion flocculated with A-C-A at pH 8.5(●) and Magnafloc® LT27AG at pH 7 (▲)

flocculated with PEO/anionic acrylamide. Beyond 1000 kJ/m^3, the flocs began to fragment and followed the same reduction patterns experienced in all other conditions. The large flocs began to fragment, producing a significant population of particles in the 10-100μm region (Figure 4.15a). Studies of the fractal dimensions[34,88] of flocculated fine suspensions have demonstrated that density increases with decreasing floc diameter. They would strongly suggest that these particles are denser than the large flocs, hence contributing to a reduced apparent volume. The sudden change in behaviour at E=1000 kJ/m^3 is a result of the mechanical degradation of PEO. PEO chains break down in response to shear stress, and the reduction can be plotted as a function of energy input[125,126].

The behaviour observed from 0 – 1000 kJ/m^3 was unique in comparison to other conditions. Flocculation continued during shearing up to 1000 kJ/m^3 which was observed through an increase in floc size and changes in chord length distribution shown in Figure 4.15a. The d[3,0] doubled from 0 – 1000

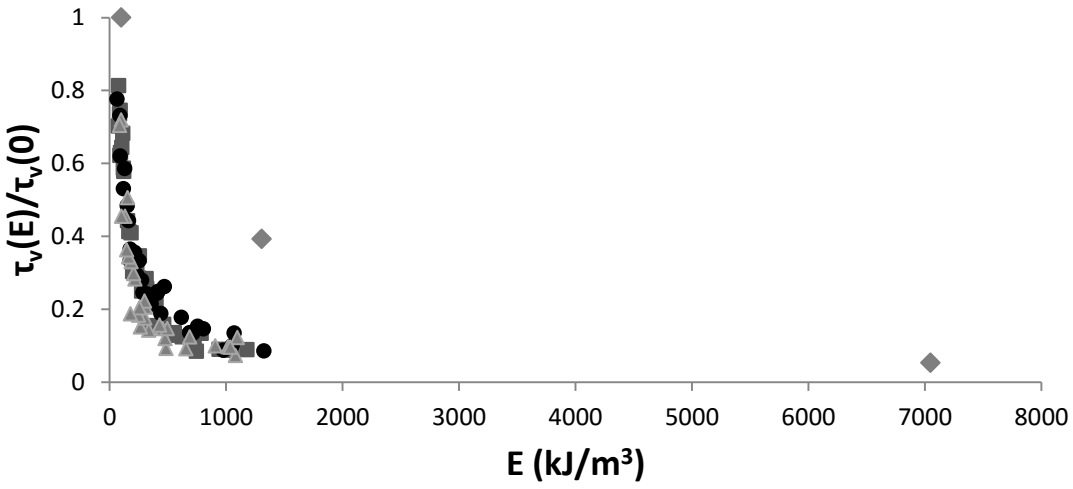

Figure 4.14: Yield stress degradation profiles as a function of energy input for conditions tested at pH 8.5. Magnafloc® LT27AG (■), Magnafloc® 1011 (●), A-C-A (▲), Magnafloc® LT27AG + PEO (◆)

kJ/m^3 (Figure 4.16a), and in fact the true value is most likely more than double as the particle size distribution is truncated, and limitations of FBRM prevented the observation of the full chord length distribution. The doubling of d[3,0] was a result of flocs increasing in size, while also flocculating the remaining fine particles in the mixture. The volume fraction of particles below 100μm decreases from 10% to 3% as 1000 kJ/m^3 is imparted for the mixture, seen in the cumulative size distributions (Figure 4.15b). In fact, the volume fraction of particles below 100μm is most likely less than reported. The chord length distributions are truncated beyond 1000μm due to instrumental limitations, and thus the volume fraction of particles with chord lengths larger than 1000μm is not included in the calculation. The ability to flocculate in high shear environments stems from the elasticity of PEO and its ability to re-conform in changing hydrodynamic environments as demonstrated by Mpofu et al. (2003)[11].

In contrast to the yield stress, the apparent viscosity of the mixture increased to E=1000 kJ/m^3 (or the peak in size distribution) followed by a power-law decay thereafter, which can be seen in Figure 4.16a. The torque steadily increases until approximately 60 seconds after which it begins to decay, seen

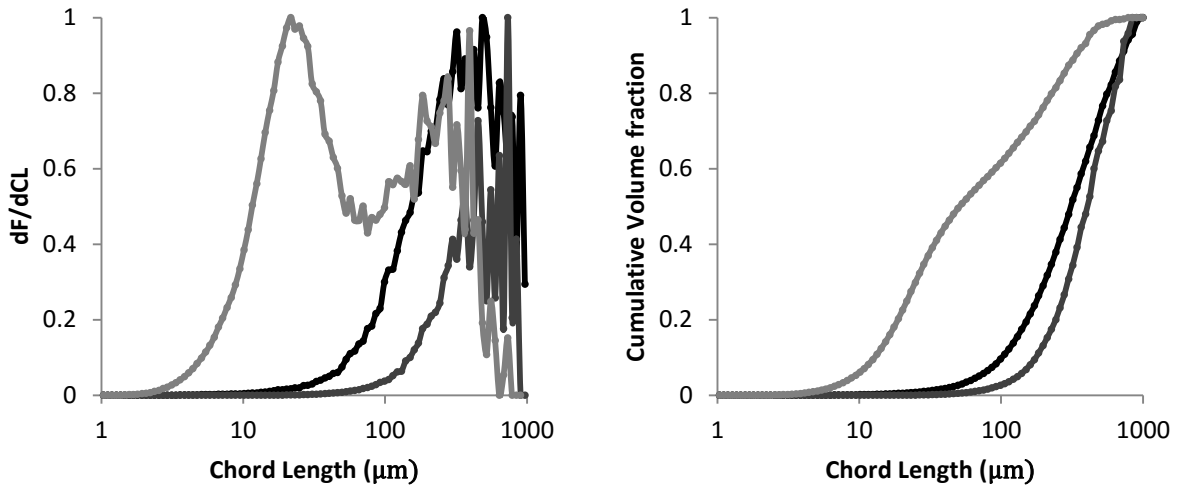

Figure 4.15: (—•—) 0 kJ/m^3, (—•—) 1000 kJ/m^3, (—•—) 7000 kJ/m^3 (**a**) Differential frequency volume distribution of Magnafloc® LT27AG + PEO. (**b**) Cumulative volume distribution of Magnafloc® LT27AG + PEO.

in Figure 4.16b. The unique behaviour in apparent viscosity is difficult to rationalize, as the available data would suggest a decrease in viscosity, as was seen with yield stress. Non-DLVO forces arising from PEO flocculated dispersions have been thoroughly investigated by Mpofu et al. (2003)[11] and Rubio (1976)[100], and may be the cause of the unusual behaviour in apparent viscosity. The entropic forces resulting from the displacement of water at the silica surface (hydrophobic forces) noted by Rubio (1976)[100] are longer range than typical van der Waals forces[78] and may be contributing to an increased momentum transfer between flocs. However, this conclusion is speculative at best and requires a thorough investigation.

The effects of the presence of Magnafloc® LT27AG on floc structure should be considered, given that the preceding discussions are for kaolinite dispersions flocculated with a PEO/Magnafloc® LT27AG mixture. Far more mixing time and higher RPM was required to flocculate kaolinite suspensions with PEO than with acrylamides. This is a result of smaller sizes of the polymer in solution due to shielding of

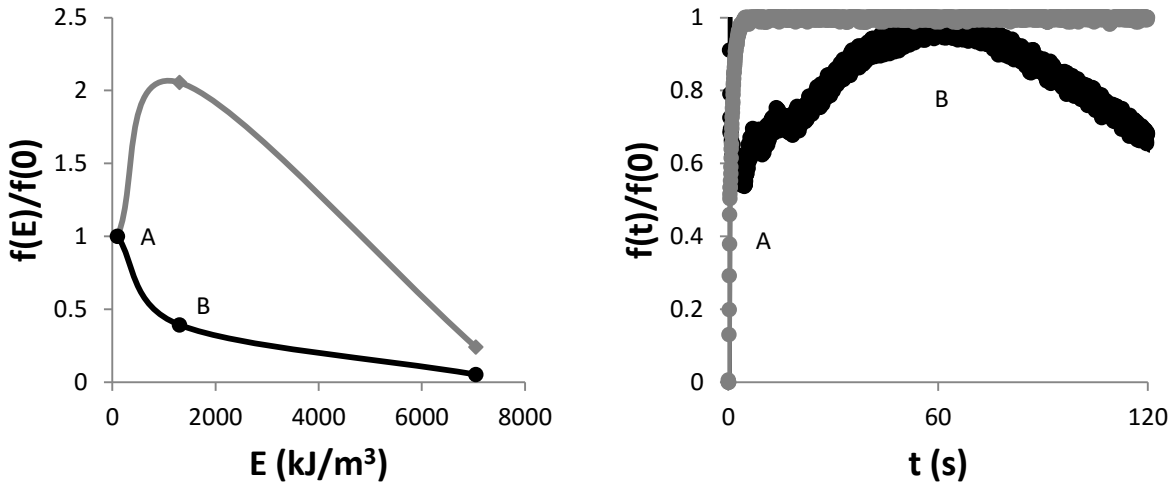

Figure 4.16: (**A**) Initial value of torque/yield stress/size. (**B**) Yield stress and size at maximum torque value. (**a**) Yield stress (—●—) and number volume mean (—◆—) as a function of energy input. (**b**) Normalized torque (—●—) and RPM (—●—) versus time of 41% wt. paste flocculated with 100g/tonne Magnafloc® LT27AG + 150g/tonne PEO at pH 8.5

hydrophobic groups in comparison to acrylamides which are extended due to electrostatic repulsions[11]. Adsorption kinetic correlations[127] have strong dependence on particle size, and hence it can be assumed that bridging occurs more rapidly for acrylamides than for PEO. For flocculation using a combination of acrylamides and PEO the majority of bridges formed during the early stages of flocculation are from acrylamide polymers and as a result initial floc structure resembles that of acrylamide-based flocs. Initially, molecular bridges formed from acrylamides; however, when these flocs are subject to shear inter-particle bonds are formed through more elastic and re-conformable PEO bridges. A study of PEO-flocculated dispersions should be conducted in the absence of acrylamides to eliminate any effects brought about by the additional polymer. A roughened spindle should be used on the concentric cylinder shearing apparatus in order to obtain complete shearing across the gap.

4.7 Tailings experiments

Tailings obtained from APEX Engineering were of approximately 15% wt. from a Teck mining site, and the full raw data are available in Appendix A. The ore was crushed and processed at APEX Engineering's research lab where roughly 90% the bitumen was removed via flotation. The tailings were flocculated using A-C-A using 300g/tonne Magnafloc® LT27AG and 180g/tonne HyChem Hyperfloc CD650. The resulting paste was difficult to shear and required very high spindle speeds with respect to the model tailings. Further investigation is required to identify what factors caused these particular tailings to have distinctly different behaviour, given that the polymer-flocculated tailings studied by Treinen et al. (2010)[16] could by studied via concentric cylinder viscometer.

The reduction in rheology of the industrial tailings sample, shown in Figure 4.17, is in general agreement with preceding model tailings experiments; however there are some slight quantitative differences. The rheology degraded in the same manner as kaolinite dispersions flocculated with acrylamides and the sample reached approximately 25% of the original yield stress which can be explained by the following parameters. The pH of the tailings was 7.9 and hence a greater equilibrium yield stress is expected than that of pH 8.5 dispersions (pH 8.5, $\frac{\tau_Y(equilibrium)}{\tau_Y(0)} = 0.1$), and less than that of pH 7 dispersions (pH 7, $\frac{\tau_Y(equilibrium)}{\tau_Y(0)} = 0.3$) from the model tailings experiments of previous sections. The dose of cationic polymer is more than double the amount used in the A-C-A experiments, and may have some contribution to equilibrium yield stress due to floc robustness[112]. Finally, the high salt concentrations and presence of divalent cations could be influencing floc structure[124] and thus contributing to equilibrium yield stress.

The flocculated industrial tailings had highly elastic properties similar to PEO-flocculated kaolinite suspensions, which could be observed macroscopically by manipulating the paste with one's

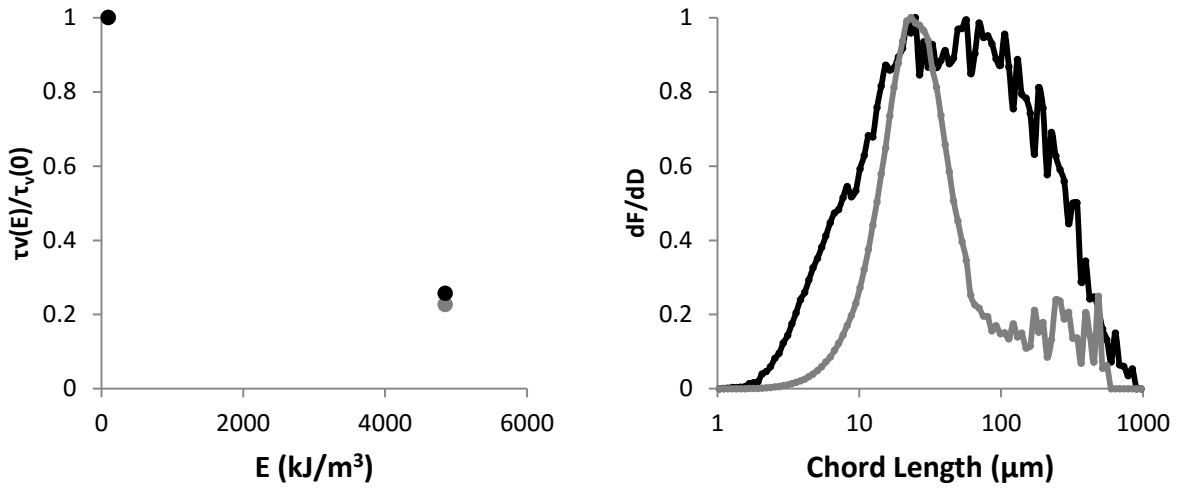

Figure 4.17: (**LEFT**) Yield stress (●) and number volume mean diameter (●) with respect to shear energy input. (**RIGHT**) Size distribution at 0 kJ/m^3 (▬) and 5000 kJ/m^3 (▬)

hand. In addition, the effect of wall slip was much greater requiring considerably greater spindle speeds to obtain complete shearing. The difficulty in obtaining complete shear of the paste may be a result of hydrophobic forces arising from bitumen and asphaltene contents which remained in the tailings. The bitumen constituted approximately 10% wt. of the ore, and only 90% was recovered which leaves a considerable amount of bitumen in the system; estimated at approximately 10 000ppm. When compared to the amount of PEO required to generate this type of behaviour (~500ppm), we can see that it is very plausible that hydrophobic forces are responsible for this behaviour.

In addition, an interesting feature is that the particles in the range of 1-10µm (flocs) actually seem to be increase in diameter during the shearing process and, in addition, the fragmentation pattern produced is ubiquitous among all conditions observed. This suggests that the ideal hydrodynamic fragmentation size may be dictated by the gap width in a concentric cylinder mixer. Clearly, this requires further investigation on the effect of gap width in order to explain this phenomenon.

Chapter 5: Conclusions and Recommendations

5.1 General Summary

The major conclusions of the preceding experiments can be summarized as follows:

- Shear induced rheology reduction was well correlated with floc breakage and an accumulation of particles in the region of 10-100μm for kaolinite suspensions. The main determining factors for yield stress decay were the reduction in apparent volume due to large floc breakdown while the nature of the kaolinite particle surface and fragmentations were the main factors dictating the equilibrium yield stress.
- Polymer structure and type had a strong influence on both rate of fragmentation, fragmentation structure and yield stress reduction.
    - Anionic acrylamide flocculants had nearly identical behaviour – significant accumulation of fragmentations between 10-100μm began at 200 kJ/m^3 of energy input after which equilibrium size and yield stress were established at approximately 400 kJ/m^3.
    - The addition of cationic polymers in a dual-polymer system resulted in more rapid fragmentation and yield stress reduction. Equilibrium behaviour began after 200 kJ/m^3 of shear energy input. Restructuring of smaller flocs occurred after energy inputs > 800 kJ/m^3 due to mixing of cationic polymer in a low shear environment. Equilibrium yield stresses were slightly higher and fragmentation structures were slightly larger
    - Suspensions flocculated with poly(ethylene oxide) showed significant wall-slip as an annulus of water formed between the paste and the concentric cylinder wall. These wall slip effects may be a result of a combination of the elasticity of poly(ethylene oxide) and hydrophobic forces

- Poly(ethylene oxide) allowed for floc densification and restructuring in high shear environments. Flocs experienced dramatic increase in size after 1000kJ/m^3 of shear energy and the volume of fine particles experienced a dramatic reduction due to the majority being bridged into larger flocs. Yield stress decreased from 0-1000kJ/m^3 of shear energy input due to floc densification and a reduction in apparent volume, however apparent viscosity increased and was most likely a result of non-DLVO forces. Excessive amounts of shear energy (7000 kJ/m^3) resulted in floc breakdown and further yield stress reduction. Floc fragmentation followed a very similar pattern to other conditions at pH 8.5

- Lowering the pH of the kaolinite slurry before flocculation from 8.5 to 7 had effects on yield stress and floc structure evolution
  - The equilibrium yield stress value of kaolinite suspensions flocculated with Magnafloc LT27AG increased markedly and plateaued at approximately 30-35% of the initial yield stress value (rather than 10-15% at pH 8.5) due to increased attractive inter-particle forces between kaolinite particles
  - Fragmented structures were considerably larger than those produced at pH 8.5 when flocculated with anionic acrylamides
  - Initial rates of yield stress and d[3,0] reduction were nearly identical to those of Magnafloc LT27AG at pH 8.5 and also resulted from a reduction in apparent volume
  - Reduction of apparent volume initially occurred through densification rather than fragmentation and a significant amount of fragmentations was not present until 500 kJ/m^3, rather than 200-250 kJ/m^3 at pH 8.5

- Experiments on real tailings showed significant wall slip and brought forth some interesting considerations for future work
    - The effect of wall slip was quite pronounced and required roughly 3-4X the spindle speed when compared to model pastes and may be the result of hydrophobic forces from remaining bitumen and other organics
    - The initial (un-sheared) size distribution was much broader than the model pastes and became more narrow with shear energy input
    - A well sheared mixture had a nearly identical size distribution to the model pastes and actually showed a reduction in the volume of particles in the 1-10µm region
    - The size distribution of the well sheared mixture may suggest that geometry of the shearing apparatus plays a significant role in determining the ideal size of fragmentations

5.2 Novel Contributions

A wide base of information is now available to predict initial yield stresses of polymer-flocculated clay dispersions. In addition, the effect of shear energy on flocculation is outlined and should be considered in bench scale flocculation studies. However a gap in information is present in connecting these properties to time dependent behaviour of these mixtures.

The present study provides the mechanism for rheological decay of flocculated suspensions in the form of reduced apparent volume concentration. In addition, the study provides methods of predicting rates of rheological decay based on polymer types and chemical environment of the dispersion. It also establishes concepts which can be used to modify the equilibrium yield stress which will be useful in long distance tailings transportation.

The study concludes in addition, that bench scale flocculation should be reported in terms of mixing energy. Simple reports of mixing speed and time are not sufficient for scaling up to industrial applications.

Lastly, the study outlines the design and use of a specialized concentric cylinder shearing apparatus which can be used to characterize tailings without the complications of a thickener or pipe-loop. The apparatus allows a simplified method to characterize tailings without requiring large volumes of sample.

5.3 Uncertainties and Challenges

5.3.1 Entrapped Air

Due to the highly shear sensitive nature of the paste produced, the entrapped air could not be removed from the samples. Hence, despite the high agreement of paste density between varying samples, the air was removed for density measurements and as a result the true density of each condition is not known, and measurement thereof would be very difficult.

In addition, due to the high yield stress of the paste pockets of air were trapped in the shearing apparatus during loading and hence a varying amount of entrapped air was entrained into the sample during shearing. In addition, this may have greatly affected shear energy inputs as the amount of wall shear stress over pockets of air is negligible. However, after approximately 30s of shearing the mixture became homogenized and wall shear stress was consistent across the length of the rotating spindle. Further investigation into the quantification of air entrapment and the removal thereof may be beneficial for future studies.

5.3.2 Instrument Noise

Due to the large scale of the shearing apparatus, vibrations from the motor and surrounding area were difficult to eliminate and generated noise, which was significant at lower torque ranges. The noise was sinusoidal in nature and hence did not affect the energy input calculation, as the integral of a sin function is near zero and can be neglected. In addition, rate of energy addition was much lower at low torques. Hence the noise did not affect the form of the graphs because low torques were only achieved at equilibrium, where resolution is not as important ($dCL/dE = d\tau_V/dE \sim 0$).

e.g. (B, A,C, K are constants, P is power)

$$E'(t) = P^{-Kt} + \sin(At)$$

Then, when t_1 is large we have:

$$E(t) = \int_{t=0}^{t=t1} (B^{-Kt} + \mathrm{Csin}(At))dt \cong \int_{t=0}^{t=t1} B^{-Kt}dt$$

5.3.3 Vane size

The use of a small vane may have contributed to inaccuracies in yield stress measurements for un-sheared samples and those at low energy input. The high yield stress of these samples lead to the formation of pockets of air and in the event that the vane was immersed into a pocket of air it would substantially lower the yield stress measurement. In the future, scaling up the experiment and using a much larger vane may produce a more consistent result.

5.3.4 FBRM Measurements

The chord length distribution of a sample was estimated using a small fraction of the sample and hence may have introduced a small margin of error. After the paste is sheared and poured into a beaker, it is inevitable that the paste from the bottom of the cup of the shearing apparatus will be at the top of the beaker. Only the paste from at the top of the beaker can be measured for size without altering the sample (e.g. to reach the paste at the bottom, the paste must be mixed or poured out resulting in some added shear). In addition the surface of the sample in the beaker is disturbed during vane yield stress measurements which may further affect the subsequent size measurement.

In order to avoid these issues, it is recommended to increase the scale of the shearing apparatus to accommodate much larger sample sizes, such that a large portion of sample can be set aside for size measurements and is not disturbed by the placement of the vane during yield stress measurements.

5.4 Recommendations for future work

The present study was conducted on a highly idealized system in order to gain insight into the time evolution of rheology and particle size distribution of polymer dosed kaolinite dispersions. However, there remain many unknowns. In terms of mixture chemistry there remains many issues to be studied:

- Effect of divalent cations should be investigated. Divalent cations have been shown to increase settling-rate and increase supernatant clarity. In addition, there was a strong presence of divalent cations in the tailings samples, thus preventing concrete conclusions from being drawn from concepts produced. Indeed the effect of divalent cations should be studied on both particle size and yield stress evolution.
- Effect of charge density of anionic acrylamides. The Frangibility of flocs changed with pH, as a result of reduced electrostatic repulsions between acrylate groups and kaolinite surface at

pH 7. In addition, acrylamides with lower charge densities produce flocs which are more deformable. The effect of shear energy on these systems should be investigated.

- Effect of dose of cationic polymers (charge neutralization). The effect of dose of cationic polymer has been shown to affect the rate of degradation of flocs, and their robustness.
- Effect of organic acids, bitumen (organic matter) on wall slip. Given the amount of slip encountered in the presence of PEO and/or organic matter from industrial tailings, the effect of these should be studied on wall slip and time-dependent rheology
- Effect of mineralogy, as only kaolinite was used in the model experiments. Full interpretation of industrial tailings experiments would require knowledge of how each type of mineral commonly encountered influences time dependent rheology and floc size evolution
- Effect of PEO (in absence of other polymers). Given the unique results produced from the PEO/Magnafloc® LT27AG blend, PEO flocculated suspensions should be studied.

From a mechanical standpoint, there are also many challenges to be addressed:

- Given the typical fragmentation pattern which developed under all conditions, a study into gap width, pipe diameter etc. should be investigated. There may be an ideal hydrodynamic size which develops that is dependent on the gap width
- The effects of spindle angular velocity or pipeline velocity should be studied to determine if there are effects on the rate of decay of both rheology and size distribution.

References

1. Alberta Energy Regulator. Directive 074: Tailings performance criteria and requirements for oil sands mining schemes. https://www-aer-ca.login.ezproxy.library.ualberta.ca/documents/directives/Directive074.pdf;. Updated 2009. Accessed October 21, 1.

2. Alberta Government. Lower athabasca region tailings management framework for the mineable athabasca oil sands. http://esrd.alberta.ca/focus/cumulative-effects/cumulative-effects-management/management-frameworks/documents/LARP-TailingsMgtAthabascaOilsands-Mar2015.pdf. Updated 2015. Accessed October 21, 2015.

3. Energy Resources Conservation Board. Decision for 2013 tailings management plan: Canadian natural resources limited, horizon mine. https://www.aer.ca/documents/oilsands/tailings-plans/2013-CNRL-TailingsPlan-DecisionReport.pdf. Updated 2013. Accessed October 21, 2015.

4. Energy Resources Conservation Board. Decision for 2013 tailings management plan: Imperial oil resources ventures limited, kearl oil sands project. https://www.aer.ca/documents/oilsands/tailings-plans/2013-Imperial-TailingsPlan-DecisionReport.pdf. Updated 2013. Accessed October 21, 2015.

5. Energy Resources Conservation Board. Decision for 2013 tailings management plan: Shell canada limited, jackpine mine. https://www.aer.ca/documents/oilsands/tailings-plans/2013-Shell-Jackpine-TailingsPlan-DecisionReport.pdf. Updated 2013. Accessed October 21, 2015.

6. Energy Resources Conservation Board. Decision for 2013 tailings management plan: Shell canada limited, muskeg river mine. https://www.aer.ca/documents/oilsands/tailings-plans/2013-Shell-MRM-TailingsPlan-DecisionReport.pdf. Updated 2013. Accessed October 21, 2015.

7. Energy Resources Conservation Board. Decision for 2013 tailings management plan: Suncor energy inc. https://www.aer.ca/documents/oilsands/tailings-plans/2013-Suncor-TailingsPlan-DecisionReport.pdf. Updated 2013. Accessed October 21, 2015.

8. Energy Resources Conservation Board. Decision for 2013 tailings management plan: Syncrude canada limited, mildred lake mine. https://www.aer.ca/documents/oilsands/tailings-plans/2013-Syncrude-ML-TailingsPlan-DecisionReport.pdf. Updated 2013. Accessed October 21, 2015.

9. Energy Resources Conservation Board. Decision for 2013 tailings management plan: Syncrude canada limited, aurora north mine. https://www.aer.ca/documents/oilsands/tailings-plans/2013-Syncrude-AN-TailingsPlan-DecisionReport.pdf. Updated 2013. Accessed October 21, 2015.

10. Boswell J, Davachi M, Sobkowicz J. Oil sands tailings technology deployment roadmap. . 2012;5.

11. Mpofu P, Addai-Mensah J, Ralston J. Investigation of the effect of polymer structure type on flocculation, rheology and dewatering behaviour of kaolinite dispersions. *Int J Miner Process*. 2003;71(1):247-268.

12. Torres FE, Russel WB, Schowalter WR. Floc structure and growth kinetics for rapid shear coagulation of polystyrene colloids. *J Colloid Interface Sci*. 1991;142(2):554-574.

13. Sobkowicz J. Oil sands tailings technology deployment roadmap. . 2012;2.

14. Hanks RW. Principles of slurry pipeline hydraulics. *Encyclopedia of fluid mechanics*. 1986;5:213-276.

15. Thomas A. A rational design philosophy for long distance slurry pipelines. *Chem.Eng.Aust*. 1977;2(1):22.

16. Treinen J.M., Cooke R., Salinas C. Energy induced rheology reduction of flocculated slurries. *BHR Group 2010*. 2010;18:487.

17. Gillies, R.G., R. Spelay, R. Sun, A. Goldszal and C. Li, 2012, "Pipeline transport of thickened oil sand tailings", Proc. Int. Oil Sand Tailings Conference, Edmonton, AB, 11 pages.

18. Salinas, C., Martinson, R., Cooke, R., Ferrada, O. Shear and rheology reduction of thickened tailings. Proceedings of Paste 2009. 2009;12(1):1.

19. Coussot P, Piau J. The effects of an addition of force-free particles on the rheological properties of fine suspensions. *Canadian geotechnical journal*. 1995;32(2):263-270.

20. Shook CA, Gillies RG, Sanders RSS. *Pipeline hydrotransport: With applications in the oil sand industry.* SRC Pipe Flow Technology Centre; 2002.

21. Thomas D. Transport characteristics of suspensions: III. laminar-flow properties of flocculated suspensions. *AI Ch.E.Journal*. 1961;7.

22. Kapur PC, Scales PJ, Boger DV, Healy TW. Yield stress of suspensions loaded with size distributed particles. *AICHE J*. 1997;43(5):1171-1179.

23. Mpofu P, Addai-Mensah J, Ralston J. Influence of hydrolyzable metal ions on the interfacial chemistry, particle interactions, and dewatering behavior of kaolinite dispersions. *J Colloid Interface Sci*. 2003;261(2):349-359.

24. Nasser M, James A. Effect of polyacrylamide polymers on floc size and rheological behaviour of kaolinite suspensions. *Colloids Surf Physicochem Eng Aspects*. 2007;301(1):311-322.

25. Nasser M, James A. The effect of polyacrylamide charge density and molecular weight on the flocculation and sedimentation behaviour of kaolinite suspensions. *Separation and purification technology*. 2006;52(2):241-252.

26. van Olphen H. Clay mineralogy. In: *An introduction to clay colloid chemistry for clay technologists, geologists and soil scientists.* New York, USA: John Wiley & Sons, Inc; 1963:59.

27. Van Olphen H, Hsu PH. An introduction to clay colloid chemistry. *Soil Sci*. 1978;126(1):59.

28. Nasser M, James A. Settling and sediment bed behaviour of kaolinite in aqueous media. *Separation and Purification Technology*. 2006;51(1):10-17.

29. Rand B, Melton IE. Particle interactions in aqueous kaolinite suspensions: I. effect of pH and electrolyte upon the mode of particle interaction in homoionic sodium kaolinite suspensions. *J Colloid Interface Sci*. 1977;60(2):308-320.

30. Addai-Mensah J. Enhanced flocculation and dewatering of clay mineral dispersions. *Powder Technol*. 2007;179(1):73-78.

31. McFarlane AJ, Addai-Mensah J, Bremmel K. Rheology of flocculated kaolinite dispersions. *Korea-Australia Rheology Journal*. 2005;17(4):181.

32. Nasser M, James A. Compressive and shear properties of flocculated kaolinite–polyacrylamide suspensions. *Colloids Surf Physicochem Eng Aspects*. 2008;317(1):211-221.

33. Nasser MS, James AE. The effect of polyacrylamide charge density and molecular weight on the flocculation and sedimentation behaviour of kaolinite suspensions. *Separation and Purification Technology*. 2006;52(2):241-252. doi: http://dx.doi.org/10.1016/j.seppur.2006.04.005.

34. Vaezi G F, Sanders RS, Masliyah JH. Flocculation kinetics and aggregate structure of kaolinite mixtures in laminar tube flow. *J Colloid Interface Sci*. 2011;355(1):96-105.

35. Klein C. *Effect of residual bitumen on polymer-assisted flocculation of fluid fine tailings.* [Master of Science]. University of Alberta; 2014.

36. Eisma D, Bale A, Dearnaley M, et al. Intercomparison of in situ suspended matter (floc) size measurements. *J Sea Res*. 1996;36(1):3-14.

37. Blanco A, De La Fuente E, Negro C, Monte MC, Tihero J. Focused beam reflectant measurement as a tool to measure flocculation. *Tappi J*. 2002;1(10):14-20.

38. Jarvis P, Jefferson B, Parsons SA. Breakage, regrowth, and fractal nature of natural organic matter flocs. *Environ Sci Technol*. 2005;39(7):2307-2314.

39. Li T, Zhu Z, Wang D, Yao C, Tang H. Characterization of floc size, strength and structure under various coagulation mechanisms. *Powder Technol*. 2006;168(2):104-110. doi: http://dx.doi.org/10.1016/j.powtec.2006.07.003.

40. Mikkelsen O, Pejrup M. The use of a LISST-100 laser particle sizer for in-situ estimates of floc size, density and settling velocity. *Geo-Mar Lett*. 2001;20(4):187-195.

41. Blanco A, Negro C, Tijero J, Hooimeijer A. Influence of salt on the interaction of polymers with the different pulp fractions. . 1994;1:55.

42. Blanco A, Negro C, Hooimeijer A, Tijero J. Polymer optimization in paper mills by means of a particle size analyser: An alternative to zeta potential measurements. *Appita J*. 1996;49(2):113-116.

43. Yoon S, Deng Y. Flocculation and reflocculation of clay suspension by different polymer systems under turbulent conditions. *J Colloid Interface Sci*. 2004;278(1):139-145.

44. Yu W, Erickson K. Chord length characterization using focused beam reflectance measurement probe-methodologies and pitfalls. *Powder Technol*. 2008;185(1):24-30.

45. Rhodes MJ. Describing populations of particles. In: *Introduction to particle technology.* 2nd ed. Chichester, England: John Wiley & Sons; 2008:4.

46. Rhodes MJ. Conversion between distributions. In: *Introduction to particle technology.* 2nd ed. Chichester, England: John Wiley & Sons; 2008:5.

47. Trotter R, Dhodapkar S. A guide to characterizing particle size and shape. *CEP Magazine*. 2014;July 2014:36.

48. Batchelor GK. *An introduction to fluid dynamics.* Cambridge university press; 2000.

49. Malkin AI. *Rheology fundamentals.* ChemTec Publishing; 1994.

50. Thornton S. The measurement of the absolute viscosity of anomalous fluids: I: The measurement of the time-dependence of viscosity of thixotropic materials. *Proceedings of the Physics Society. Section B*. 1953;66:115.

51. Walls H, Caines SB, Sanchez AM, Khan SA. Yield stress and wall slip phenomena in colloidal silica gels. *Journal of Rheology (1978-present)*. 2003;47(4):847-868.

52. Scott Blair GW. *Physics*. 1933;4:113.

53. Yoshimura A, Prud'homme RK. Wall slip corrections for couette and parallel disk viscometers. *Journal of Rheology (1978-present)*. 1988;32(1):53-67.

54. Shook CA, Rocco MC. *Slurry flow: Principles and practice.* Boston: Butterworth-Heinemann; 1991.

55. Dzuy NQ, Boger DV. Yield stress measurement for concentrated suspensions. *Journal of Rheology*. 1983;27(4):321-349.

56. Pullum L. Homogeneous slurries: An applied rheology lesson. BHR 19 Pre-Conference Workshop, Golden Co . 2014;1(1):1-13.

57. Rahman MH. *Yield stresses of mixtures with bimodal size distrubutions.* [Master of Science]. University of Alberta; 2011.

58. Zhou Z, Solomon MJ, Scales PJ, Boger DV. The yield stress of concentrated flocculated suspensions of size distributed particles. *Journal of Rheology (1978-present)*. 1999;43(3):651-671.

59. Rhodes MJ, Franks G. V. Colloids and fine particles. In: *Introduction to particle technology.* 2nd ed. Chichester, England: John Wiley & Sons; 2008:117.

60. Masliyah J, Zhou ZJ, Xu Z, Czarnecki J, Hamza H. Understanding water-based bitumen extraction from athabasca oil sands. *The Canadian Journal of Chemical Engineering*. 2004;82(4):628-654.

61. Butt H, Graf K, Kappl M. Surface forces. In: *Physics and chemistry of interfaces.* Wiley-VCH; 2003:80-116.

62. Butt H, Graf K, Kappl M. The electric double-layer. In: *Physics and chemistry of interfaces.* Wiley-VCH; 2003:42.

63. Israelachvilli JN. The charging of surfaces in liquids: The electric "double-layer". In: *Intermolecular and surface forces.* 3rd ed. Amsterdam, Netherlands: Elsevier Inc.; 2011:291.

64. Israelachvilli JN. Van der waals forces in a medium. In: *Intermolecular and surface forces.* 3rd ed. Elsevier Inc.; 2011:122.

65. Michaels AS, Bolger JC. The plastic flow behavior of flocculated kaolin suspensions. *Industrial & Engineering Chemistry Fundamentals*. 1962;1(3):153-162.

66. Addai-Mensah J. Colloidal forces, rheology and implications. BHR 19 Pre-Conference Workshop, Golden Co. 2014;1(1):1-3.

67. Thomas DG. Transport characteristics of suspensions VII. relation of hindered-settling floc characteristics to rheological parameters. *AIChE J*. 1963;9(3):310-316.

68. Michaels AS, Bolger JC. The plastic flow behavior of flocculated kaolin suspensions. *Industrial & Engineering Chemistry Fundamentals*. 1962;1(3):153-162.

69. KwongáLeong Y. Rheological evidence of adsorbate-mediated short-range steric forces in concentrated dispersions. *Journal of the Chemical Society, Faraday Transactions*. 1993;89(14):2473-2478.

70. Leong Y, Scales PJ, Healy TW, Boger DV. Effect of particle size on colloidal zirconia rheology at the isoelectric point. *J Am Ceram Soc*. 1995;78(8):2209-2212.

71. Pignon F, Magnin A, Piau J, Cabane B, Lindner P, Diat O. Yield stress thixotropic clay suspension: Investigations of structure by light, neutron, and x-ray scattering. *Physical Review E*. 1997;56(3):3281.

72. Lifschitz EM. *Soviet Physics JEPT (english translation)*. 1956;2:73.

73. Dzyaloshinskii IE, Lifschitz EM, Pitaevski LP. *Advanced Physics*. 1961;10:165.

74. Israelachvilli JN. Nonretarded Hamaker constants calculated on the basis of the Lifshitz theory. In: *Intermolecular and surface forces.* 3rd ed. Elsevier; 2011:260.

75. Scales PJ, Johnson SB, Healy TW, Kapur PC. Shear yield stress of partially flocculated colloidal suspensions. *AIChE J*. 1998;44(3):538-544.

76. Johnson SB, Franks GV, Scales PJ, Boger DV, Healy TW. Surface chemistry–rheology relationships in concentrated mineral suspensions. *Int J Miner Process*. 2000;58(1):267-304.

77. Butt H, Graf K, Kappl M. Types of potentials. In: *Physics and chemistry of inerfactes.* Wiley-VCH Verlag & Co. KGaA; 2003:77.

78. Masliyah J, Czarnecki J, Xu Z. *Handbook on theory and practice of bitumen recovery from Athabasca oil sands.* Canada: Kinsgley; 2011.

79. Klein C, Hurlbut CSJ. *Manual of mineralogy.* 21st ed. New York, USA: John Wiley & Sons; 1993.

80. Braggs B, Fornasiero D, Ralston J, Smart RS. The effect of surface modification by an organosilane on the electrochemical properties of kaolinite. *Clays Clay Miner*. 1994;42(2):123-136.

81. Fleer G, Stuart C. MA; scheutjens, JMHM; cosgrove, T.; vincent, B. *Polymers at interfaces*. 1993;2.

82. Hogg R. Flocculation and dewatering. *Int J Miner Process*. 2000;58(1):223-236.

83. Hogg R, Bunnaul P, Suharyono H. Chemical and physical variables in polymer-induced flocculation. *Minerals and Metallurgical Processing*. 1993;10:81-81.

84. Ray D, Hogg R. Agglomerate breakage in polymer-flocculated suspensions. *J Colloid Interface Sci*. 1987;116(1):256-268.

85. Keys RO, Hogg R. Mixing problems in polymer flocculation. *AIChE Symposium Series*. 1979;75(190):63.

86. Johnson CP, Li X, Logan BE. Settling velocities of fractal aggregates. *Environ Sci Technol*. 1996;30(6):1911-1918.

87. Vreeker R, Hoekstra L, Den Boer D, Agterof W. Fractal aggregation of whey proteins. *Food Hydrocoll*. 1992;6(5):423-435.

88. Gregory J. The density of particle aggregates. *Water Science and Technology*. 1997;36(4):1-13. doi: http://dx.doi.org/10.1016/S0273-1223(97)00452-6.

89. Lee D, Chen G, Liao Y, Hsieh C. On the free-settling test for estimating activated sludge floc density. *Water Res*. 1996;30(3):541-550.

90. Bushell G, Yan Y, Woodfield D, Raper J, Amal R. On techniques for the measurement of the mass fractal dimension of aggregates. *Adv Colloid Interface Sci*. 2002;95(1):1-50.

91. Li D, Ganczarczyk J. Advective transport in activated sludge flocs. *Water Environ Res*. 1992;64(3):236-240.

92. Brakalov L. A connection between the orthokinetic coagulation capture efficiency of aggregates and their maximum size. *Chemical Engineering Science*. 1987;42(10):2373-2383.

93. Matsuo T, Unno H. Forces acting on floc and strength of floc. *Journal of the Environmental Engineering Division*. 1981;107(3):527-545.

94. Yukselen MA, Gregory J. The reversibility of floc breakage. *Int J Miner Process*. 2004;73(2–4):251-259. doi: http://dx.doi.org/10.1016/S0301-7516(03)00077-2.

95. Gregory J. Polymer adsorption and flocculation in sheared suspensions. *Colloids and Surfaces*. 1988;31:231-253.

96. Klimpel R, Somasundaran P, Moudgil B. Reagents in mineral technology. *Marcel Dekker, New York*. 1988;27:663.

97. Hogg R. The role of polymer adsorption kinetics in flocculation. *Colloids Surf Physicochem Eng Aspects*. 1999;146(1):253-263.

98. Biggs S. Steric and bridging forces between surfaces bearing adsorbed polymer: An atomic force microscopy study. *Langmuir*. 1995;11(1):156-162.

99. Alagha L, Wang S, Yan L, Xu Z, Masliyah J. Probing adsorption of polyacrylamide-based polymers on anisotropic basal planes of kaolinite using quartz crystal microbalance. *Langmuir*. 2013;29(12):3989-3998.

100. Rubio J, Kitchener J. The mechanism of adsorption of poly (ethylene oxide) flocculant on silica. *J Colloid Interface Sci*. 1976;57(1):132-142.

101. Pelssers E, Stuart MC, Fleer G. Kinetic aspects of polymer bridging: Equilibrium flocculation and nonequilibrium flocculation. *Colloids and Surfaces*. 1989;38(1):15-25.

102. Sengupta D, Kan J, Al Taweel A, Hamza H. Dependence of separation properties on flocculation dynamics of kaolinite suspension. *Int J Miner Process*. 1997;49(1):73-85.

103. Farrow J, Johnston R, Simic K, Swift J. Consolidation and aggregate densification during gravity thickening. *Chem Eng J*. 2000;80(1):141-148.

104. Sworska A, Laskowski J, Cymerman G. Flocculation of the syncrude fine tailings: Part II. effect of hydrodynamic conditions. *Int J Miner Process*. 2000;60(2):153-161.

105. Scheiner B, Smelley A. Dewatering of fine particle mining wastes using polyethylene oxide flocculant. *Minerals and Metallurgical processing*. 1984;1(1):71-75.

106. McFarlane AJ, Bremmell K, Addai-Mensah J. Optimising the dewatering behaviour of clay tailings through interfacial chemistry, orthokinetic flocculation and controlled shear. *Powder Technol*. 2005;160(1):27-34.

107. Fan A, Turro NJ, Somasundaran P. A study of dual polymer flocculation. *Colloids Surf Physicochem Eng Aspects*. 2000;162(1):141-148.

108. Ovenden C, Xiao H. Flocculation behaviour and mechanisms of cationic inorganic microparticle/polymer systems. *Colloids Surf Physicochem Eng Aspects*. 2002;197(1):225-234.

109. Nabzar L, Pefferkorn E. An experimental study of kaolinite crystal edge-polyacrylamide interactions in dilute suspensions. *J Colloid Interface Sci*. 1985;108(1):243-248.

110. Lee L, Rahbari R, Lecourtier J, Chauveteau G. Adsorption of polyacrylamides on the different faces of kaolinites. *J Colloid Interface Sci*. 1991;147(2):351-357.

111. Pearse M, Barnett J. Chemical treatments for thickening and filtration. *Filtr Sep*. 1980;17(5):465-468.

112. Zhou Y, Yu H, Wanless EJ, Jameson GJ, Franks GV. Influence of polymer charge on the shear yield stress of silica aggregated with adsorbed cationic polymers. *J Colloid Interface Sci*. 2009;336(2):533-543.

113. Koksal E, Ramachandran R, Somasundaran P, Maltesh C. Flocculation of oxides using polyethylene oxide. *Powder Technol*. 1990;62(3):253-259.

114. Pinder KL. Time dependent rheology of the tetrahydrofuran-hydrogen sulphide gas hydrate slurry. *The Canadian Journal of Chemical Engineering*. 1964;42(3):132-138.

115. Bruice PY. *Organic chemistry.* 6th ed. United States of America: Prentice Hall; 2011.

116. Spicer PT, Pratsinis SE. Shear-induced flocculation: The evolution of floc structure and the shape of the size distribution at steady state. *Water Res*. 1996;30(5):1049-1056. doi: http://dx.doi.org/10.1016/0043-1354(95)00253-7.

117. Li T, Zhu Z, Wang D, Yao C, Tang H. Characterization of floc size, strength and structure under various coagulation mechanisms. *Powder Technol*. 2006;168(2):104-110.

118. Sun R, Neelakantan R. Conversation regarding relative doses of anionic and cationic flocculant in A-C-A type flocculation systems. . 2015.

119. Bailey FE, Powell GM, Smith KL. *Industrial & Engineering Chemistry*. 1958;50(4).

120. Bailey FE, Callard RW. *Journal of Applied Polymer Science*. 1959;1:56-373.

121. Bluestone S, Mark JE, Flory PJ. *Macromolecules*. 1974;7:325.

122. Franks GV. Zeta potentials and yield stresses of silica suspensions in concentrated monovalent electrolytes: Isoelectric point shift and additional attraction. *J Colloid Interface Sci*. 2002;249(1):44-51.

123. Neelakantan R, Romaniuk N. Conversation regarding APEX tailings samples from Teck mine site. . 2015.

124. Fitzsimmons R, Posner A, Quirk J. Electron microscopic and kinetic study of the flocculation of calcium montmorillonite. *Isr J Chem*. 1970;8(3):301-314.

125. McGary C. Degradation of poly (ethylene oxide). *Journal of Polymer Science*. 1960;46(147):51-57.

126. Bailey FJ. *Poly (ethylene oxide).* Elsevier; 2012.

127. Hogg R. The role of polymer adsorption kinetics in flocculation. *Colloids Surf Physicochem Eng Aspects*. 1999;146(1–3):253-263. doi: http://dx.doi.org/10.1016/S0927-7757(98)00723-7.

Appendix A: Supplementary data

Table A.1: MagnaFloc 1011 density data

Batch 1			
Sample	**Mass (g)**	**% by mass**	**Volume fraction**
1	6.68	40.4	0.204
2	6.67	40.2	0.202
3	6.75	41.6	0.212
4	6.65	39.8	0.200
5	6.69	40.6	0.205
6	6.76	41.8	0.213
7	6.67	40.2	0.202
8	6.66	40.0	0.201
9	6.8	42.5	0.218
10	6.68	40.4	0.204
Batch 2			
Sample	**Mass (g)**	**% by mass**	**Volume fraction**
1	6.62	39.3	0.196
2	6.75	41.6	0.212
3	6.74	41.5	0.211
4	6.76	41.8	0.213
5	6.77	42.0	0.215
6	6.63	39.5	0.198
7	6.67	40.2	0.202
8	6.77	42.0	0.215
9	6.71	40.9	0.207
10	6.74	41.5	0.211
Batch 3			
Sample	**Mass (g)**	**% by mass**	**Volume fraction**
1	6.71	40.9	0.207
2	6.72	41.1	0.208
3	6.77	42.0	0.215
4	6.7	40.8	0.206
5	6.7	40.8	0.206
6	6.66	40.0	0.201
7	6.67	40.2	0.202
8	6.71	40.9	0.207
9	6.66	40.0	0.201
10	6.74	41.5	0.211

Table A.2: Magnafloc LT27G density data

Batch 1			
Sample	**Mass (g)**	**% by mass**	**Volume fraction**
1	6.72	41.1	0.208
2	6.76	41.8	0.213
3	6.77	42.0	0.215
4	6.76	41.8	0.213
5	6.75	41.6	0.212
6	6.74	41.5	0.211
7	6.71	40.9	0.207
8	6.78	42.2	0.216
9	6.74	41.5	0.211
10	6.76	41.8	0.213
Batch 2			
Sample	**Mass (g)**	**% by mass**	**Volume fraction**
1	6.8	42.5	0.218
2	6.8	42.5	0.218
3	6.82	42.9	0.221
4	6.8	42.5	0.218
5	6.8	42.5	0.218
6	6.76	41.8	0.213
7	6.82	42.9	0.221
8	6.85	43.4	0.224
9	6.76	41.8	0.213
10	6.78	42.2	0.216
Batch 3			
Sample	**Mass (g)**	**% by mass**	**Volume fraction**
1	6.82	42.9	0.221
2	6.76	41.8	0.213
3	6.75	41.6	0.212
4	6.79	42.3	0.217
5	6.75	41.6	0.212
6	6.76	41.8	0.213
7	6.76	41.8	0.213
8	6.77	42.0	0.215
9	6.78	42.2	0.216
10	6.77	42.0	0.215

Table A.3: A-C-A density data

Batch 1			
Sample	**Mass (g)**	**% by mass**	**Volume concentration**
1	6.67	40.2	0.202
2	6.67	40.2	0.202
3	6.7	40.8	0.206
4	6.58	38.6	0.192
5	6.72	41.1	0.208
6	6.53	37.6	0.185
7	6.76	41.8	0.213
8	6.65	39.8	0.2
9	6.57	38.4	0.190
10	6.7	40.8	0.206
Batch 2			
Sample	**Mass (g)**	**% by mass**	**Volume concentration**
1	6.68	40.4	0.204
2	6.77	42.0	0.215
3	6.66	40.0	0.201
4	6.58	38.6	0.192
5	6.62	39.3	0.196
6	6.69	40.6	0.205
7	6.69	40.6	0.205
8	6.73	41.3	0.210
9	6.74	41.5	0.211
10	6.65	39.8	0.200
Batch 3			
Sample	**Mass (g)**	**% by mass**	**Volume concentration**
1	6.67	40.2	0.202
2	6.72	41.1	0.208
3	6.74	41.5	0.211
4	6.61	39.1	0.195
5	6.59	38.8	0.193
6	6.69	40.6	0.205
7	6.66	40.0	0.201
8	6.66	40.0	0.201
9	6.69	40.6	0.205
10	6.69	40.6	0.205

Table A.4: LT27AG pH 7 density data

Batch 1			
Sample	**Mass (g)**	**% by mass**	**Volume concentration**
1	6.82	43.8	0.221
2	6.87	43.7	0.227
3	6.89	44.0	0.229
4	6.74	41.5	0.211
5	6.83	43.0	0.222
6	6.85	43.4	0.224
7	6.83	43.0	0.222
8	6.81	42.7	0.219
9	6.73	41.3	0.210
10	6.85	43.4	0.224
Batch 2			
Sample	**Mass (g)**	**% by mass**	**Volume concentration**
1	6.8	42.5	0.218
2	6.94	44.9	0.235
3	6.88	43.9	0.228
4	6.77	42.0	0.215
5	6.95	45.0	0.236
6	6.87	43.7	0.227
7	6.81	42.7	0.219
8	6.89	44.0	0.229
9	6.93	44.7	0.234
10	6.88	43.9	0.228
Batch 3			
Sample	**Mass (g)**	**% by mass**	**Volume concentration**
1	6.74	41.5	0.211
2	6.84	43.2	0.223
3	6.86	43.5	0.226
4	6.74	41.5	0.211
5	6.76	41.8	0.213
6	6.72	41.1	0.208
7	6.79	42.3	0.217
8	6.88	43.9	0.228
9	6.76	41.8	0.213
10	6.81	42.7	0.219

Table A.5: Magnafloc® LT27AG pH 8.5 yield stress data. T_{MAX} values are represented as an average of the three measurements taken from each pre-shear and sheared sample

		Pre-Shear		Sheared	
Sample	**Energy (kJ/m^3)**	**T_{MAX} (μN·m)**	**τ_v (Pa)**	**T_{MAX} (μN·m)**	**τ_v (Pa)**
1	84	2430	137	1788	101
2	91	2440	138	1815	102
3	87	2447	138	1477	83
4	104	2327	131	1535	87
5	75	2343	132	1630	92
6	77	2545	143	2070	117
7	94	2390	135	1505	85
8	184	2370	134	970	55
9	120	2120	120	1225	69
10	112	2300	130	1570	89
11	117	2370	134	1390	78
12	153	1920	108	850	48
13	165	1985	112	820	46
14	201	2168	122	690	39
15	197	2200	124	667	38
16	234	2253	127	713	40
17	252	1990	112	567	32
18	256	2003	113	693	39
19	284	2147	121	557	31
20	314	2415	136	685	39
21	275	2200	124	557	31
22	318	2367	133	607	34
23	367	2297	129	527	30
24	397	2017	114	453	26
25	377	2140	121	453	26
26	463	1913	108	303	17
27	364	2057	116	318	18
28	538	2487	140	320	18
29	555	2217	125	300	17
30	624	2432	137	303	17
31	787	2168	122	290	16
32	726	2022	114	197	11
33	745	2150	121	182	10
34	1178	2165	122	193	11
35	1046	2395	135	210	12
36	941	2080	117	187	11

Table A.6: Magnafloc® 1011 pH 8.5 yield stress data. T_{MAX} values are represented as an average of the three measurements taken from each pre-shear and sheared sample

		Pre-Shear		Sheared	
Sample	**Energy (kJ/m^3)**	**T_{MAX} (μN·m)**	**τ_v (Pa)**	**T_{MAX} (μN·m)**	**τ_v (Pa)**
1		2200	124	1708	96
2		2358	133	1725	97
3		2208	124	1370	77
4		2133	120	1250	70
5		1923	108	1020	57
6		2238	126	1083	61
7		2280	129	1010	57
8		2493	141	910	51
9		2013	113	670	38
10		2190	123	773	44
11		2085	118	743	42
12		2432	137	810	46
13		2155	121	630	36
14		2207	124	617	35
15		2450	138	527	30
16		2227	126	547	31
17		2230	126	540	30
18		1983	112	483	27
19		2058	116	513	29
20		2098	118	550	31
21		1940	109	365	21
22		2270	128	403	23
23		1965	111	263	15
24		2140	121	313	18
25		1848	104	250	14
26		2023	114	310	17
27		2148	121	217	12
28		2147	121	187	11
29		2433	137	327	18
30		2340	132	200	11

Table A.7: A-C-A pH 8.5 yield stress data. T_{MAX} values are represented as an average of the three measurements taken from each pre-shear and sheared sample

		Pre-Shear		Sheared	
Sample	**Energy (kJ/m^3)**	**T_{MAX} (μN·m)**	**τ_v (Pa)**	**T_{MAX} (μN·m)**	**τ_v (Pa)**
1	86	2895	163	2038	115
2	100	2673	151	1923	108
3	102	2000	113	910	51
4	13	2597	146	1183	67
5	155	2328	131	1178	66
6	146	2287	129	830	47
7	164	2152	121	740	42
8	183	2510	141	830	47
9	205	2437	137	727	41
10	218	2428	137	687	39
11	180	2360	133	442	25
12	255	2722	153	555	31
13	247	2567	145	473	27
14	299	2680	151	597	34
15	302	2855	161	503	28
16	263	2482	140	375	21
17	309	2655	150	547	31
18	337	2585	146	370	21
19	429	2510	141	393	22
20	495	2910	164	428	24
21	688	2232	126	277	16
22	475	2398	135	287	16
23	484	2590	146	240	14
24	453	2678	151	393	22
25	655	2147	121	198	11
26	908	2097	118	210	12
27	1036	3118	176	300	17
28	1018	1713	97	167	9
29	1081	2047	115	150	8
30	1096	1727	97	212	12

Table A.8: Magnafloc® LT27AG pH 7 yield stress data. T_{MAX} values are represented as an average of the three measurements taken from each pre-shear and sheared sample

		Pre-Shear		Sheared	
Sample	**Energy (kJ/m^3)**	**T_{MAX} (μN·m)**	**τ_v (Pa)**	**T_{MAX} (μN·m)**	**τ_v (Pa)**
1	80	2892	2245	163	127
2	167	2908	1163	164	66
3	291	2835	1178	160	66
4	306	3048	1023	172	58
5	506	2622	887	148	50
6	693	2668	850	150	48
7	977	2767	740	156	42
8	1580	2923	727	165	41
9	2145	2773	740	156	42
10	2690	2535	715	143	40

Table A.9: Magnafloc® LT27AG + poly(ethylene oxide) pH 8.5 yield stress data. T_{MAX} values are represented as an average of the three measurements taken from each pre-shear and sheared sample

		Pre-Shear		Sheared	
Sample	**Energy (kJ/m^3)**	**T_{MAX} (μN·m)**	**τ_v (Pa)**	**T_{MAX} (μN·m)**	**τ_v (Pa)**
1	1306	6990	394	2747	155
2	7048	5908	333	313	18

Table A.10: Teck Ore data

Mass Bitumen	Mass Solids	Mass Water	Mass Total	Bitumen	Solids	Water	Recovery	MBI	MBI corrected
11.31	86.52333	4.033333	101.6467	11.12667	85.12333	3.966667	100.2167	1.2343	1.2343

Pan (-45 µm) corrected	Sieve - #10 (+2000 µm)	Sieve - #18 (+1000 µm)	Sieve - #25 (+710 µm)	Sieve - #35 (+500 µm)	Sieve - #45 (+355 µm)	Sieve - #60 (250 µm)	Sieve - #80 (+180 µm)	Sieve - #120 (+125 µm)	Sieve - #200 (+75 µm)	Sieve - #325 (+45 µm)	Pan (-45 µm)	Recovery
23.5090522	0	0.053248	0.119808	0.612354	1.277955	1.863685	3.700746	23.62886	33.41321	11.82109	23.50905	99.23382

Percent Passing 2000 µm	Percent Passing 1000 µm	Percent Passing 710 µm	Percent Passing 500 µm	Percent Passing 355 µm	Percent Passing 250 µm	Percent Passing 180 µm	Percent Passing 125 µm	Percent Passing 75 µm	Percent Passing 44 µm	Percent Passing 31 µm	Percent Passing 22 µm	Percent Passing 16 µm	Percent Passing 11 µm	Percent Passing 7.8 µm	Percent Passing 6.6 µm	Percent Passing 3.9 µm	Percent Passing 2.8 µm	Percent Passing 1.9 µm	Percent Passing 1.3 µm
100	100	100	100	100	100	100	100	99.98	92.9	81.7	70.1	60.6	50.4	40.4	35.6	21.7	14.9	8.66	4.36
Differential 2000 µm	Differential 1000 µm	Differential 710 µm	Differential 500 µm	Differential 355 µm	Differential 250 µm	Differential 180 µm	Differential 125 µm	Differential 75 µm	Differential 44 µm	Differential 31 µm	Differential 22 µm	Differential 16 µm	Differential 11 µm	Differential 7.8 µm	Differential 6.6 µm	Differential 3.9 µm	Differential 2.8 µm	Differential 1.9 µm	Differential 1.3 µm
0	0	0	0	0	0	0	0	0.016	7.04	11.2	11.6	9.46	10.2	9.99	4.87	13.8	6.87	6.19	4.3

d10	d50	d90	< 2 µm	< 45 µm	< 74 µm
2.088	10.83	39.93	9.38	93.5	99.98

pH*	Conductivity	Ba	Ca	Fe	Mg	K	Na	cation	Cl	Alkalinity (as CaCO3)	Bicarbonate (HCO3)	Carbonate (CO3)	Hydroxide (OH)	Sulphate (SO4)
7.99	565		0.1		0.04	2.37	117.94		92.34		139.9524			14.47

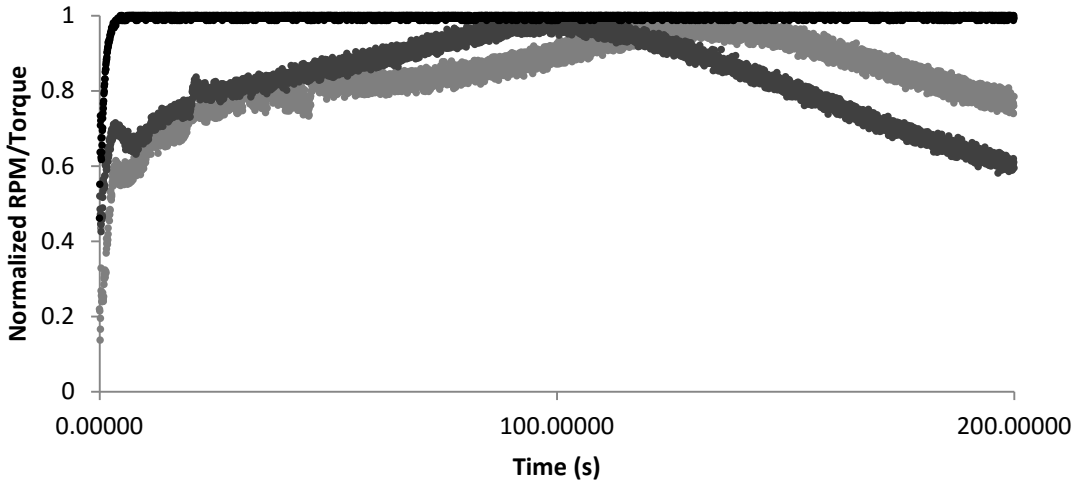

Figure A.1: (BLACK) Normalized RPM versus time. (DARK GREY) Sample 1 using 100g/tonne Magnafloc LT27AG and 200g/tonne poly(ethylene oxide), oeak torque occurs at approximately 95s. (LIGHT GREY) Sample 2, using 100g/tonne Magnafloc LT27AG and 200g/tonne poly(ethylene oxide), peak torque occurs at 135s.

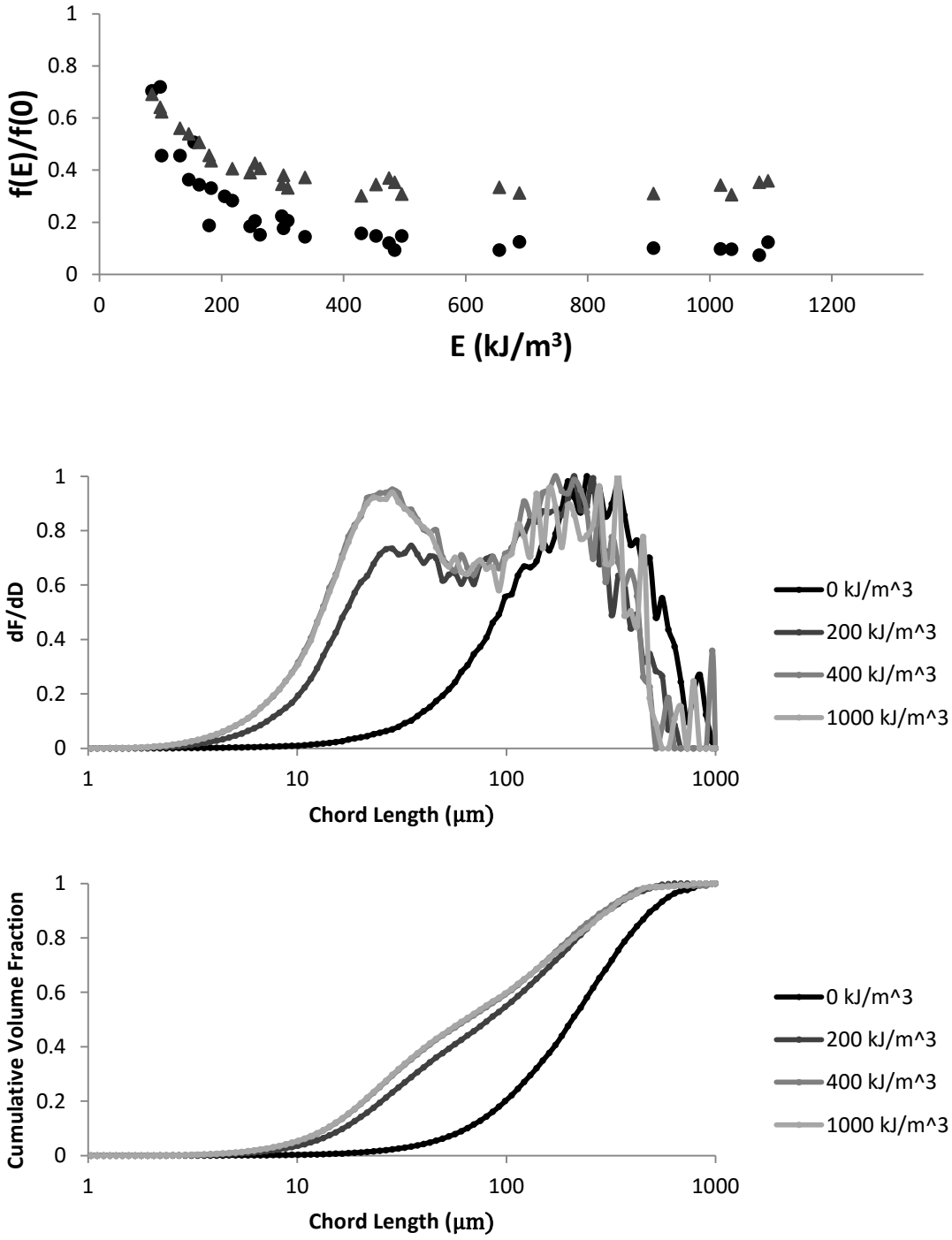

Figure A.2: Normalized functions of yield stress (●) and number volume mean diameter(▲) plotted as a function of shear energy input for 41% wt. paste flocculated with an A-C-A system (Magnafloc LT27AG at 100g/tonne + Hychem Hyperfloc CD 650 85g/tonne)(MIDDLE) Differential frequency distribution of particle volume of 41% by mass paste produced with **A-C-A** (100g/tonne Magnafloc LT27AG + 85g/tonne Hychem Hyperfloc CD650) at pH 8.5. (BOTTOM) Cumulative volume distribution of 41% by mass paste produced **A-C-A** (100g/tonne Magnafloc LT27AG + 85g/tonne Hychem Hyperfloc CD650)at pH 8.5

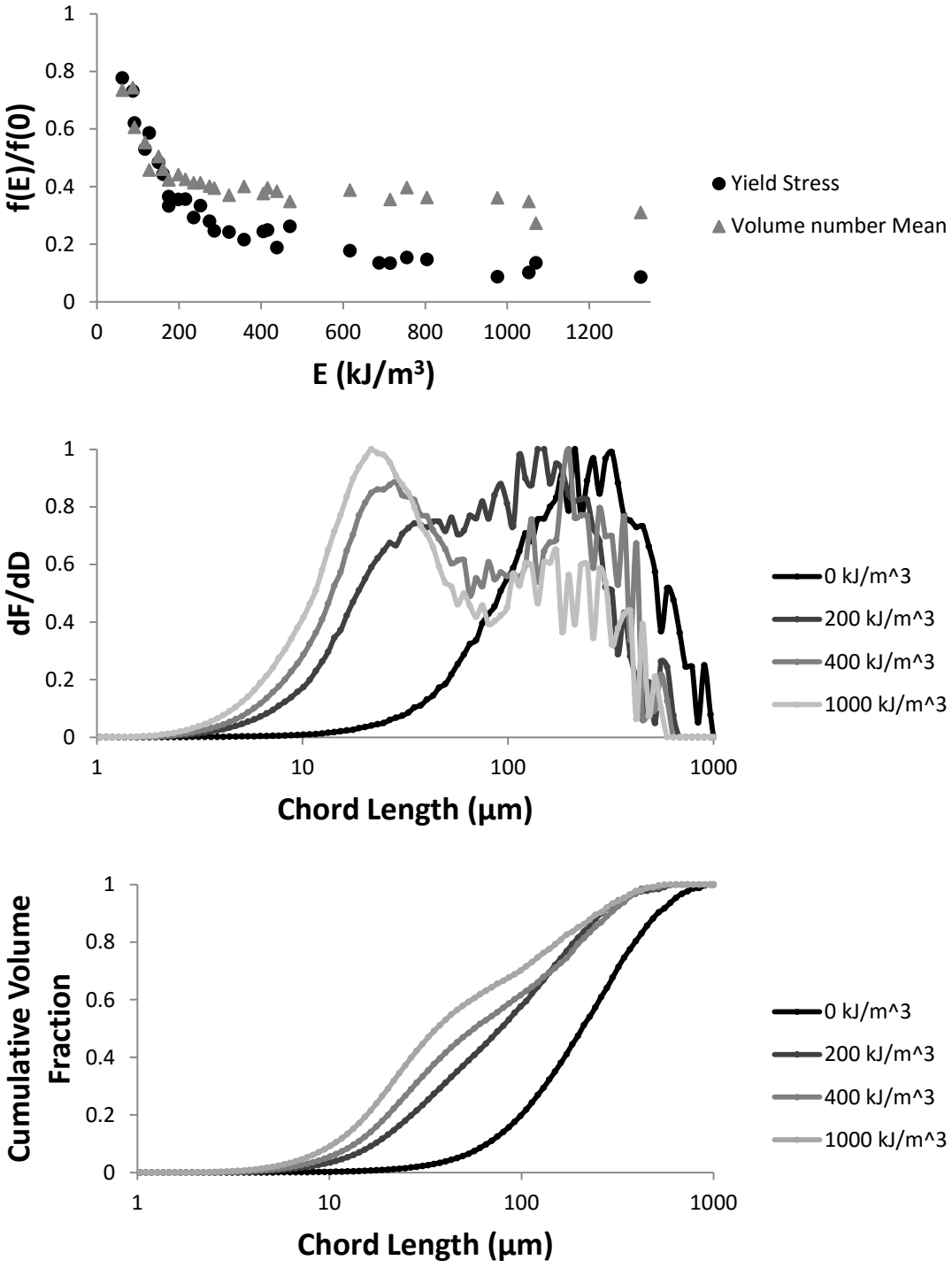

Figure A.3: (TOP) Normalized functions of yield stress and number volume mean diameter plotted as a function of shear energy input for 41% by mass paste flocculated with **Magnafloc® 1011** at 100g/tonne pH 8.5 (MIDDLE) Differential frequency distribution of particle volume of 41% by mass paste produced with 100g/tonne Magnafloc® 1011 at pH 8.5. (BOTTOM) Cumulative volume distribution of 41% by mass paste produced with 100g/tonne Magnafloc® 1011 at pH 8.5

Appendix B: Chord length distribution statistics and selection of proper chord length

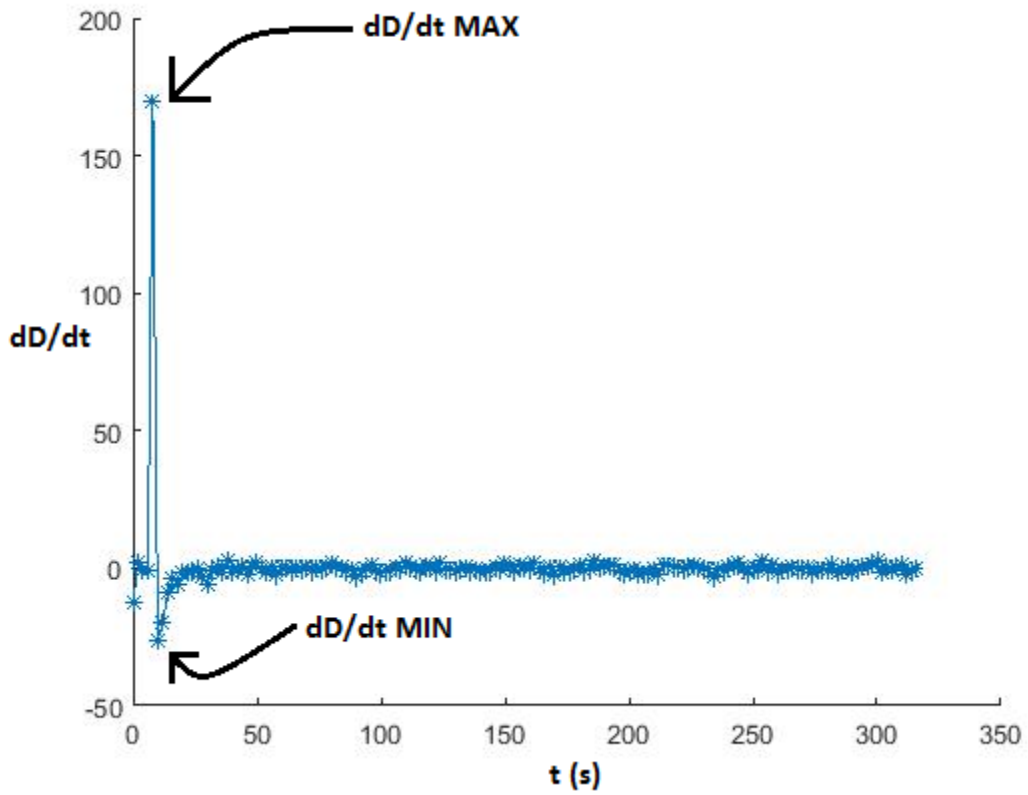

Figure B.1: dCL/dt versus t when dropping 41% by mass paste into stirring solution of de-ionized water

A Matlab code was formulated to select the most accurate particle chord length distribution, which based the selection on the establishment of a dynamic equilibrium. The model reported Sauter mean d_{50} values, and, with reference to figure A.2.1, the initial spike in dCL/dt (dCL/dt MAX) is a result of the addition of the addition of paste to the stirring de-ionized water with the larger particles settling more rapidly and the subsequent minimum dCL/dt (dCL/dt MIN) results from the larger particles being suspended as the mixture is homogenized. The dCL/dt reaches equilibrium when the mixture is homogeneous, and at this point the d_{50} measurement is the most accurate representation of particle

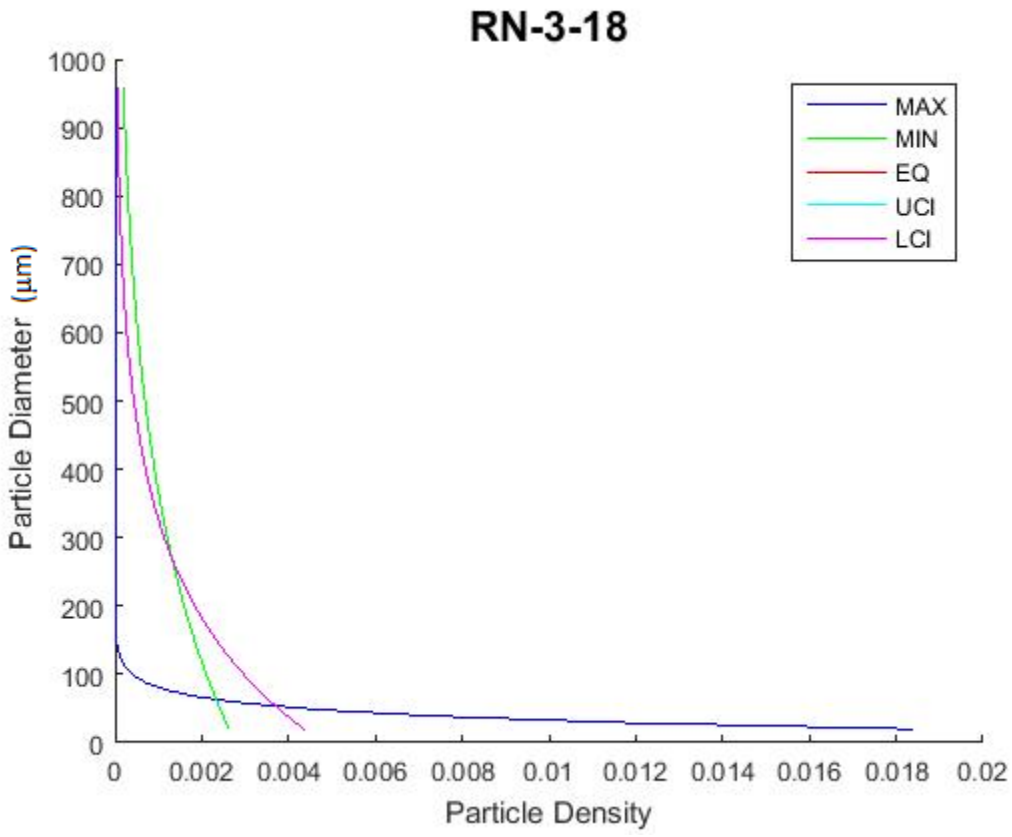

Figure B.2: Particle density functions of min dCL/dt, max dDdt and equilibrium showing the difference between these points

chord length distribution. The code selected the first point after dCL/dt MIN A where dCL/dt>-3 as the first point at equilibrium.

First, the chord length distributions at dCL/dt max and dCL/dt min were proven to be statistically different from the equilibrium points using an exponential fit model in Matlab. The null hypothesis (the null hypothesis being that the populations are equal, or, '$\mu=\mu_o$') of the distributions was rejected under all confidence intervals tested (95%, 90%, 80%). A typical result is shown in figure B.2 and distinctly shows that the chord length distributions at dCL/dt MAX and dCL/dt MIN diverge from the equilibrium value. In addition, the Matlab code also took the average and standard deviation of dCL/dt for the first 20 seconds

Table B.1: Statistical data for equilibrium conditions

Condition	dCL/dt (μm/s) MAX	dCL/dt (μm/s) MIN	Equilibrium (μm/s) dCL/dt mean	Equilibrium (μm/s) dCL/dt stdev	Range Max (μm/s) (+3 STDEV)	Range Min (μm/s) (-3 STDEV)
MF LT27AG pH 8.5 RN-3-15	129.1105	-16.3565	0.121999785	1.804476906	5.535430502	-5.291430932
MF LT27AG pH 8.5 RN-2-274	157.3824	-32.8307	-0.817214386	1.81767829	4.635820485	-6.270249256
MF LT27AG pH 8.5 RN-3-12	83.44614	-16.0029	-0.348879194	1.832374192	5.148243383	-5.846001771
MF LT27AG pH 7 RN-3-39	132.669	-3.58328	-0.822368397	1.539036506	3.79474112	-5.439477913
MF LT27AG pH 7 RN-3-40	201.9476	-45.6338	-0.626246254	0.963624964	2.264628638	-3.517121147
MF LT27AG pH 7 RN-3-42	149.6338	-13.883	-0.429464998	1.068898927	2.777231784	-3.63616178
MF 1011 pH 8.5 RN-2-288	155.6221	-22.7513	-0.745835869	2.891334807	7.928168553	-9.41984029
MF 1011 pH 8.5 RN-2-316	175.3124	-37.0134	-0.937234365	2.135646038	5.469703748	-7.344172478
MF 1011 pH 8.5 RN-3-24	159.5339	-21.8934	-0.179997081	1.656288164	4.78886741	-5.148861572
ACA pH 8.5 RN-2-345	161.6491	-19.185	-0.85662122	0.901568556	1.848084448	-3.561326887
ACA pH 8.5 RN-3-18	169.4879	-26.2074	-0.05733245	1.277384836	3.774822057	-3.889486957
ACA pH 8.5 RN-3-21	193.1439	-26.9366	-0.196063109	1.089785692	3.073293968	-3.465420186

starting from the first equilibrium point. The initial values, dCL/dt MAX and dCL/dt MIN, did not fall within three standard deviations of the equilibrium for all experiments except one, further demonstrating that dCL/dt max and dCL/dt min are not in equilibrium and hence do not sufficiently represent the true chord length distribution of the mixture. The data is shown in table B.1, clearly showing that dCL/dt MAX and dCL/dt MIN lie well outside the range of equilibrium.

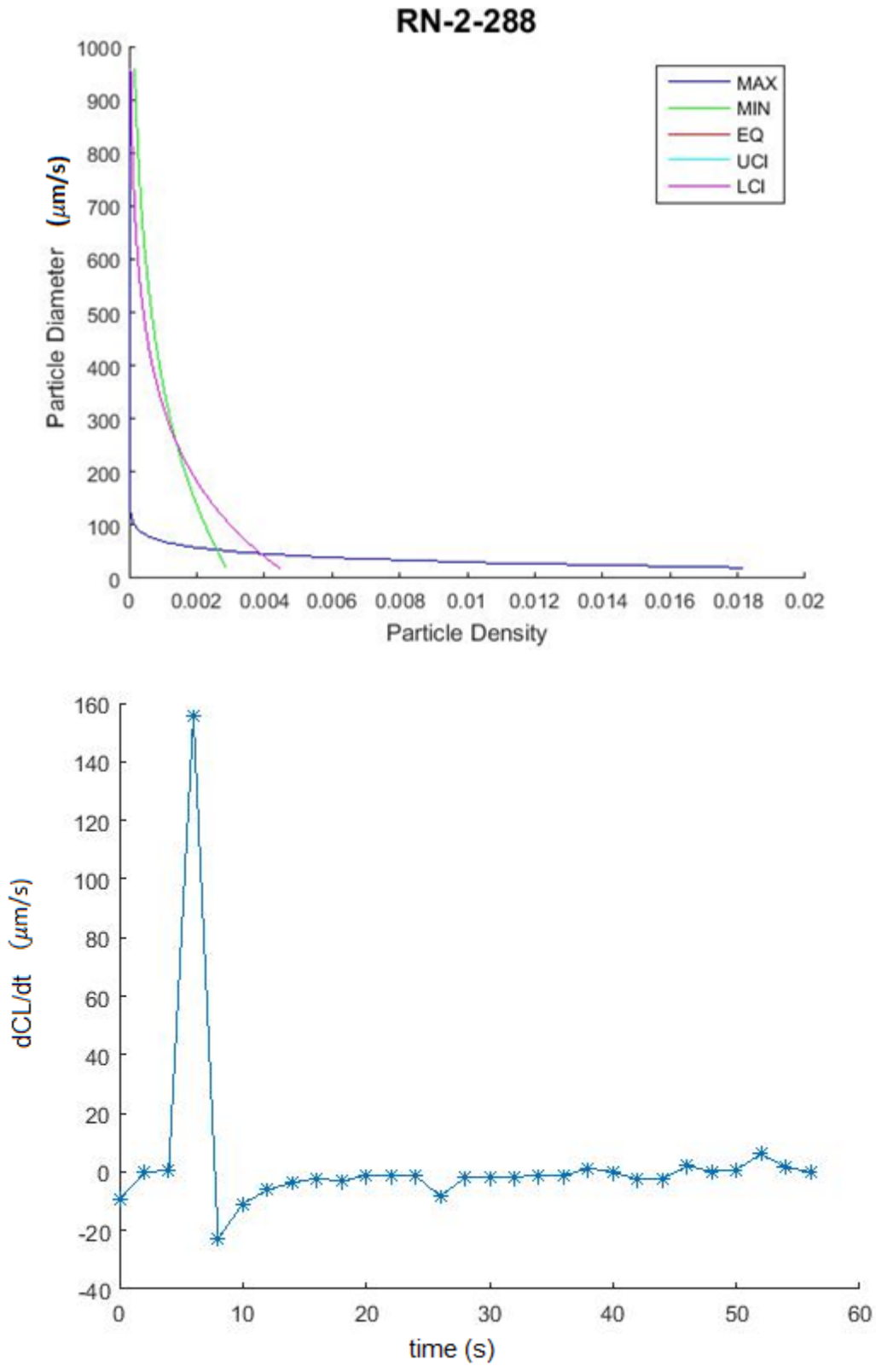

Figure B.3: Magnafloc 1011 pH 8.5 (TOP) Chord length distribution analysis (BOTTOM) dCL/dt vs t

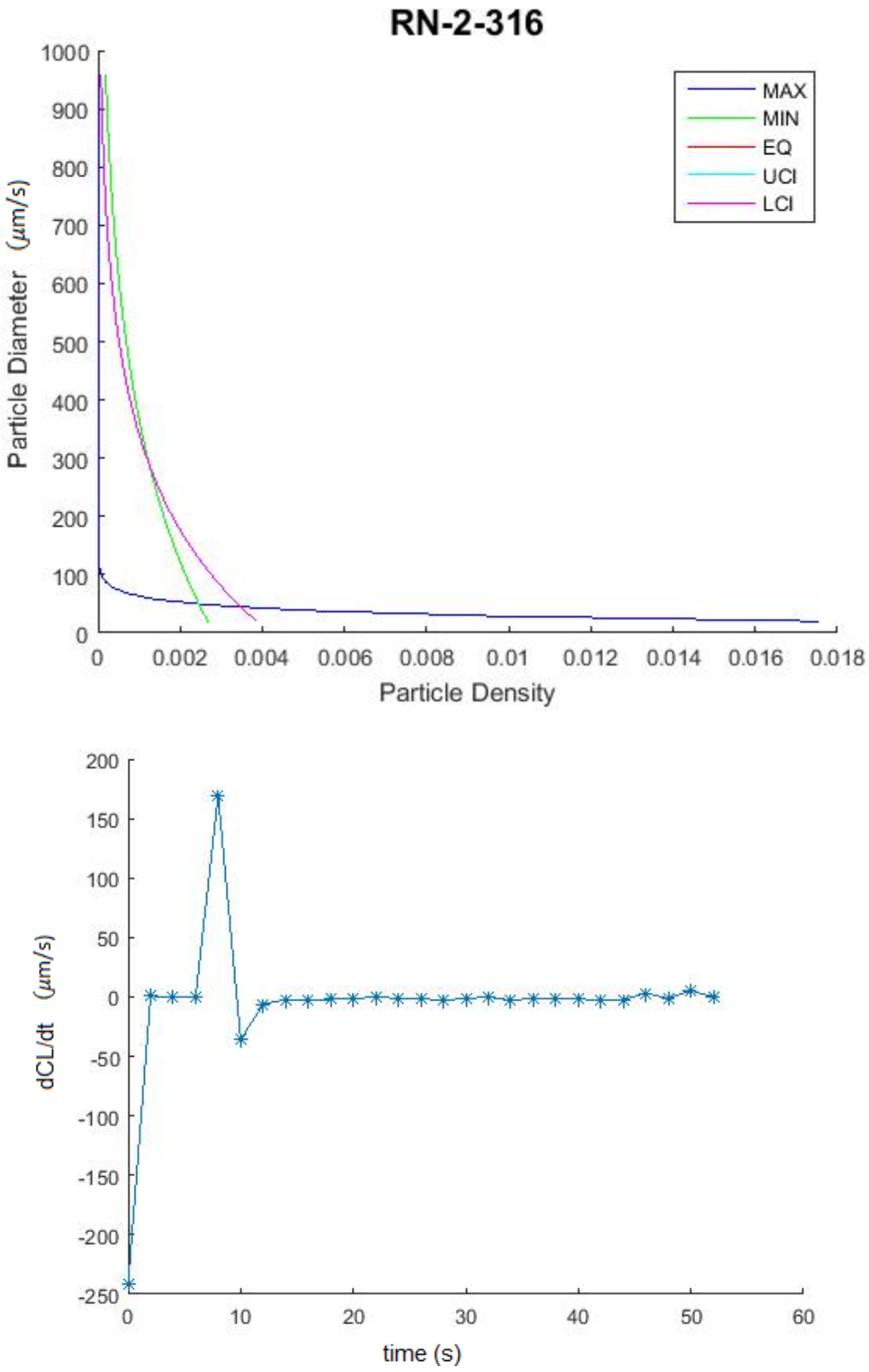

Figure B.4: Magnafloc 1011 pH 8.5 (TOP) Chord length distribution analysis (BOTTOM) dCL/dt vs t

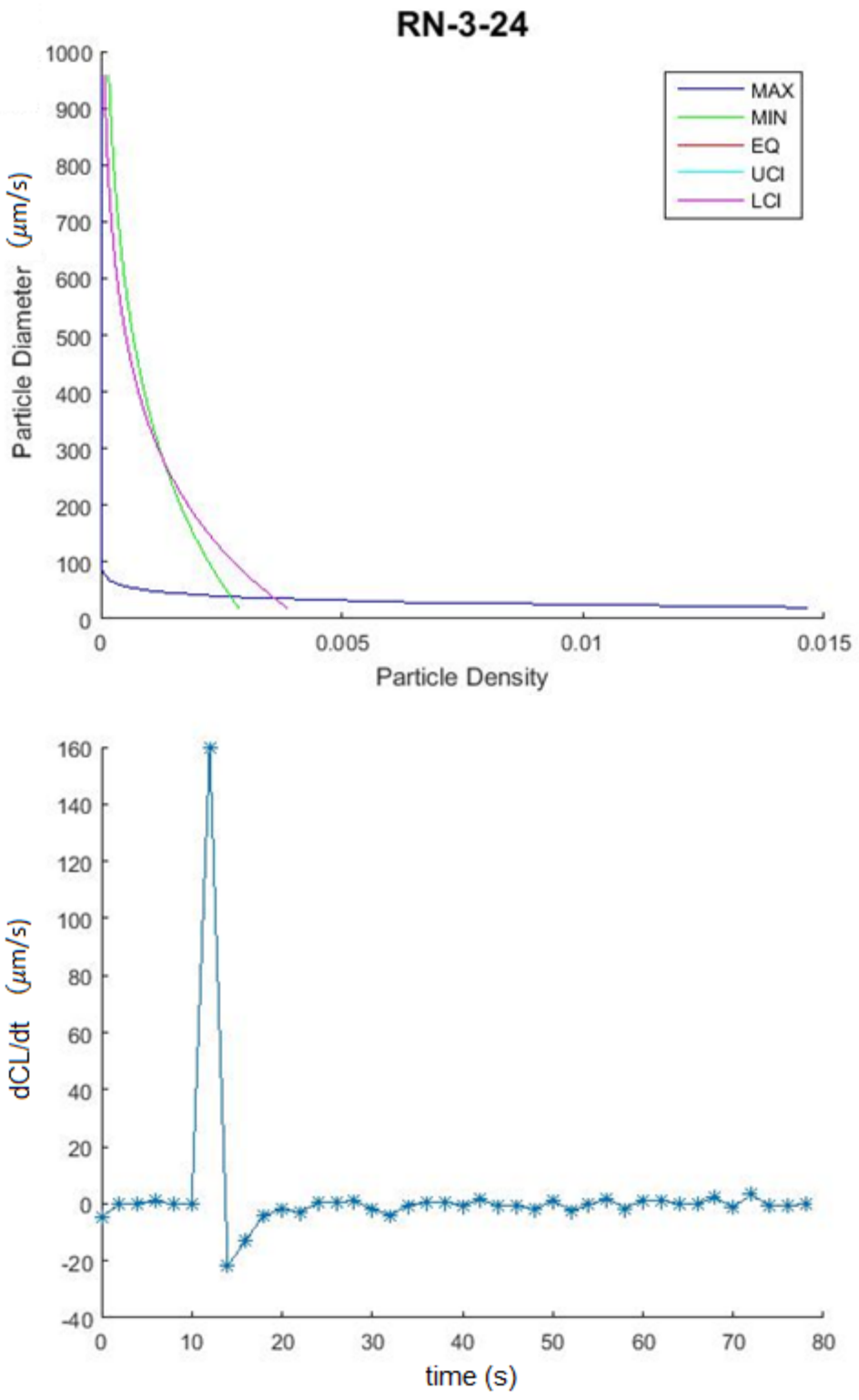

Figure B.5: Magnafloc 1011 pH 8.5 (TOP) Chord length distribution analysis (BOTTOM) dCL/dt vs t

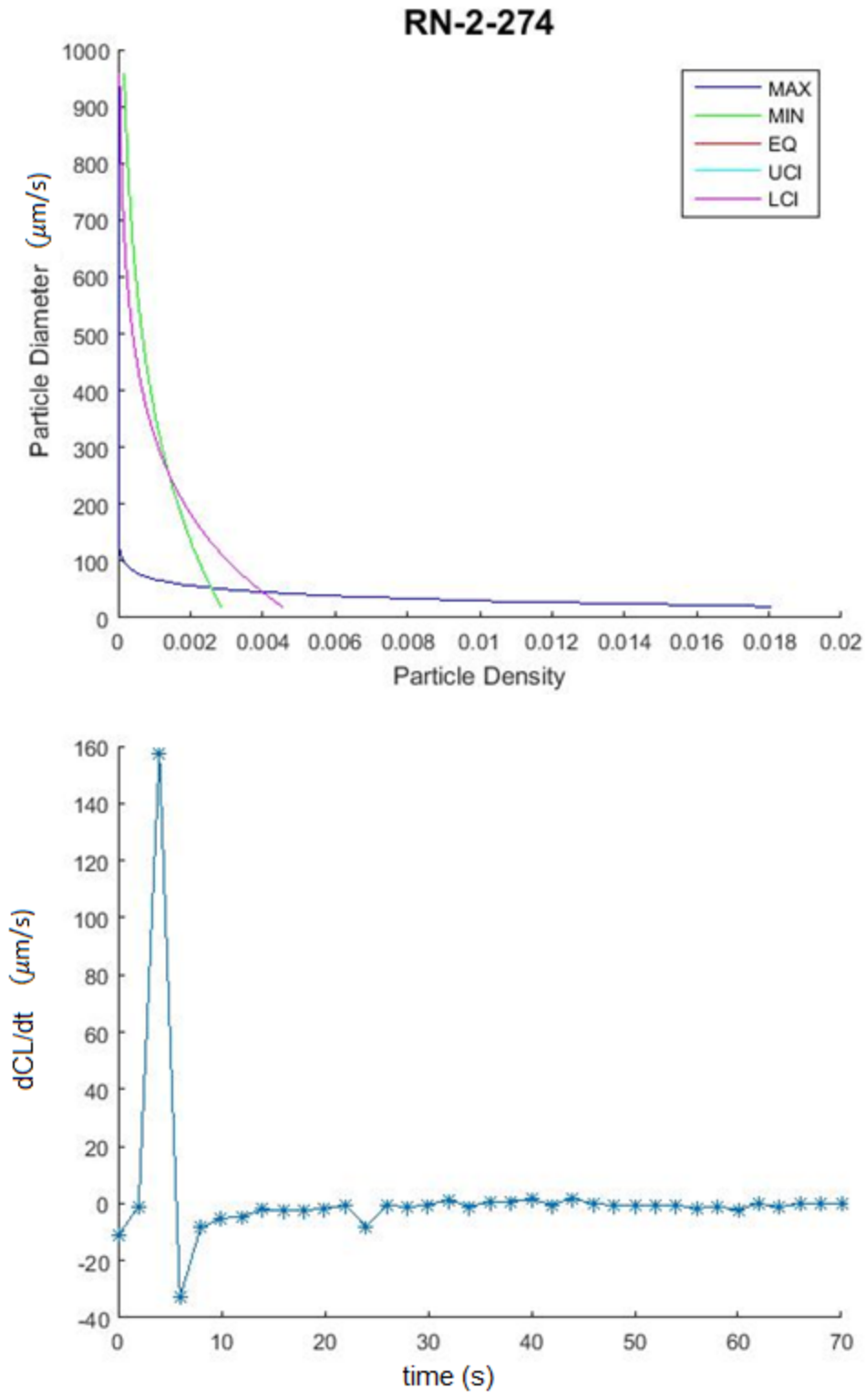

Figure B.6: Magnafloc LT27AG pH 8.5 (TOP) Chord length distribution analysis (BOTTOM) dCL/dt vs t

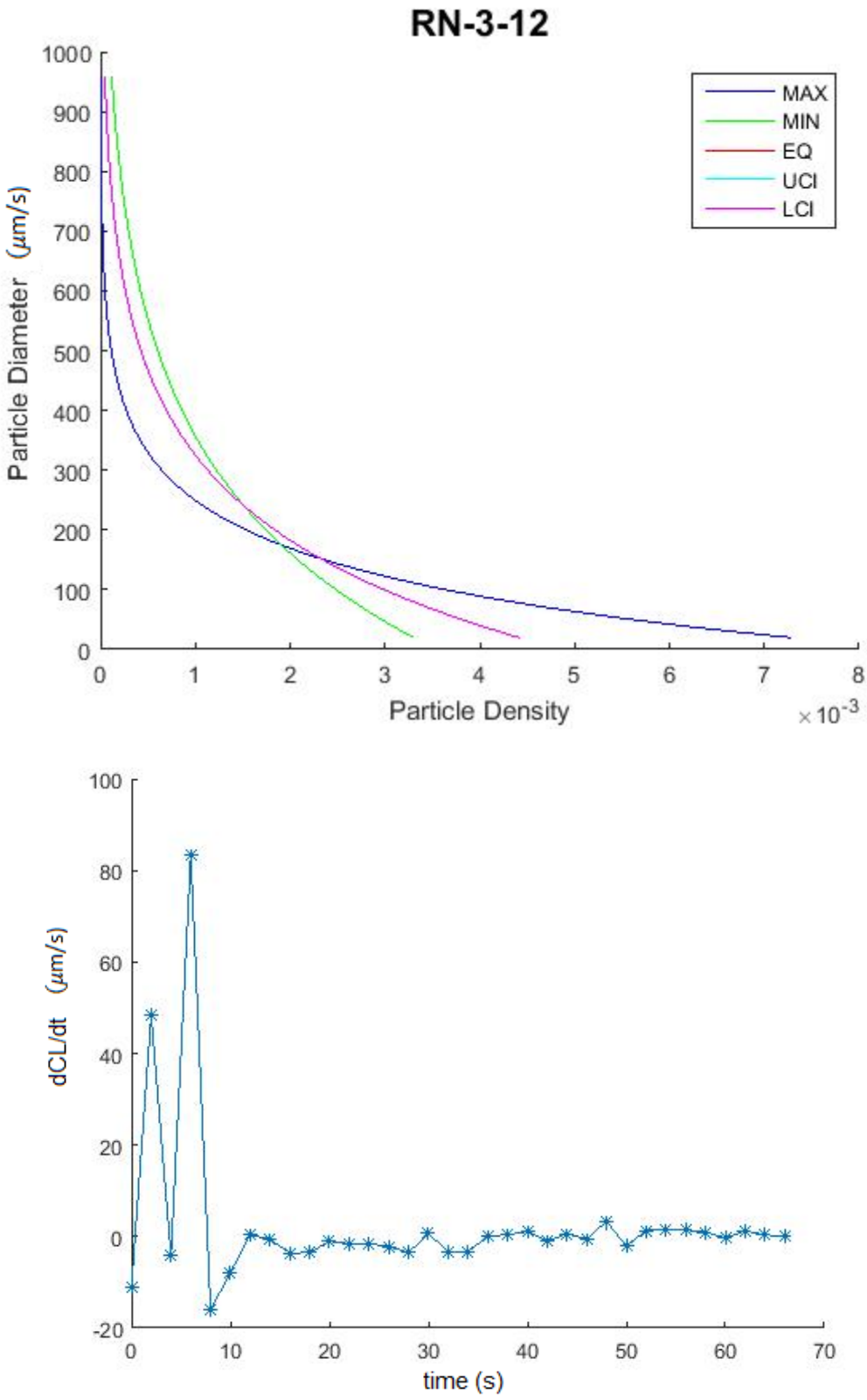

Figure B.7: Magnafloc LT27AG pH 8.5 (TOP) Chord length distribution analysis (BOTTOM) dCL/dt vs t

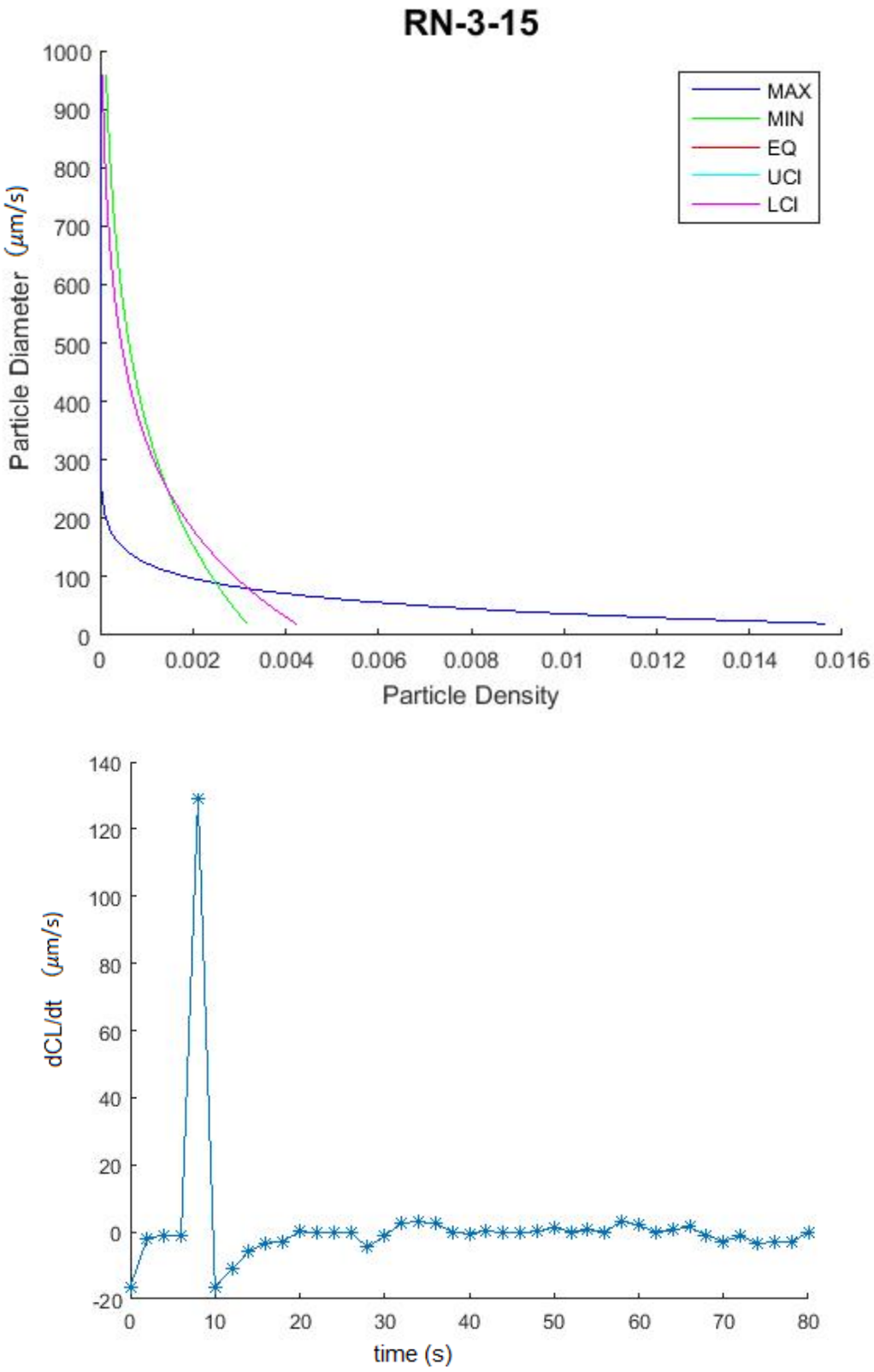

Figure B.8: Magnafloc LT27AG pH 8.5 (TOP) Chord length distribution analysis (BOTTOM) dCL/dt vs t

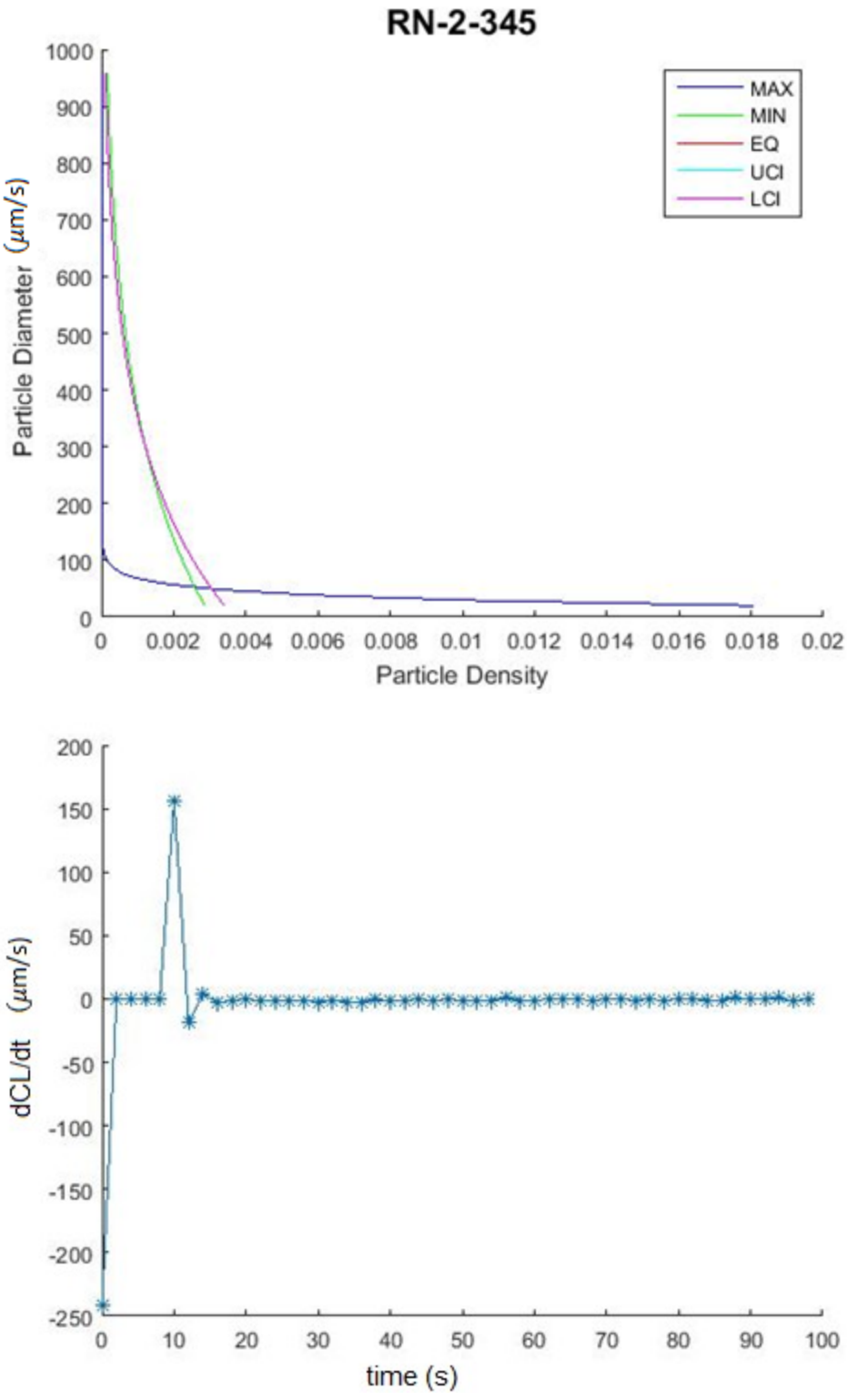

Figure B.9: A-C-A pH 8.5 (TOP) Chord length distribution analysis (BOTTOM) dCL/dt vs t

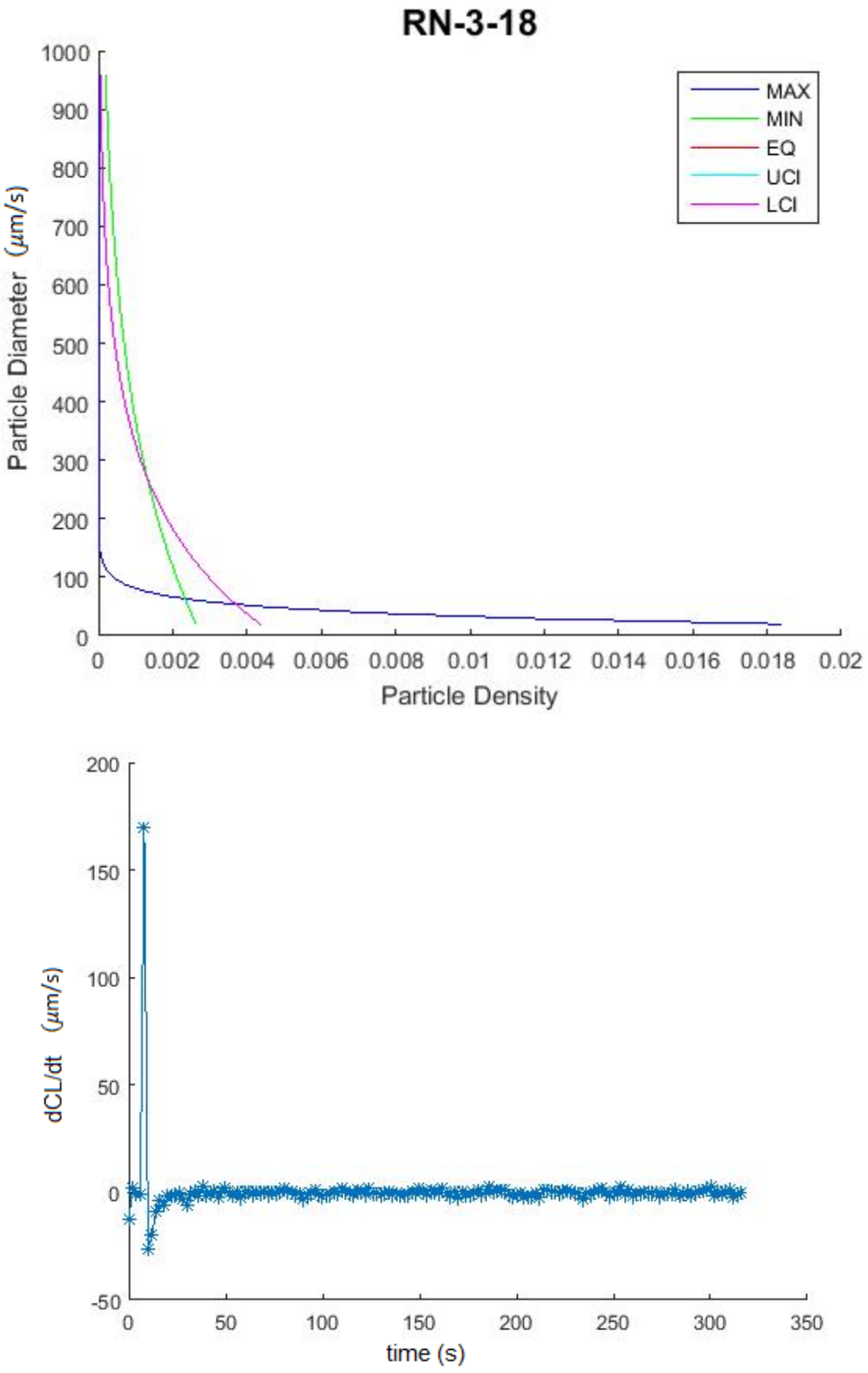

Figure B.10: A-C-A pH 8.5 (TOP) Chord length distribution analysis (BOTTOM) dCL/dt vs t

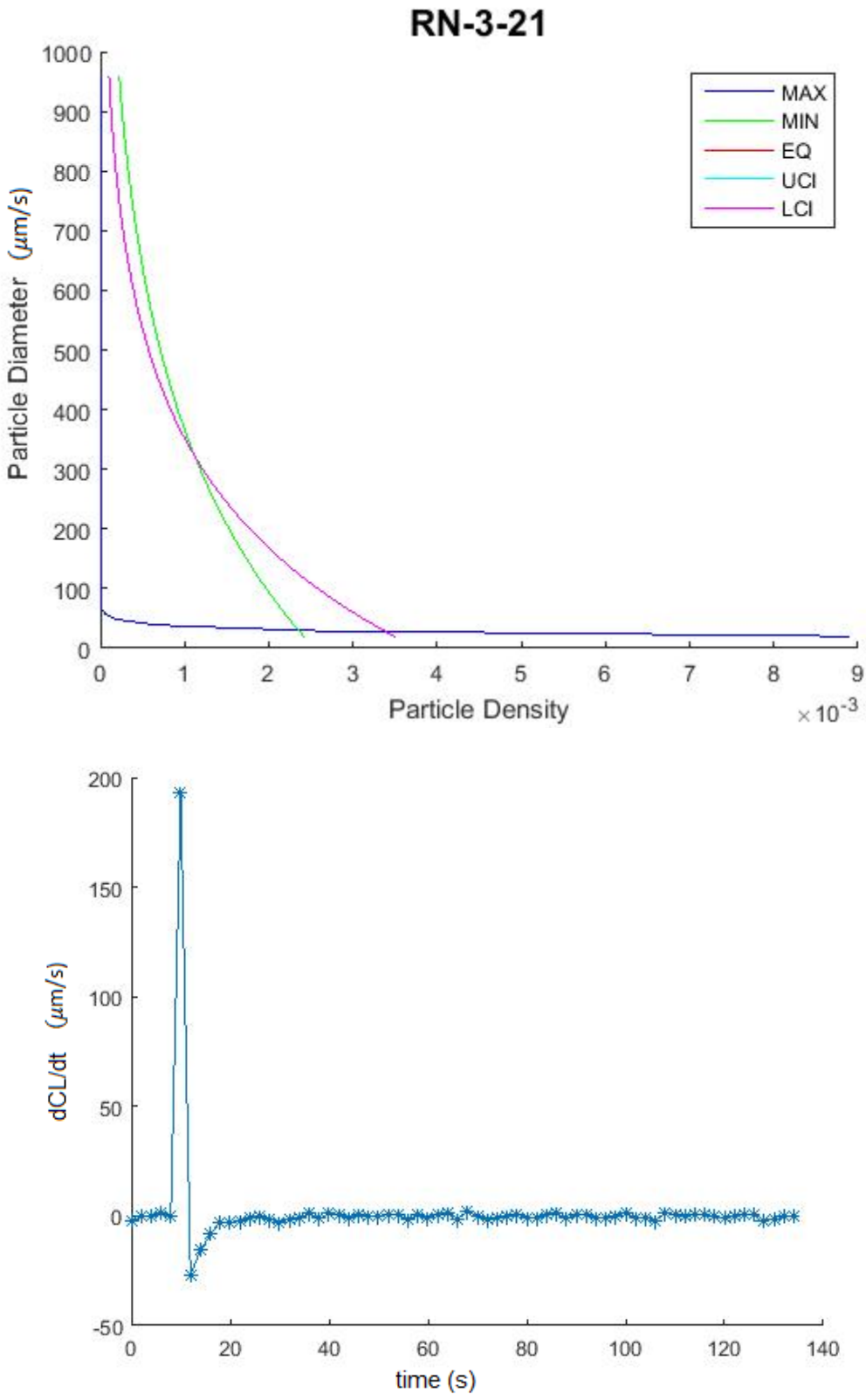

Figure B.11: A-C-A pH 8.5 (TOP) Chord length distribution analysis (BOTTOM) dCL/dt vs t

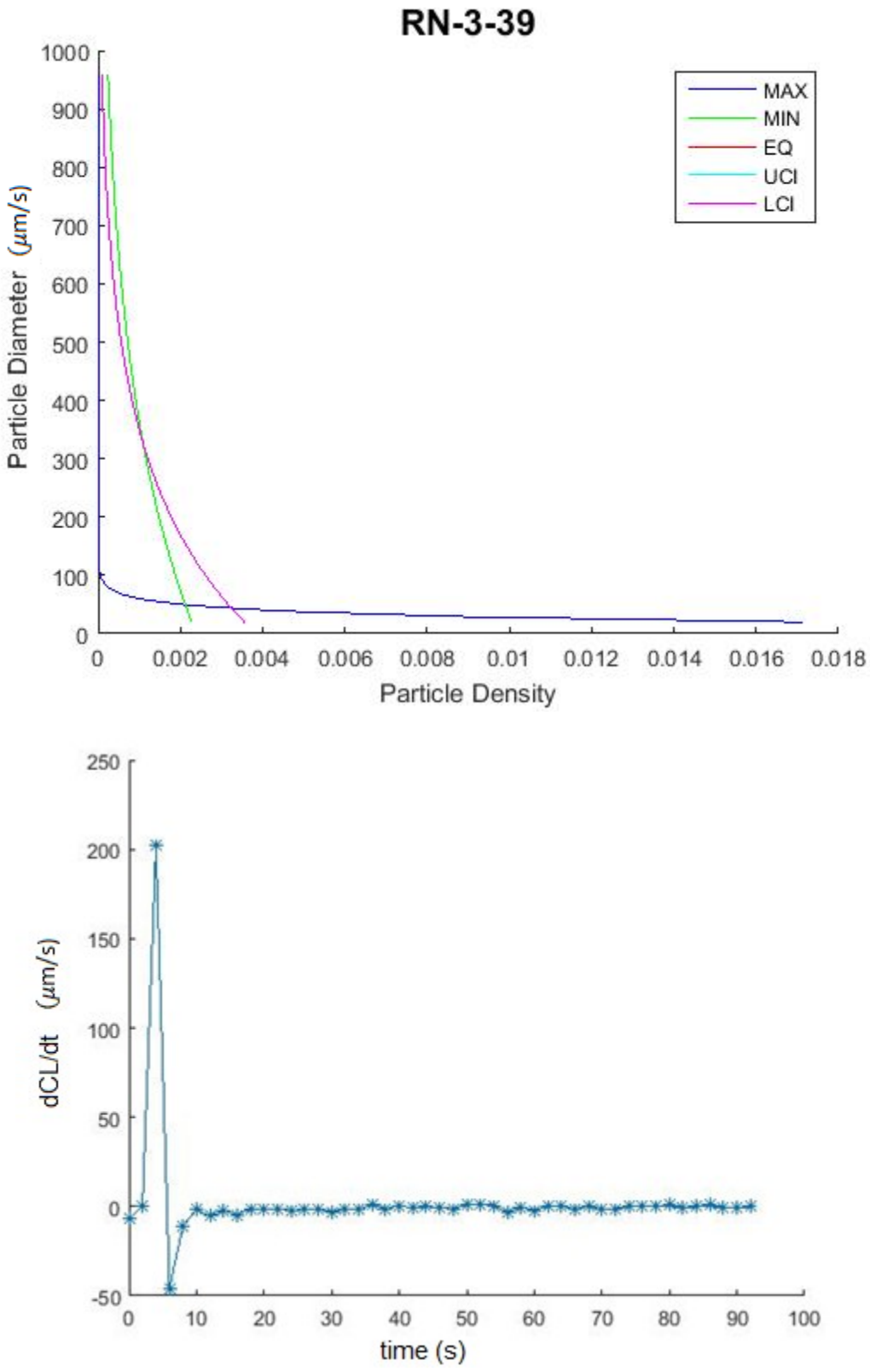

Figure B.12: Magnafloc LT27AG pH 7 (TOP) Chord length distribution analysis (BOTTOM) dCL/dt vs t

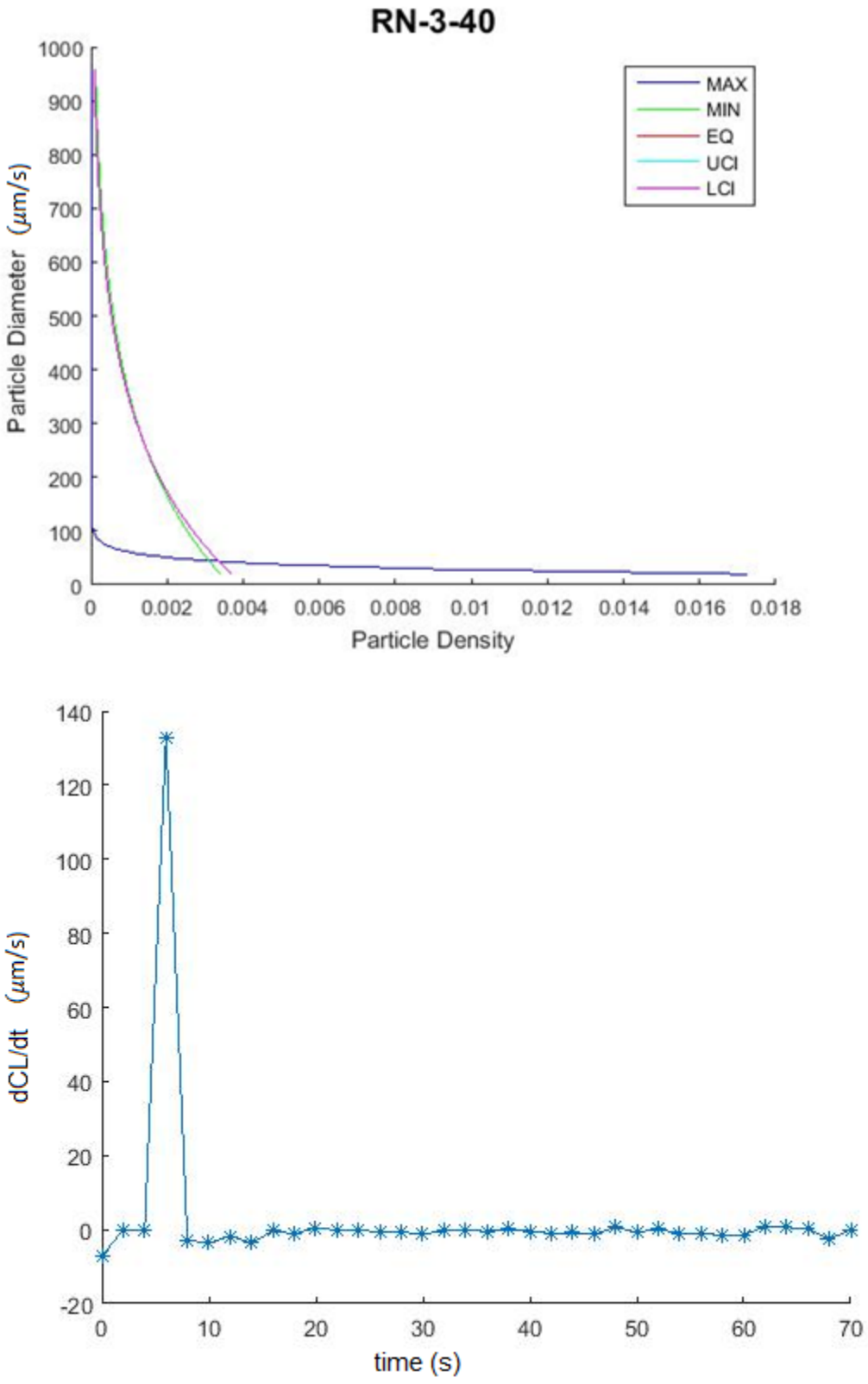

Figure B.13: Magnafloc LT27AG pH 7 (TOP) Chord length distribution analysis (BOTTOM) dCL/dt vs t

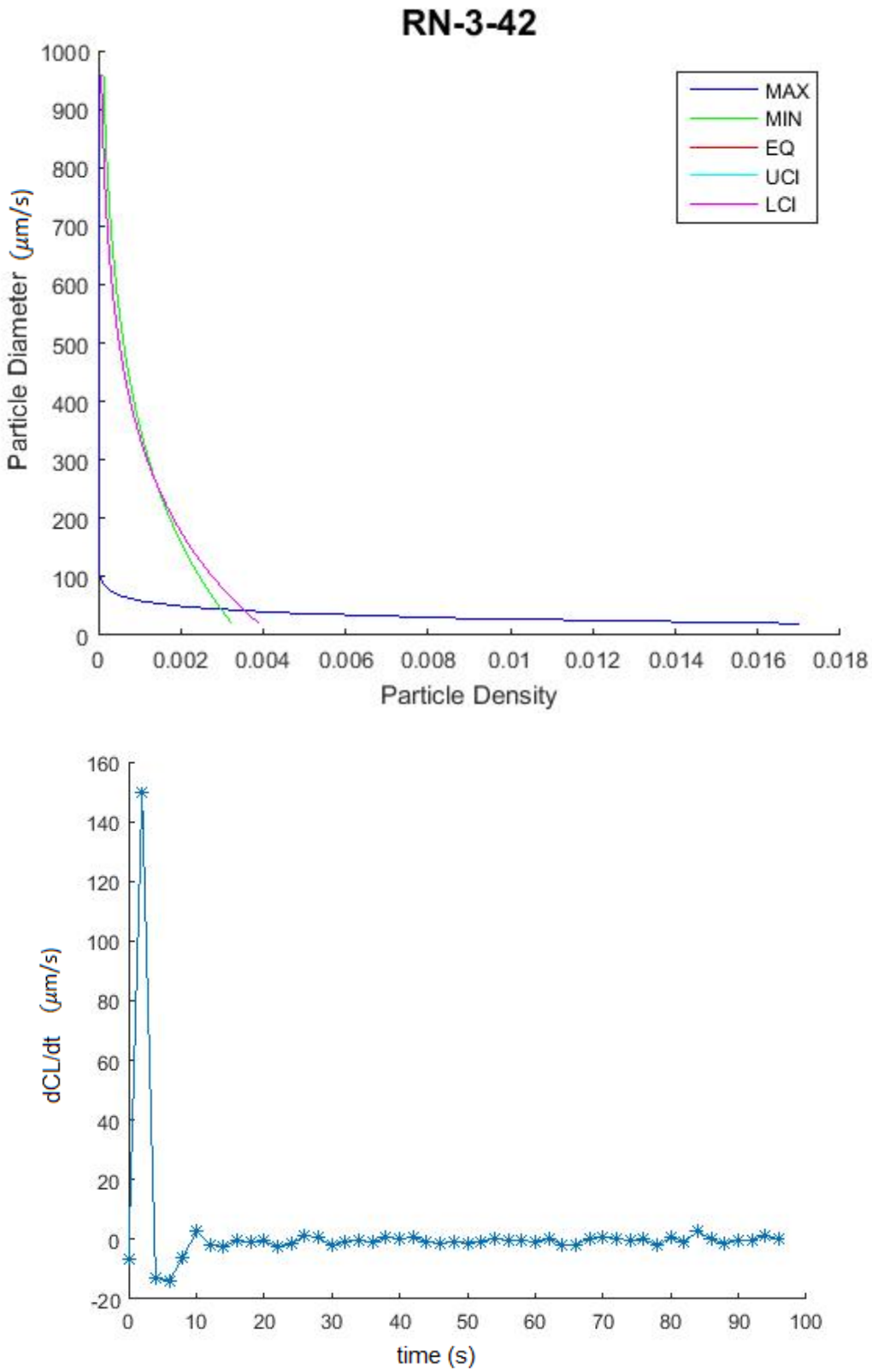

Figure B.14: Magnafloc LT27AG pH 7 (TOP) Chord length distribution analysis (BOTTOM) dCL/dt vs t

Appendix C: Effect of volume concentration of measured chord length

The first reason for dilution of the 41% by mass paste was that the samples would foul very quickly and size measurements were not reproducible. At this concentration range, the FBRM probe could not discriminate between adjacent particles in many cases which lead to very large mean diameters and unreliable measurements. In addition, bubbles of entrained air drastically affected size measurements, as a comparison with the peak floc size during flocculation was less than that of the initial floc size of moderately sheared paste. Lastly, the dilution allowed for low energy input into the flocs thus reducing the rate at which the d_{50} would decrease. The conditions attempted are shown below in Table C.1.

The effect of dilution was tested for all three conditions. Mixtures were tested at three different dilutions – 6% by mass, 8%by mass, and 12% by mass As the solids content of the system increased, the size measurements became more problematic due to a clear mudline being established, which can be seen by the gradual decrease to a pseudo-equilibrium value shown in Figure C.1. At low solids content, the larger particles were quickly suspended and no mudline was observed. On the other hand, at 12% by mass in all three conditions a distinct mudline was present which altered the measurement of the particles. The particles below the mudline consisted of the macroscopically visible flocs and above the mudline was turbid water containing a considerable amount of the smaller particles. Hence the probe tip was not measuring a homogenous mixture so the size measured was not representative of the entire system. This phenomenon is apparent when observing dCL/dt (where 'CL' represents chord length) and size versus time of an FBRM experiment at 6% by mass versus one measured at 12% by mass shown in figure 3.9. As a result of the equilibrium taking longer to establish itself, the flocs are subject to more shear forces in order to take a representative measurement of the system which could affect the size distributions. A relationship was established between particle d_{50} and solids concentration in the system

Table C.1: Conditions tested for reproducibility of particle size measurement from 41% by mass paste

Condition	Reproducibility
Un-diluted paste, stirring with FBRM probe (no over-head stirrer)	- Initial measurements were consistent but affected by air entrapment. - Sheared paste fouled within 10-20 seconds and was not reproducible
Un-diluted paste Overhead stirrer at 90RPM	- Initial d_{50} continued to increase with time, no equilibrium value obtained. Produced air bubbles as mass-volume d_{50} seemed to increase to over 700µm - Final d_{50} did not reach an equilibrium quickly (20 seconds) hence energy input becomes consideration. Fouled for some samples
Un-diluted paste Overhead stirrer at 150RPM	- Initial d_{50} did not establish equilibrium within 20 seconds. Fouling for many samples, not reproducible. - Final d_{50} reached an equilibrium quickly within 4-6 seconds.
Un-diluted paste Overhead stirrer at 60RPM	- Initial d_{50} fouled - Final d_{50} fouled
Paste diluted to 6% by mass in 500mL pH 8.5 de-ionized water Overhead stirrer at 350RPM	Produced a consistent result. Both initial and final measurements established an equilibrium within 2-4 seconds from addition of paste.

where measured d_{50} seemed to increase with solids concentration. With references to Figures C.1, C.2 and C.3, we can see that size measurement seemed to peak at 8% by mass – this is most likely a result of the interplay of two factors. The mudline present at 8% by mass was present only for the first few seconds and hence equilibrium was established much more quickly when compared to 12% by mass mixtures and flocs were subject to less shear. Secondly, while also reaching equilibrium in a similar time frame as the 6% by mass mixtures and hence being subject to similar amounts of shear, the solids concentration was higher.

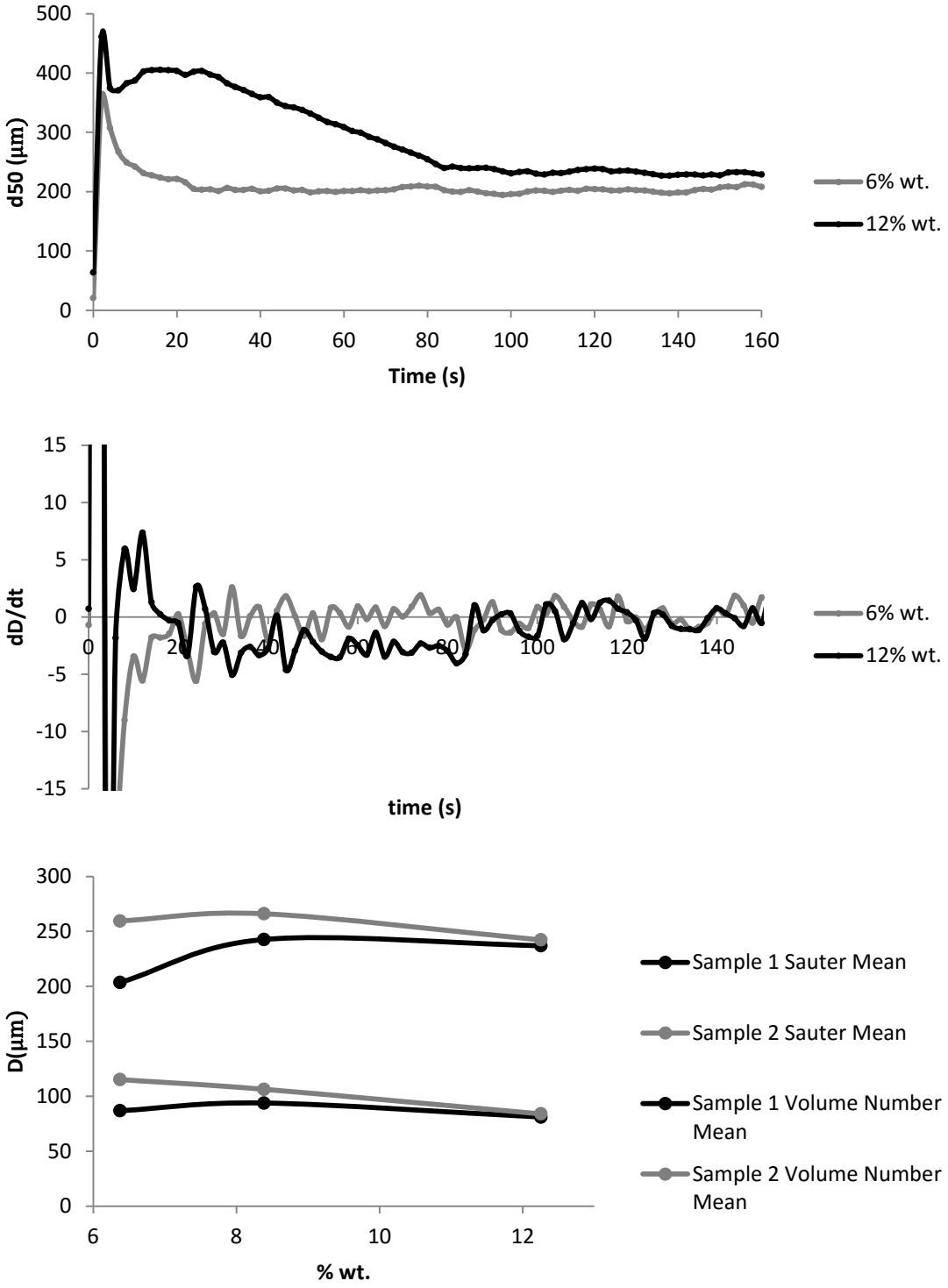

Figure C.1: A-C-A dilution tests. (TOP) Size measurement evolution profiles for varying solids concentrations of suspension from FBRM experiment. (MIDDLE) Time derivative of size showing the presence of a mudline at 12% by mass which is not present at 6% by mass (BOTTOM) Equilibrium size measurements of paste at varying solids concentration

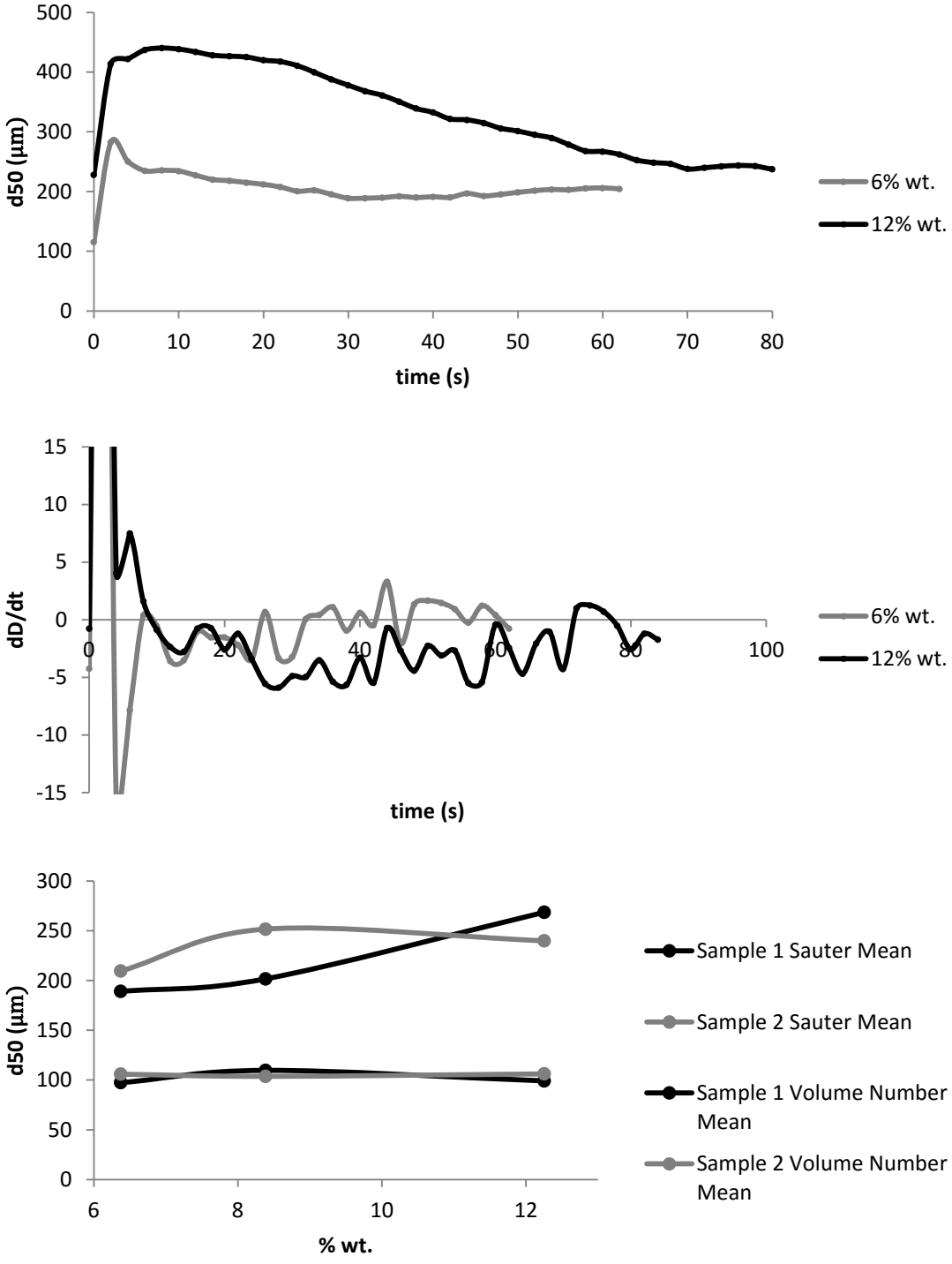

Figure C.2: Magnafloc LT27AG dilution tests. (TOP) Size measurement evolution profiles for varying solids concentrations of suspension from FBRM experiment. (MIDDLE) Time derivative of size showing the presence of a mudline at 12% by mass which is not present at 6% by mass (BOTTOM) Equilibrium size measurements of paste at varying solids concentration

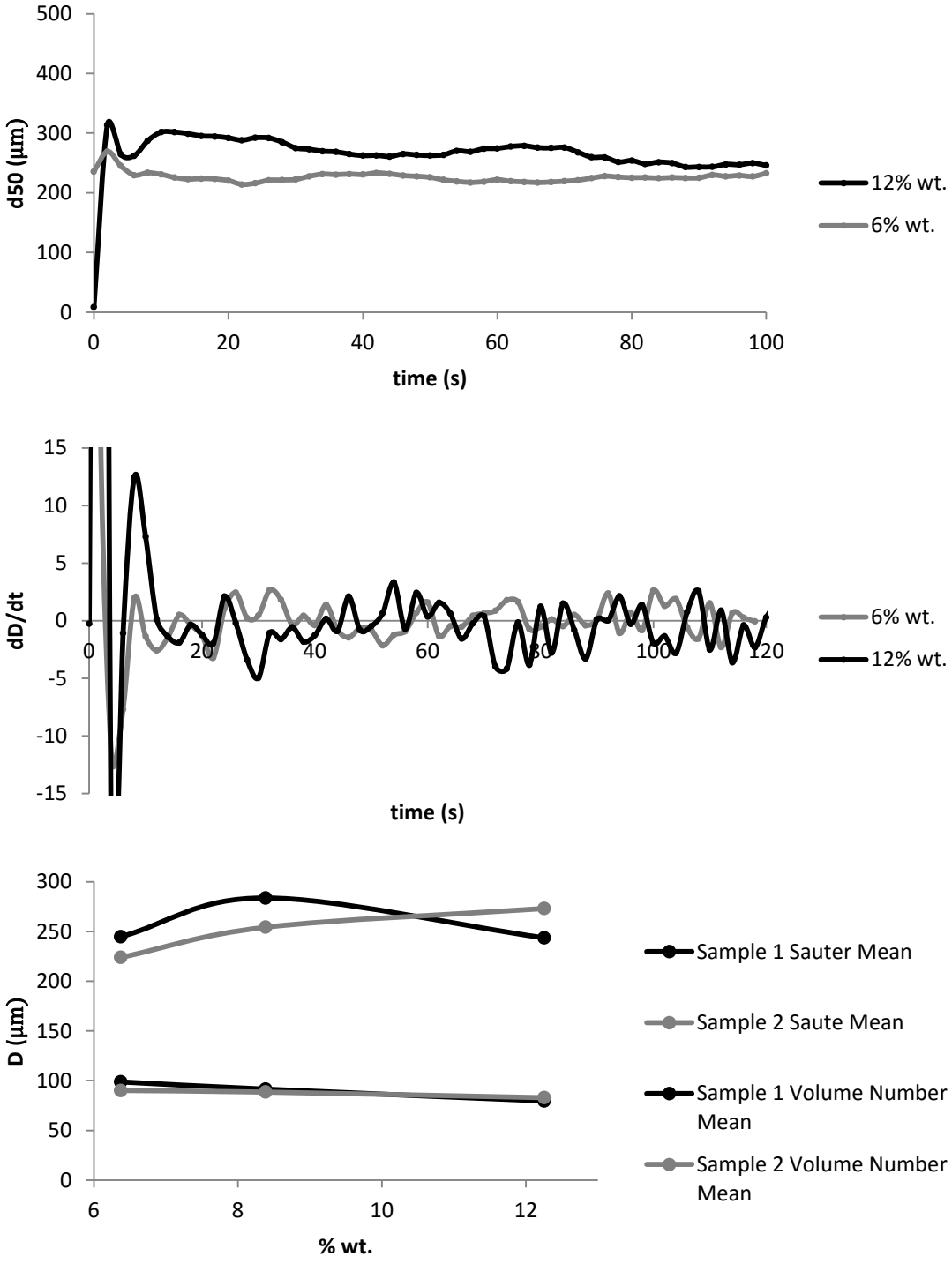

Figure C.3: Magnafloc 1011 dilution tests. (TOP) Size measurement evolution profiles for varying solids concentrations of suspension from FBRM experiment. (MIDDLE) Time derivative of size showing the presence of a mudline at 12% by mass which is not present at 6% by mass (BOTTOM) Equilibrium size measurements of paste at varying solids concentration

Appendix D: Supplemental Data Regarding Development of Procedures

Table D.1: Mixing conditions of poly(ethylene oxide) solutions, all glass containers were 3" in diameter

Conditions	Result
1. Cylindrical container geometry with sharp edges 2. 70mL, 1% by mass 2h30min, 100RPM (impeller 3mm above bottom) 3. Diluted to 280mL, 100RPM, 1min (impeller 3mm above bottom) 4. 100RPM, 6h (impeller 3cm above bottom)	Not solubilized
1. Cylindrical container geometry with sharp edges 2. 80mL, 1% by mass 5h, 100RPM (impeller 3mm above bottom) 3. Diluted to 320mL, 100RPM, 12h (impeller 3cm above bottom)	Not solubilized
1. Cylindrical container geometry with sharp edges 2. 80mL, 1% by mass 8h, 150RPM, ice bath (impeller 3mm above bottom) 3. Diluted to 320mL, 150RPM, 12h (impeller 3cm above bottom)	Solubilized μ=0.0374 Pa·s
1. Cylindrical container geometry with sharp edges 2. 80mL, 0.5% by mass 4h, 150RPM, ice bath (impeller 3mm above bottom) 3. Diluted to 160mL, 150RPM, 4h (impeller 3cm above bottom)	Not solubilized
1. Cylindrical container geometry with rounded edges 2. 100mL, 0.8% by mass 1h, 150RPM, ice bath (impeller at bottom) 3. Added 10mL, stirred for additional 7h, 150RPM ice bath(impeller at bottom) 4. Diluted to 320mL, 300RPM, 1min (impeller at bottom) 5. Diluted to 320mL, 150RPM, 12h (impeller 3cm above bottom)	Solubilized μ=0.0374 Pa·s
1. Cylindrical container geometry with rounded edges 2. 80mL, 1% by mass 30min, 150RPM (impeller 3mm above bottom) 3. Added 20mL, stirred for additional 5h, 150RPM (impeller 3mm above bottom) 4. Diluted to 320mL, 300RPM, 1min (impeller 3mm above bottom) 5. Diluted to 320mL, 150RPM, 10h (impeller 3cm above bottom)	Solubilized μ=0.0395 Pa·s

FBRM flocculation

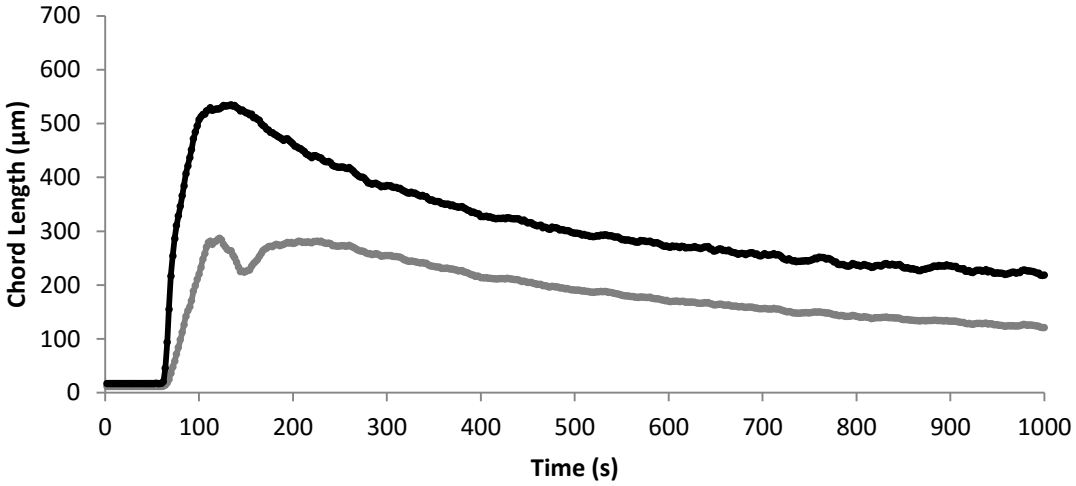

Figure D.1: FBRM chord length versus time data of a flocculation experiment of an 8% by mass kaolinite suspension at pH 8.5 where 100g/tonne of Magnafloc® LT27AG is added as 0.1% by mass solution over 40 seconds, and left to flocculate for 1000 seconds. Sauter mean diameter (—•—) and Number volume mean (—•—) are shown.

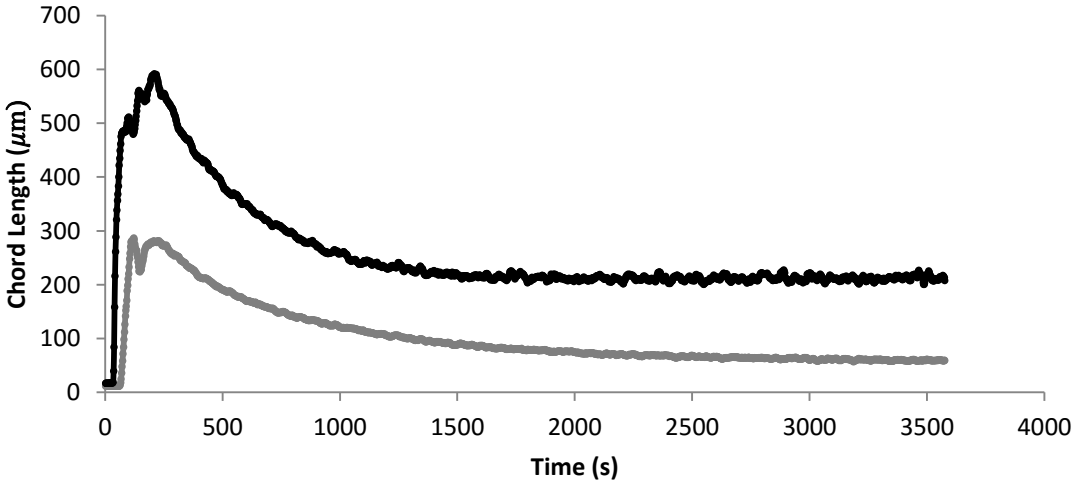

Figure D.2: FBRM chord length versus time data of a flocculation experiment of an 8% by mass kaolinite suspension at pH 8.5 with A-C-A (100g/tonne of Magnafloc® LT27AG +HyChem Hyperfloc CD650) is added as 0.1% by mass solution over 40 seconds, and left to flocculate for 1000 seconds. Sauter mean diameter (—•—) and Number volume mean (—•—) are shown.

Dual-polymer flocculation conditions tested:

Condition 1:

1) 5cm diameter impeller placed 6cm from base
2) Stirred at 350RPM
3) 100g/tonne Magnafloc® LT27AG dispensed as 0.1% by mass solution over 50 seconds
4) Stirred for 10 seconds after polymer addition
5) 100g/tonne HyChem Hyperfloc CD650 dispensed as 0.1% by mass solution over 50 seconds
6) Stirred for 20 seconds after polymer addition

Observations: Too much cationic polymer was added. Settled beds were volumous and the flocs adhered to the wall of the glass and thus were difficult to collect.

Condition 2:

1) 5cm diameter impeller placed 6cm from base
2) Stirred at 350RPM
3) 100g/tonne Magnafloc® LT27AG dispensed as 0.1% by mass solution over 50 seconds
4) Stirred for 10 seconds after polymer addition
5) 60g/tonne HyChem Hyperfloc CD650 dispensed as 0.1% by mass solution over 30 seconds
6) Stirred for 20 seconds after polymer addition

Observations: Too little cationic polymer was added. Settled bed properties were very similar to those from anionic acrylamide flocculated suspensions (volume, yield stress, appearance) and water was not as clear as condition 1.

Condition 3:

1) 5cm diameter impeller placed 6cm from base
2) Stirred at 350RPM
3) 100g/tonne Magnafloc® LT27AG dispensed as 0.1% by mass solution over 50 seconds
4) Stirred for 10 seconds after polymer addition
5) 80g/tonne HyChem Hyperfloc CD650 dispensed as 0.1% by mass solution over 50 seconds
6) Stirred for 20 seconds after polymer addition

Observations: Too much cationic polymer was added. Flocs adhered to the wall of the glass and thus were difficult to collect. Cationic should be added first, adding cationic after anionic acrylamides results in flocs which adhere to wall of glass and are difficult to collect for dewatering.

Condition 4:

1) 5cm diameter impeller placed 6cm from base
2) Stirred at 350RPM
3) 65g/tonne Magnafloc® LT27AG dispensed as 0.1% by mass solution over 30 seconds
4) Stirred for 10 seconds after polymer addition
5) 100g/tonne HyChem Hyperfloc CD650 dispensed as 0.1% by mass solution over 50 seconds
6) Stirred for 10 seconds after polymer addition
7) 35g/tonne Magnafloc® LT27AG dispensed as 0.1% by mass solution over 20 seconds
8) Stirred for 20 seconds after polymer addition

Observations: Flocs adhere to glass. Good supernatant clarity. Large fast-settling flocs

Condition 5:

1) 5cm diameter impeller placed 6cm from base
2) Stirred at 350RPM
3) 65g/tonne Magnafloc® LT27AG dispensed as 0.1% by mass solution over 30 seconds
4) Stirred for 10 seconds after polymer addition
5) 85g/tonne HyChem Hyperfloc CD650 dispensed as 0.1% by mass solution over 50 seconds
6) Stirred for 10 seconds after polymer addition
7) 35g/tonne Magnafloc® LT27AG dispensed as 0.1% by mass solution over 20 seconds
8) Stirred for 10 seconds after polymer addition

Observations: Flocs are easy to collect and don't adhere to glass. Good supernatant clarity. Large fast-settling flocs